A STUDY OF THE PROPERTIES THAT INFLUENCE VEHICLE ROLLOVER PROPENSITY

Except where reference is made to work of others, the work described in this thesis is my own or was done in collaboration with my advisory committee. This thesis does not include proprietary or classified information

Randall John Whitehead

Certificate of Approval:

George T. Flowers
Professor
Mechanical Engineering

David M. Bevly, Chair
Assistant Professor
Mechanical Engineering

Nels Madsen
Associate Professor
Mechanical Engineering

Stephen L. McFarland
Dean
Graduate School

A STUDY OF THE PROPERTIES THAT INFLUENCE VEHICLE ROLLOVER PROPENSITY

Randall John Whitehead

A Thesis

Submitted to

the Graduate Faculty of

Auburn University

in Partial Fulfillment of the

Requirements for the

Degree of

Masters of Science

Auburn, Alabama
December 16, 2005

A STUDY OF THE PROPERTIES THAT INFLUENCE VEHICLE ROLLOVER PROPENSITY

Randall John Whitehead

Signature of the Author

Date of Graduation

THESIS ABSTRACT

A STUDY OF THE PROPERTIES THAT INFLUENCE VEHICLE ROLLOVER PROPENSITY

Randall John Whitehead

Master of Science, December 16, 2005
(B.M.E., Auburn University, 2003)

180 Typed Pages

Directed by David M. Bevly

In this thesis, a vehicle's load condition is varied to investigate its impact on roll stability and a stability threshold is derived empirically using vehicle simulation. A vehicle model is developed and simulated using MATLAB. Experiments performed by the National Highway Transportation and Safety Administration (NHTSA), are used to validate the simulation. Data from these experiments is also used to validate a stability threshold developed from the simulation.

Scaled passenger vehicles in conjunction with computer simulation have proven to be a valuable tool in determining rollover propensity. The stability threshold is also validated by scaled vehicle experiments. This is made possible with the lower cost and increased safety of using a scaled vehicle versus full size passenger vehicles. A simple electronic stability control (ESC) is then developed to keep the scaled vehicle within the

stability threshold. The ESC is tested using varying vehicle properties with a constant vehicle model to see how these property changes affect the ESC's effectiveness to prevent rollover. The ESC is then implemented with an Intelligent Vehicle Model (IVM) which updates the controller's vehicle model as vehicle properties such as loading conditions change. It is shown that an IVM greatly increases the success of ESC in keeping the vehicle in the stability region.

ACKNOWLEGEMENTS

This thesis is dedicated to my Dad and Mom, Larry and Judy Whitehead, whose support throughout the past six years allowed this research to be conducted.

Special thanks to my faulty advisor Dave Bevly. You guided me through this process and spurred me on to completion. Thank you for the opportunity to further my education.

To the Auburn University GAVLAB, thank you for the technical advice, physical data, and good laughs. To Rob Daily, lab manager, your MATLAB expertise and wealth of knowledge on all other technical matters was invaluable to my studies. To Christof Hamm, the 'token' lab EE, without his knowledge of circuits and computer software, I would have had to learn things the "hard way." To Will Travis, thanks for your hard work on our research together. To Matt Heffernan, the "intellectual" discussions about vehicle dynamics and racing aroused my curiosity and motivated me to search for answers. To the rest of the Wilmore gang, Evan Gartley, Ren Flennigan, and Paul Pearson, thanks for the company and long nights cramming for exams and final projects. Thanks to the "Dungeon" inmates who fought valiantly beside me against the swarms of fruit flies.

Thanks to Dr. George Flowers and Dr. Nels Madsen, "Mad Dog," for being on my thesis defense committee. Dr. Flowers thanks for revelation that Diet Coke is great,

even at 8 a.m. classes. Dr. Madsen thanks for three seasons of Hitchcock League baseball, and enlightening me to the power of the FBD ($\Sigma F \neq 0$)!

Thanks to Undergrad research assistants for staying up late with me and on weekends to get projects complete. Thanks to Taylor Owens for all the engineering jokes and teaming up with me in classes and triathlons. Thanks to the Auburn Formula SAE Team for getting me started and interested in vehicle dynamics. Thanks to Bradley Kirkland for being a good friend and roommate. Thanks to all my other friends who gave me great memories in my years at Auburn University.

Thanks to my LORD, Jesus Christ, who taught me to trust and follow. There is peace in knowing that no matter how bad I mess things up, He never gives up on me. That is where I find hope. He directed all my paths. Proverbs 3:5-6.

Style of Journal Used:

ASME Journal of Dynamic Systems, Measurement, and Control

Computer Software Used:

Microsoft Word 2003

TABLE OF CONTENTS

LIST OF FIGURES

LIST OF TABLES

CHAPTER 1

INTRODUCTION

1.1 Motivation

Over the past decade, the occurrence of rollover incidents in vehicle accidents has received much attention due to the increase in Sport Utility Vehicle (SUV) miles driven on the roadways and litigation claiming that engineers are to blame for designing unsafe vehicles. The National Highway Traffic Safety Administration (NHTSA) reported in 2002 that 3% of all light passenger vehicle crashes on United States roads involve rollover, yet rollover accidents are responsible for 1/3 of all passenger vehicle occupant fatalities [Hilton, 2003]. The statistics reveal that SUVs rollover fatalities are more prevalent than in cars; 59% of total fatalities in SUV accidents occurred in rollover crashes, while rollovers accounted for only 23% of total fatalities in car accidents [Ponticel, 2003]. There are many differences in the vehicle properties of SUVs versus those of passenger cars. Understanding how these vehicle properties affect rollover is important when designing a safe vehicle. 10,376 fatalities and 229,000 injuries were caused by crashes that involved rollover in 2003 alone [FARS, 2005]. Along with lives, there is an economic cost that can be decreased by designing vehicles that are less prone to rollover. Motor vehicle crashes in the United States cost an estimated $231 billion in economic costs [NHTSA, 2002]. It is easy to see that a reduction in the number of

vehicle rollovers can have a positive impact on the economy. By utilizing research to understand how vehicle properties and vehicle dynamics affect rollover, both human life and economic dollars can be saved.

1.2 Background and Literature Review

The vehicle dynamics and properties that affect the occurrence of vehicle rollover have been studied for many years. Early vehicle rollover studies consisted of static tests to determine a vehicle's rollover propensity [Allen, 1990]. Statistical studies of vehicle rollover accidents were also performed to correlate vehicle properties with rollover propensity [Klein, 1992]. The most notable of these parameters are the vehicle center of gravity (CG) height and track width. In fact, they are the sole parameters that determine the Static Stability Factor (SSF). The rollover studies that used static tests proposed the SSF as a measure to quantify vehicle rollover propensity. As stated before, the SSF is a static measure of two variables: the average of the vehicle's front and rear track widths and the vehicle's CG height, as shown in Equation (1.1).

$$\text{SSF} = \frac{\text{Track Width}}{2 \cdot \text{CG Height}} \tag{1.1}$$

An illustration of the SSF taken from NHTSA's website is shown in Figure 1.1. Note that an increase in SSF corresponds to a decrease in rollover propensity. The SSF is a very accurate measure of a vehicle's static rollover stability during tripped and non-

tripped rollover. However, static rollover tests neglect the transient dynamics and tire dynamics that are involved in the abrupt changes in velocity and steer angle that come before crashes [Chrstos, 1992]. It is noted that suspension characteristics during dynamics tests are important when determining a vehicle's rollover stability and since tires are non-linear, the tires' lateral forces saturate during extreme maneuvers [Hac, 2002].

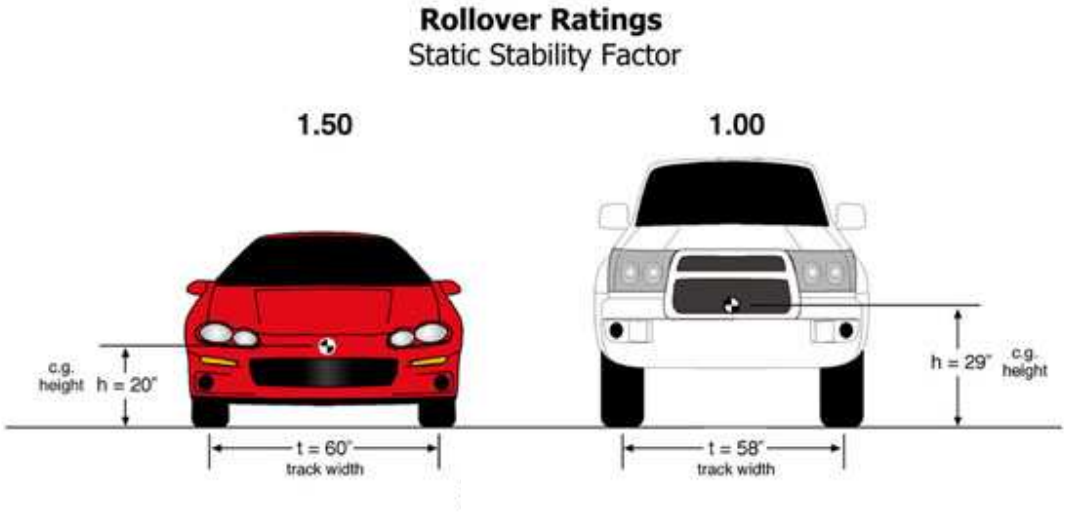

Figure 1.1. Static Stability Factor [NHTSA, 2005]

In the 1990's, the National Highway Traffic Safety Administration's (NHTSA) vehicle safety star rating system used only the SSF to determine a vehicle's rollover propensity. However, due to the high fatality rate of rollover crashes, Congress passed the "Transportation Recall, Enhancement, Accountability and Documentation Act," (TREAD), in November of 2000. TREAD charged NHTSA to conduct dynamic rollover resistance rating tests, which NHTSA in turn made part of its New Car Assessment Program (NCAP). For the purposes of a dynamic rollover resistance rating test, NHTSA selected the Fishhook steering maneuver as a primary candidate to use in conducting

rollover experiments. An illustration of the Fishhook maneuver, taken from NHTSA's website is shown in Figure 1.2.

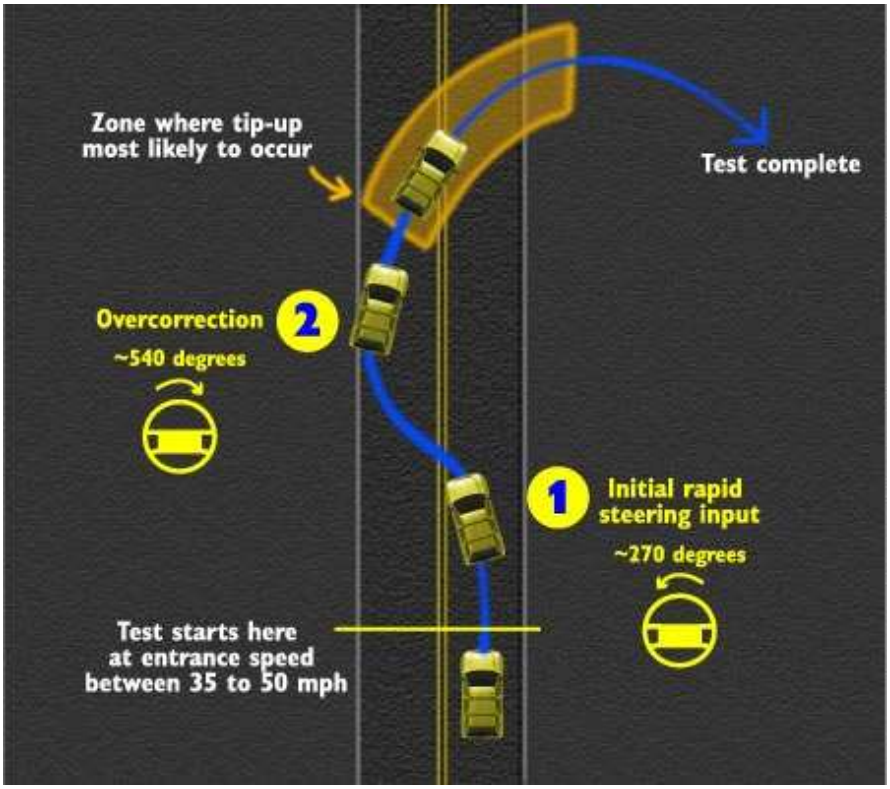

Figure 1.2. Fishhook Maneuver [NHTSA, 2005]

For vehicle dynamic testing, the rollover propensity of a vehicle is determined from the highest speed for which the vehicle can complete the selected maneuver without achieving two-wheel lift. Since the vehicle testing is conducted on-road, the results are more repeatable and give more control over the test environment than off-road tripped tests [Forkenbrock, 2003]. The evaluation procedure is only meant to test vehicles for on-road, un-tripped, rollover propensity. Although this only accounts for a small percentage of rollover crashes, the results are still a valuable measure of overall rollover stability for relative comparison of vehicles [Viano, 2003]. In 2004, NHTSA added the dynamic test to its star rating system for rollover propensity. Figure 1.3 shows NHTSA's

chart for determining a vehicle's rollover propensity star rating. It uses both the SSF and dynamic test results in order to determine rollover propensity. However, because the majority of rollover events are tripped and the CG height and track width are the vehicle properties that have the greatest effect on tripped rollover propensity, the new rating system placed more weight on the SSF [Cooperrider, 1990].

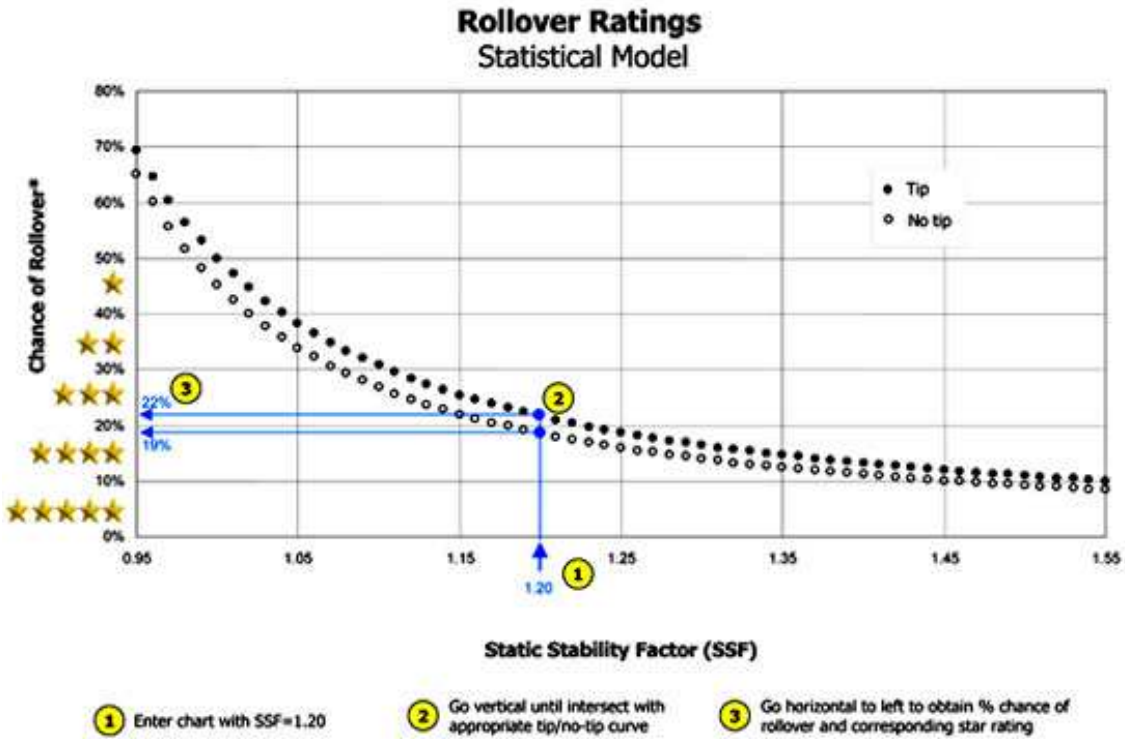

Figure 1.3. NHTSA's Rollover Propensity Star Rating System [NHTSA, 2005]

Along with developing a rollover propensity rating system, the Department of Transportation (DOT) has taken other action to make vehicles safer. In 2004, all new vehicles were mandated by the DOT to have a tire pressure monitor in each tire and a tire pressure warning light visible to the driver. The light acts as an indicator to the driver that the tire with low pressure is a hazard and needs to be repaired. This mandate was a

result of the occurrence of multiple incidents in which tires with low pressure blew-out on highways and resulted in rollover fatalities.

Electronic Stability Control (ESC) is the current buzz technology in automotive industry, and rightly so. NHTSA has published reports stating that ESC reduces single vehicle crashes by 67% and fatal crashes by 64%. The 10,376 rollover related fatalities in 2003 and the 8,476 single vehicle rollover fatalities reveal the potential that ESC has to save lives [FARS, 2005]. The ESC is designed and implemented in order to help the driver maintain vehicle stability, while tracking the` driver's desired path. The first generation of ESC uses a lateral accelerometer and a yaw rate gyroscope (gryo) to monitor the yaw dynamics and use the vehicle's antilock braking system to brake the wheels independently to minimize understeer and oversteer [van Zanten, 2000]. ESC's effectiveness is so impressive that Daimler-Chrysler, Ford, and General Motors have announced that ESC, once only an option on SUVs, will be a standard feature in all of their 2007 SUV models [Voelcker, 2005].

Since the first generation of ESC systems were so successful, continuous efforts to improve ESC are ongoing [Hac, 2004]. The accurate detection of vehicle rollover and vehicle state estimation are current topics being studied [Johansson, 2004]. The ability to precisely estimate vehicle states such as side slip angle and slip angle rate greatly increases the ESC's ability to detect instability and prevent rollover [Bevly, 2001; Ryu, 2004; Nishio, 2001]. Many researchers are putting emphasis on the design and implementation of new actuators, such as active suspension and steer-by-wire, to improve ESC performance [Wilde, 2005; Huang, 2004; Vilaplana, 2004]. And even more ESC research is being conducted on improving control algorithms by optimizing the use of the

actuators and sensors in conjunction with vehicle state estimation [Carlson, 2003; Plumlee, 2004; Schubert, 2004].

Vehicle modeling of rollover and vehicle dynamics that influence rollover has been studied much in recent years in order to better understand and prevent rollover [Nalecz, 1993]. LaGrange's method, an energy method, works well with impact modeling such as tripping [Ginsberg, 1998]. Tripped rollover scenarios are most commonly modeled using LaGrange's method, although researchers have used both Lagrange's and Newton's method to develop models for untripped rollover events [Garrott, 1992; Day, 2000;]. Newton's method works in modeling non-impact dynamics like a vehicle's yaw dynamics as seen in the bicycle model [Baumann, 2004].

Scaled vehicles are being used as valuable research tools to investigate vehicle yaw dynamics and test ESC algorithms [Travis, 2004; Brennan, 2003]. The rollover testing of full-size vehicles is an expensive and dangerous endeavor, unlike scaled vehicles where the vehicles are cheaper and experiments are safer [Yih, 2000]. If results from scaled vehicles tested in a controlled environment can be related to the dynamic behavior of full-size vehicles, then the use of scaled vehicles can be an effective means of investigating rollover [Brennan, 2001]. Brennan and Alleyne developed the Illinois Roadway Simulator for design and evaluation of yaw dynamics controllers [Brennan, 1998]. The Illinois Roadway Simulator research and scaled vehicle experiments at Auburn University have shown that scaled vehicle test beds are successful in capturing the vehicle's dynamics and can be used to develop ESC technologies for full size passenger vehicles [Whitehead, 2004; Brennan, 2004].

1.3 Purpose of Thesis and Contribution

It is well known that center of gravity height and track width, the two parameters that make up the SSF, are the major vehicle parameters that contribute to rollover propensity. In this thesis, the effects of other vehicle properties, such as longitudinal weight distribution, are evaluated to determine its influence on rollover propensity, while holding the SSF constant. The purpose of this work is to analyze vehicle rollover utilizing vehicle simulation and vehicle experimental data. A non-linear vehicle model is created in order to study how vehicle properties affect rollover propensity. A detailed development and description of a vehicle simulation, including validation testing, and a discussion of the results for several parametric variation studies are provided.

An instrumented scaled vehicle is used for the first time to study vehicle rollover and relate it to full scale passenger vehicles. The scaled vehicle is used to acquire vehicle dynamics data leading to rollover and to evaluate a stability threshold created by simulation. The vehicle simulation correlates the scaled vehicle with a full scale passenger vehicle in order to validate the use of scaled vehicles for studying rollover. The vehicle simulation is also used to develop a stability threshold which is a function of the vehicle's loading condition.

This work also develops a method to increase the effectiveness of ESC. Although ESC's ability to prevent single vehicle rollover is already high, there is room for even more improvement by using an Intelligent Vehicle Model (IVM). The IVM utilizes information about the vehicle to update the ESC's vehicle model and controller limits with a new stability threshold as the vehicle's loading condition changes. This thesis uses simulation in conjunction with an ESC on a scaled vehicle test bed to determine the

effectiveness of the ESC as vehicle properties change. The simulation is used to determine the vehicle's stability threshold at different vehicle properties. The ESC with the IVM utilizes the property changes to the vehicle model and the controller gains are adjusted to keep the vehicle within the stability threshold. This is different from a regular ESC where the vehicle model does not change, and one stability threshold is used at all times. Vehicle loading conditions are the most common way vehicle properties are varied. This thesis focuses on the influence of two of those properties, CG height and weight split, and compares the effectiveness of ESC with and without the use of an IVM.

1.4 Outline of Thesis

The purpose of this study is to evaluate and determine the parameters that influence or change vehicle rollover propensity using both experimental data and simulation. The first step was to derive a vehicle model for the simulation. The vehicle model was developed using Newton's laws of motion. The free body diagrams, equations, and assumptions are shown in Chapter 2 [Newton, 1687]. The computer simulation uses a transient roll and yaw dynamic model to capture the dynamics of the vehicle. The vehicle model is verified via comparison with experimental data from a passenger vehicle in Chapter 3. The vehicle properties' values used are given in Appendix A.

The loading conditions that effect vehicle rollover are evaluated in Chapter 4. The vehicle model developed in Chapters 2 and 3 is used to create a stability threshold for variations of these loading conditions. In Chapter 5, an ESC that uses throttle and steering control to maintain vehicle stability is developed. The ESC is evaluated in simulation and a method to improve its effectiveness is tested. The IVM, which updates the ESC's vehicle model and stability threshold for variations in vehicle load configuration, is developed in this chapter and is shown to increase the ESC's effectiveness.

Finally, to aid in studying rollover propensity, this research uses an instrumented scaled vehicle test bed to validate the vehicle model, the stability threshold, the ESC and the IVM that were developed in Chapters 2-5. The scaled vehicle is instrumented with a six degree of freedom (DOF) inertial measurement unit (IMU) and a global positioning system (GPS). The scaled test bed is also equipped with a CG relocator which allows the vehicle's loading condition to be varied in the longitudinal and vertical axes. The detailed analysis of rollover using a $1/10^{th}$ scaled vehicle is given in Chapter 6. Appendix B contains the values of the scaled vehicle properties and a description of how the roll mass moment of inertia was quantified.

CHAPTER 2

VEHICLE MODEL

2.1 Introduction

In this chapter, the model of a typical four-wheel passenger vehicle is developed. The developed vehicle model has three degrees of freedom (DOF) and was developed by deriving the equations of motion (EOM) using the free body diagrams (FBD) of the sprung and un-sprung masses. The vehicle coordinate system can be seen in Figure 2.1. The primary dynamics of concern in this thesis are the yaw and roll motions.

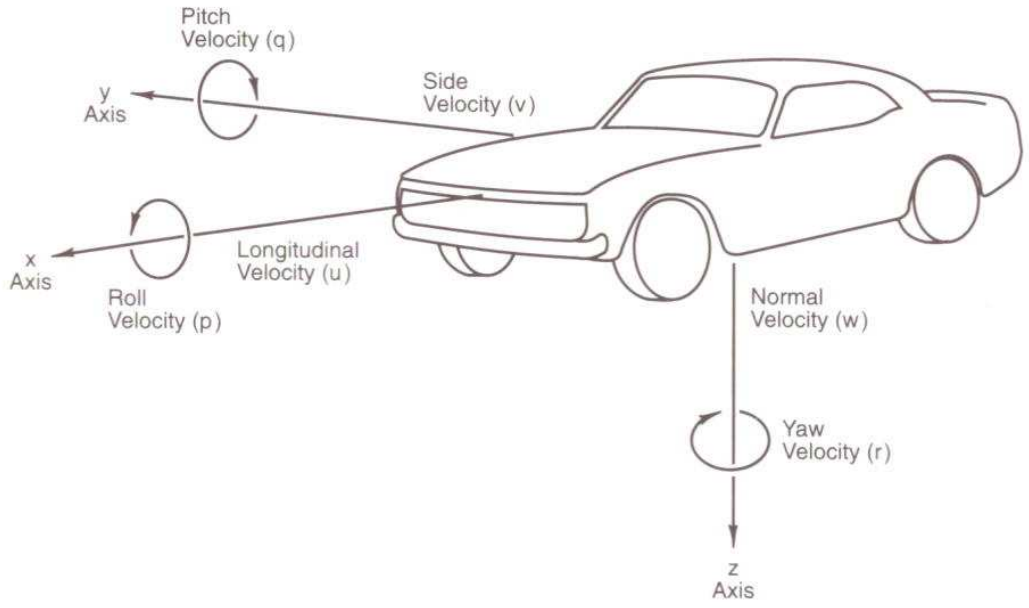

Figure 2.1. SAE Vehicle Coordinate System [Milliken, 1995]

The pitch dynamics (which cause longitudinal weight transfer) are neglected since longitudinal accelerations were kept small in the experiments considered in this thesis. The model, which is implemented using the MATLAB programming language, was developed to be extremely flexible. Individual vehicle properties such as center of gravity location and suspension setup are easily changed. Additionally, the simulation can utilize either use the transient yaw equations with either the steady state roll dynamic equations or the transient roll dynamic equations. The difference in these two models is apparent when analyzing the vehicle dynamics of transient maneuvers. However, in steady state maneuvers, the difference is small, as is shown in Chapter 3.

2.2 Bicycle Model

The transient yaw equations are derived from the "bicycle model" free body diagram shown in Figure 2.2. The 2-wheel bicycle model is the most commonly known version; however, for the purposes of this research, a 4-wheel bicycle model is used so that lateral weight transfer can be included in the yaw dynamics. The 4-wheel bicycle model, assumes that the slip angles are symmetric about the x-axis of the vehicle, which is valid at high speeds and zero Ackerman Effect [Gillespie, 1992].

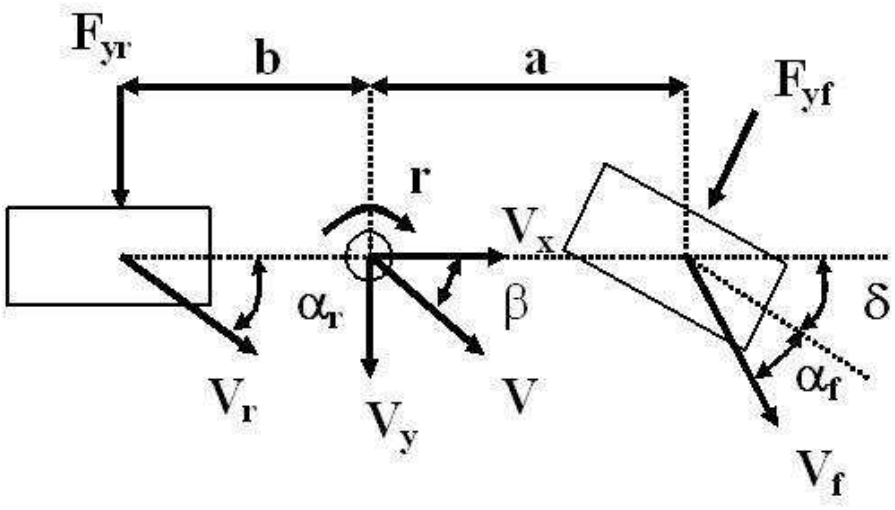

Figure 2.2. Bicycle Model, Yaw FBD

The tire forces and slip angles in Figure 2.2 are drawn using a positive sign convention. In actuality, the tire slip angles as shown would produce a negative lateral tire force as shown in Figure 2.2. Summation of moments about the center of gravity yields the yaw acceleration found in Equations (2.1 and 2.2).

$$\Sigma M_z = I_z \cdot \dot{r} \cdot [N \cdot m] \tag{2.1}$$

$$\dot{r} = \frac{1}{I_z} \cdot \left[-F_{yr} \cdot b + F_{yf} \cdot a \cdot \cos(\delta) \right] \cdot \left[rad / s^2 \right] \tag{2.2}$$

where:

a = Length between the CG and front tire patch

b = Length between the CG and rear tire patch

δ = Steer angle

F_y = Tire lateral forces

r = Yaw rate

V = Vehicle velocity vector

V_f = Front tire velocity vector

V_r = Rear tire velocity vector

V_x = Vehicle velocity in the x-axis

V_y = Vehicle velocity in the y-axis

The lateral dynamics are shown in Equations (2.3 and 2.4) by summing forces in the y-axis direction.

$$\Sigma F_y = M_t \cdot \left(\dot{V}_y + V \cdot r \cdot \cos(\beta)\right) \cdot [N] \tag{2.3}$$

$$\dot{V}_y = \frac{F_{yr} + F_{yf} \cdot \cos(\delta)}{(M_t)} - V \cdot r \cdot \cos(\beta) \cdot [m/s^2] \tag{2.4}$$

The tire slip angles are calculated as the angle between the velocity vector of the tire and the direction that the tire centerline is pointing. Equation (2.5) represents the front tire slip angle, which includes the steer angle, δ, since the vehicle being modeled is front wheel steer. Equation (2.6) corresponds to the rear tire slip angle.

$$\alpha_f = \left(\tan^{-1}\left(\frac{V_y + r \cdot a}{V_x} \right) - \delta \right) \cdot [rad] \tag{2.5}$$

$$\alpha_r = \tan^{-1}\left(\frac{V_y - r \cdot b}{V_x} \right) \cdot [rad] \tag{2.6}$$

Similarly, the vehicle side slip angle, shown in Equation (2.7), is the angle between the vehicle velocity vector and the direction the vehicle centerline is heading. The side slip rate, shown in Equation (2.8), is an important dynamic property in stability control systems. A large spike in the $\dot{\beta}$ value is an indicator of yaw instability since it is the rate at which the vehicle's velocity vector and heading are changing [Ryu, 2004]. Additionally, the side slip rate is more accurately estimated than side slip angle which current technology.

$$\beta = \sin^{-1}\left(\frac{V_y}{V} \right) \cdot [rad] \tag{2.7}$$

$$\dot{\beta} = \left(\frac{\beta(n+1) - \beta(n)}{dt} \right) \cdot [rad/s] \quad (2.8)$$

The lateral acceleration, shown in Equation (2.9), is comprised of $\dot{V}_y$ and the component of centripetal acceleration, shown in Equation (2.10), that is perpendicular to the vehicle velocity vector.

$$a_y = \left(\dot{V}_y + a_{cen} \cdot \cos(\beta) \right) \cdot \left[m/s^2 \right] \quad (2.9)$$

$$a_{cen} = r \cdot V \cdot \left[m/s^2 \right] \quad (2.10)$$

The vehicle's longitudinal and lateral velocities are defined by Equations (2.11 and 2.12).

$$V_x = V \cos(\beta) \cdot [m/s] \quad (2.11)$$

$$V_y = V \sin(\beta) \cdot [m/s] \quad (2.12)$$

2.3 Roll Model

The roll equations are derived by separating the sprung and un-sprung masses in the y-z plane, as shown in Figures 2.3 and 2.4, and applying Newton's second law (as formulated for rigid bodies). 'Inside' and 'Outside' represent the sides of the car that correspond to the inside and outside of a turn. In the figures shown below, the front of the vehicle is pointing into the page resulting in a positive roll angle towards the outside of the vehicle.

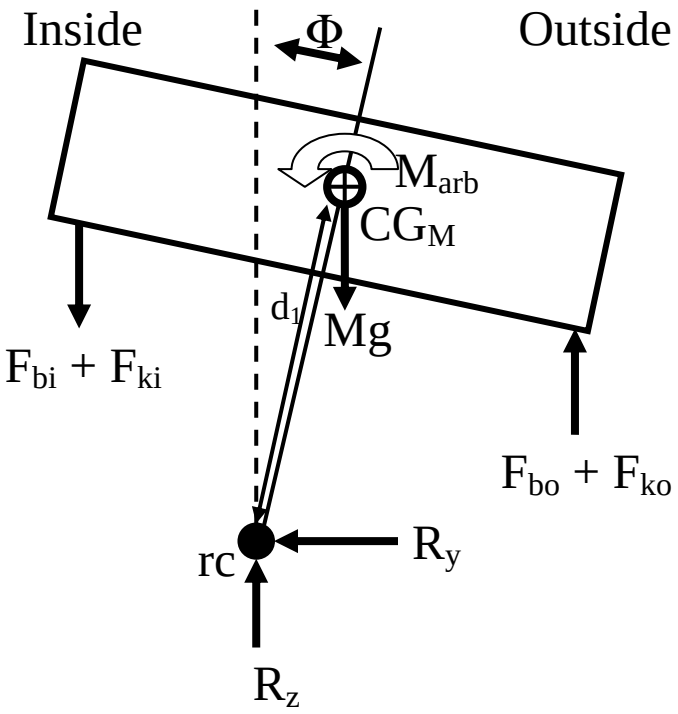

Figure 2.3. Roll FBD Sprung Mass

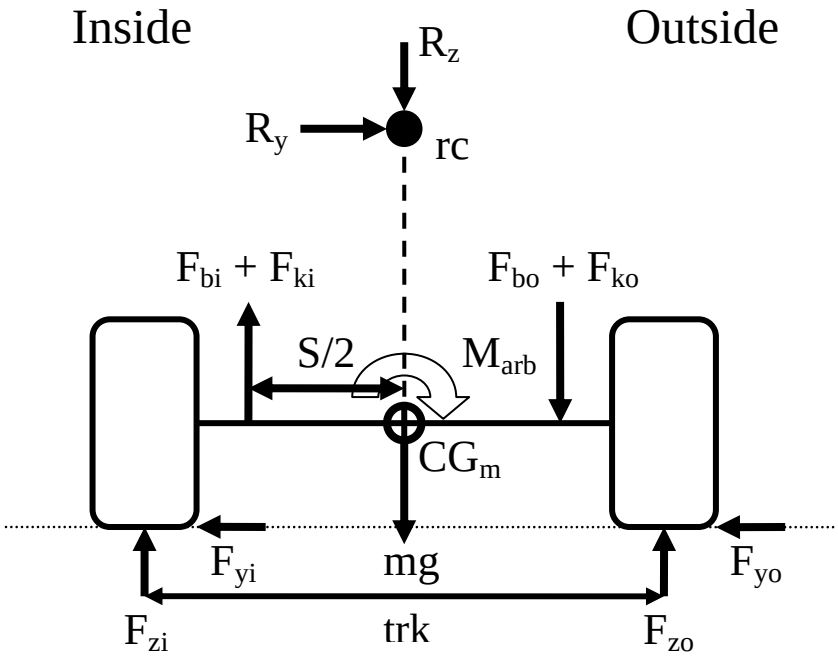

Figure 2.4. Roll FBD Un-Sprung Mass

The forces, moment, and lengths on Figures 2.3 and 2.4 are defined as:

CG_M = Sprung mass center of gravity

CG_m = Un-sprung mass center of gravity

d_1 = Length between the rc and CG_M

F_b = Damper force

(o – outside, i – inside)

F_k = Spring force

(o – outside, i – inside)

F_y = Tire lateral force

F_z = Tire normal force

M_{arb} = Anti-roll bar moment

Φ = Roll angle

rc = Roll center

R_y = Reaction force in the y-axis

R_z = Reaction force in the z-axis

S = Length between the springs and dampers

trk = Track width

The steady state roll model can be derived, by setting the acceleration and velocity dynamic states to zero. With this simplification, roll angle is analyzed as a linear function of lateral acceleration. This assumes that the total roll stiffness is linear and d_1 is constant due to the small angle linearization. Equation (2.13) is the linearized roll angle equation.

$$\Phi_{ss} = \frac{W_t \cdot d_1}{k_{\Phi t} - W_t \cdot d_1} \cdot \frac{a_y}{g} [rad] \qquad 2.13$$

where:

a_y = Lateral acceleration

g = Gravitational constant

$k_{\Phi t}$ = Total roll stiffness

W_t = Total sprung weight

The transient roll model is more complex than the steady state version since it is non-linear and includes the acceleration and velocity states. The transient roll model is very useful in that it incorporates the transient dynamics into the lateral weight transfer equations which monitor the normal forces on the wheels. Also, roll rate is a vehicle state of much importance in anti-rollover stability control systems. With the roll EOM, the roll rate magnitude can be compared with rollover incidents to develop limits for a new stability control systems. The roll equation of motion is found in Equations (2.14 and 2.15) by summing the moments about the x-axis.

$$\Sigma M_x = I_x \cdot \ddot{\Phi} \cdot [N \cdot m] \tag{2.14}$$

$$\ddot{\Phi} = \left(\frac{1}{I_x}\right) \cdot \left[-RSM - RDM + \left(R_z \cdot d_1 \cdot \sin(\Phi)\right) + \left(R_y \cdot d_1 \cdot \cos(\Phi)\right)\right] \cdot [rad/s^2] \tag{2.15}$$

In the above equation, $\ddot{\Phi}$ is the roll acceleration, RSM is the torque from the roll stiffness, and RDM is the torque from the roll damping. The roll stiffness (RS) and roll stiffness moment (RSM) values are calculated in Equations (2.16 and 2.17).

$$RS = \left[\left(0.5 \cdot k_{sf} \cdot {S_{kf}}^2\right) + \left(0.5 \cdot k_{sr} \cdot {S_{kr}}^2\right) + k_{arbf} + k_{arbr}\right] \cdot [N \cdot m/rad] \tag{2.16}$$

$$RSM = \left[\left[\left(0.5 \cdot k_{sf} \cdot {S_{kf}}^2\right) + \left(0.5 \cdot k_{sr} \cdot {S_{kr}}^2\right) + k_{arbf} + k_{arbr}\right] \cdot \Phi\right] \cdot [N \cdot m] \tag{2.17}$$

Additionally, the roll damping (RD) and roll damping moment (RDM) are represented by Equations (2.18 and 2.19) respectively.

$$RD = \left[\left(0.5 \cdot b_f \cdot {S_{bf}}^2\right) + \left(0.5 \cdot b_r \cdot {S_{br}}^2\right)\right] \cdot [N \cdot m/(rad/s)] \tag{2.18}$$

$$RDM = \left[\left[\left(0.5 \cdot b_f \cdot {S_{bf}}^2\right) + \left(0.5 \cdot b_r \cdot {S_{br}}^2\right)\right] \cdot \dot{\Phi}\right] \cdot [N \cdot m] \tag{2.19}$$

where:

b_f = Front shock damping

b_r = Rear shock damping

k_{arbf} = Front anti-roll bar stiffness

k_{arbr} = Rear anti-roll bar stiffness

k_{sf} = Front spring stiffness

k_{sr} = Rear spring stiffness

S_{bf} = Length between front shocks

S_{br} = Length between rear shocks

S_{kf} = Length between front springs

S_{kr} = Length between rear springs

The x and y axes reaction Forces at the roll center are given by Equations (2.20 and 2.21). Where M is the sprung mass.

$$R_y = M \cdot a_y \cdot [N] \tag{2.20}$$

$$R_z = M \cdot g \cdot [N] \tag{2.21}$$

It is important to note that the roll centers are assumed to be stationary to simplify the model. Also note that the spring and damper forces are assumed to be symmetric about the x-axis. This is due to the complexity of calculating the suspension kinematics during simulation. By not calculating the suspension kinematics during maneuvers, the simulation runtime is decreased. By comparison with experimental data, it is revealed in following chapters that this simplification is valid.

In order to simplify the lateral weight transfer calculation, the un-sprung mass roll dynamics are neglected. The un-sprung mass transient dynamics are neglected because rollover detection is possible by using the less complex steady state equations. The transient dynamics for the un-sprung mass are needed to determine the height of wheel lift. However, for this study, only the instant that the wheel is lifted is required to signal a rollover event.

2.4 Lateral Weight Transfer and Normal Wheel Loads

The lateral weight transfer is derived from the un-sprung mass FBD. The lateral weight transfer is measured as the difference between the inside and outside tire normal forces as shown in Equation (2.22).

$$dF_z = \left[F_{zo} - F_{zi}\right] \cdot \left[N\right] \tag{2.22}$$

To accurately determine the normal force on each wheel, the FBD of the un-sprung mass must be configured using both front and rear components. However, only the steady state roll dynamics of the un-sprung mass are modeled since the simulation is only concerned with rollover occurrences. Once wheel lift is detected, (which is when the transient roll dynamics of the un-sprung mass would be critical), the vehicle simulation is terminated and declared a rollover event. Therefore, the lateral weight transfer of the front and rear axles are found using Equations (2.23 and 2.24), respectively.

$$dF_{zf} = \frac{2}{trk_f} \cdot \left[M_{arbf} + S_{kf} \cdot F_{kf} + S_{bf} \cdot F_{bf} + R_{yf} \cdot \left(h_{rcf} - h_{cgm}\right) + F_{yf} \cdot h_{cgm}\right] \cdot \left[N\right] \tag{2.23}$$

$$dF_{zr} = \frac{2}{trk_r} \cdot \left[M_{arbr} + S_{kr} \cdot F_{kr} + S_{br} \cdot F_{br} + R_{yr} \cdot \left(h_{rcr} - h_{cgm}\right) + F_{yr} \cdot h_{cgm}\right] \cdot \left[N\right] \tag{2.24}$$

where:

F_{bf} = Front damper force

F_{br} = Rear damper force

F_{kf} = Front spring force

R_{yf} = Reaction force on the front

R_{yr} = Reaction force on the rear

S_{bf} = Length between front shocks

F_{kr} = Rear spring force

F_{yf} = Front axle lateral force

F_{yr} = Rear axle lateral force

h_{cgm} = Un-sprung mass CG height

h_{rcf} = Front roll center height

h_{rcr} = Rear roll center height

S_{br} = Length between rear shocks

S_{kf} = Length between front springs

S_{kr} = Length between rear springs

trk_f = Front track width

trk_r = Rear track width

Since the suspension kinematics of the vehicle's modeled are hard to calculate, and require additional time for simulation, the roll center height is assumed remain in the stationary static position. In order to obtain the front and rear reaction forces in the y-axis, the weight split of the vehicle must be incorporated. This allows the magnitude of the reaction force to be distributed proportionally to the mass on the front (M_f) and rear (M_r) axles as shown in Equations (2.25 and 2.26).

$$R_{yf} = R_y \cdot \frac{M_f}{M} \cdot [N] \qquad 2.25$$

$$R_{yr} = R_y \cdot \frac{M_r}{M} \cdot [N] \qquad 2.26$$

The normal forces of each tire are then calculated using the initial static force on each axle and the lateral weight transfer of each axle. W_f and W_r are the static forces on the front and rear axle respectively. The front and rear inside normal tire forces, F_{zfi} and F_{zri}, are shown in Equations (2.27 and 2.28), while the front and rear outside normal tire, F_{zfo} and F_{zro}, forces are shown in Equations (2.29 and 2.30).

$$F_{zfi} = \left[\frac{W_f}{2} - dF_{zf} \right] \cdot [N] \qquad 2.27$$

$$F_{zri} = \left[\frac{W_r}{2} - dF_{zr} \right] \cdot [N] \tag{2.28}$$

$$F_{zfo} = \left[\frac{W_f}{2} + dF_{zf} \right] \cdot [N] \tag{2.29}$$

$$F_{zro} = \left[\frac{W_r}{2} + dF_{zr} \right] \cdot [N] \tag{2.30}$$

2.5 The Pacejka Tire Model: The 'Magic Formula'

The normal forces of the tires are not only used to determine vehicle rollover; they must be used in order to determine the lateral force of each tire. Through the years, many tire studies have been conducted resulting in various tire models. As early as 1925, a researcher named Broulhiet discovered the concept of side slip and its role in producing lateral forces in a pneumatic tire [Broulhiet, 1925]. Fromm also contributed to the early studies of tire side slip and yaw [Fromm, 1954]. In the '50s and '60s, the "friction circle" was developed and experiments were conducted in order to understand its effects on handling [Radt, 1960; Ellis, 1963; Radt, 1963; Morrison, 1967]. In 1970, Dugoff, in conjunction with the Highway Safety Research Institute at the University of Michigan, published a study in which tire experiments were conducted resulting in an analytical tire model [Dugoff, 1969; Dugoff, 1970]. A lead engineer in tire research throughout the '60s, Hans Pacejka, published the 'Magic Formula' in 1987 for use in determining the lateral forces for a pneumatic passenger vehicle tire in vehicle simulations [Pacejka,

1987]. In the 1987 study, Pacejka and his colleagues recorded tire data on vehicles and developed an equation that models the empirical data of the tire's dynamics quite well. In 1989, Pacejka published an even more refined and detailed "Magic Formula" [Pacejka, 1989]. This tire model is a highly non-linear model where lateral force is a function of the tire slip angle and tire normal force. Additionally, the tire model contains parameters such as peak tire lateral force, cornering stiffness, and tire model curvature which can be modified to capture the effects for different tires. Not only does the "Magic Formula" model the tire's lateral dynamics, it contains the tire's longitudinal dynamics as well. The vehicle model in this research uses the Pacejka model because of its accuracy and ease of use.

Figure 2.5 shows the difference between the linear and non-linear "Magic Formula" tire model. The linear model has a constant tire cornering stiffness, C_α, with no saturation, while the Pacejka tire model has a non-constant C_α as the tire curve transitions into the non-linear region. In the non-linear Pacejka tire model, once the peak force is reached, the lateral tire force decreases with increasing tire slip angle. This is called tire saturation.

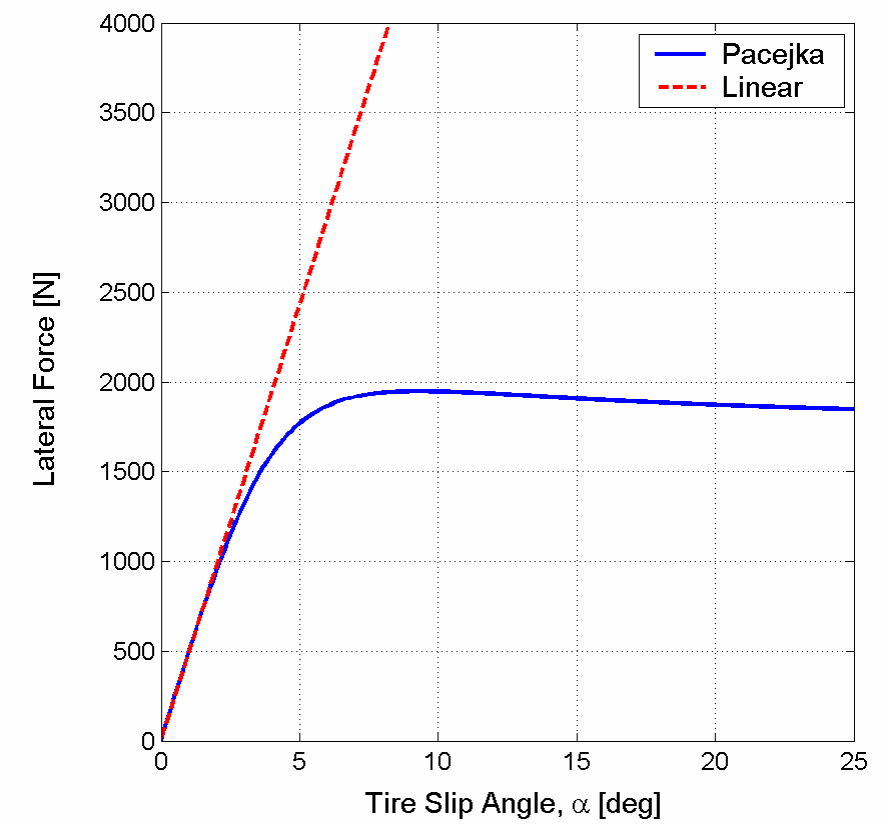

Figure 2.5. Linear vs. Non-Linear Pacejka Tire Model with a Normal Force of 5 kN

Note that the linear tire model approximates the non-linear Pacejka model for small slip angles; however, Table 2.2 shows that this approximation rapidly loses validity as tire slip angle increases.

Table 2.1. Linear Tire Model vs. Non-Linear Pacejka Tire Model

Tire Slip Angle, α, [deg]	2.5º	5.0º	7.5º
Lateral Force difference between Linear and Non-Linear Tire Models	5.6%	37.1%	88.4%

The peak tire lateral force is a function of tire slip angle and normal load. Note that increasing normal load reaches a point where it no longer produces significant gains in lateral force. This relationship is seen in Figure 2.6, which shows that both the C_α and peak force change with changing normal load.

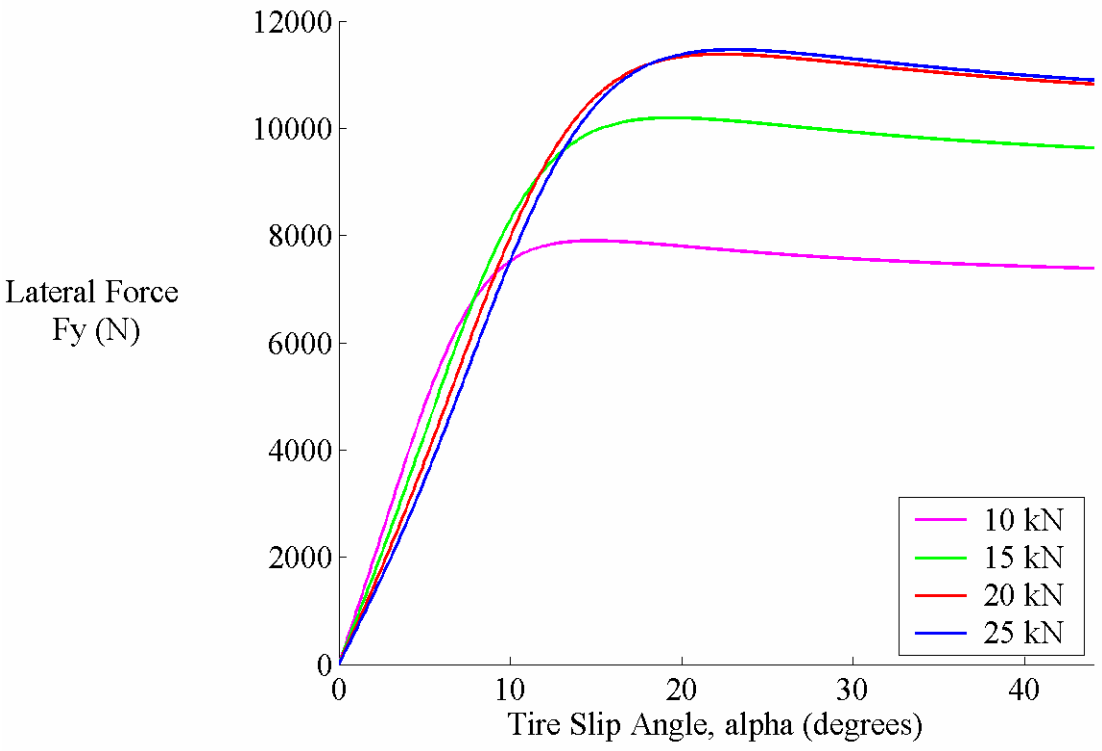

Figure 2.6. Non-Linear Tire Model with Varying Normal Forces

The inputs of the Pacejka tire model are tire slip angle and tire normal force, and the output is tire lateral force. The non-linear Pacejka lateral tire force is calculated using the Equation (2.31).

$$F_y = D \cdot \sin\left(C \cdot a\tan\left(B \cdot \phi\right)\right) \tag{2.31}$$

Equations (2.32 to 2.36) show the constants that are found in Equation (2.31). Equation (2.32) is known as the shape factor, which is independent of the tire normal force.

$$C = 1.3 \tag{2.32}$$

Equation 2.29 represents the peak factor which determines the peak lateral force of the tire curve.

$$D = a_1 \cdot F_z^{\,2} + a_2 \cdot F_z \tag{2.33}$$

Equation 2.30 controls the curvature of the tire curve, thus it is called the curvature factor.

$$E = a_6 \cdot F_z^{\,2} + a_7 \cdot F_z + a_8 \tag{2.34}$$

The cornering stiffness, C_α, factor is found in equation 2.31. Where the BCD variable is effectively C_α.

$$BCD = a_3 \cdot \sin\left(a_4 \cdot a\tan\left(a_5 \cdot F_z\right)\right) \tag{2.35}$$

Equation 2.32 is developed to be used later in equation 2.33.

$$\phi = (1 - E) \cdot \alpha + \left(\frac{E}{B}\right) \cdot a\tan(B \cdot \alpha) \tag{2.36}$$

The Pacejka parameters used in the model are those found in Pacejka, 1987, and can be seen in Table 2.2. Note that these parameters assume that the dimensional unit for the tire slip angle is degrees and for the tire normal force is kilo-Newton. The output of the Pacejka model, lateral tire force, has units of Newtons.

Table 2.2 Pacejka Parameters

a_0 = 0	a_5 = 0.208
a_1 = -22.1	a_6 = 0
a_2 = 1011	a_7 = -0.354
a_3 = 1078	a_8 = 0.707
a_4 = 1.82	

Steps were taken to simplify the non-linear tire model in this vehicle model. In Figure 2.8, the radius of the friction circle represents the maximum magnitude of force that the tire can produce at any one time. If the vehicle is braking or accelerating (longitudinal axis), the maximum lateral force decreases from the non-braking, non-accelerating scenario. The longitudinal effects of braking and acceleration were neglected since the majority of the experiments were conducted at a constant longitudinal velocity.

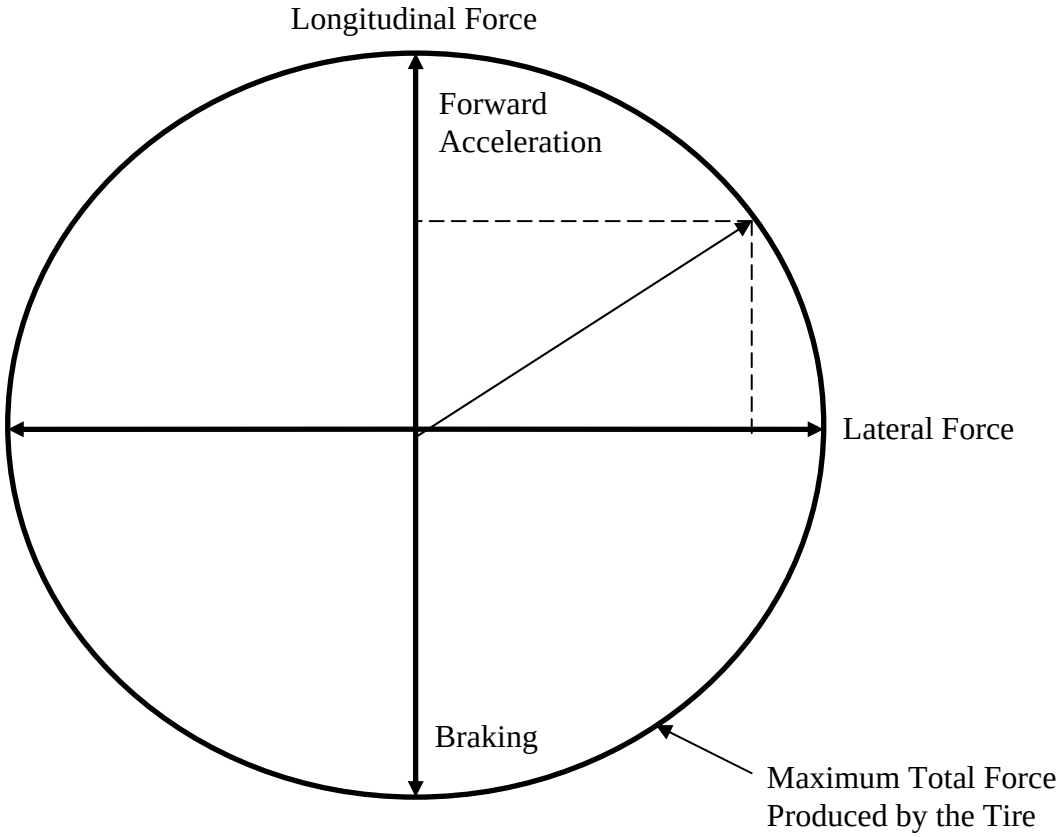

Figure 2.7. The Friction Circle

Only the lateral forces of the tire model are considered in this model, and some of those are left out as well. For instance, all forces that come from camber thrust and all moments from the self aligning torque are neglected. However, following chapters will

show how the model accurately captures a passenger vehicle's dynamics without these tire parameters.

2.6 Garage

The simulation uses a MATLAB m-file entitled 'Garage.' This appropriately entitled garage contains multiple vehicles and their vehicle properties. The 2001 Chevy Blazer in the 4-door, 2 wheel drive package that is loaded into to the garage contains the most accurate vehicle property data. Other vehicles that are in the garage include modified Blazers that match NHTSA Phase IV experiments along with a scaled vehicle. The accuracy of these vehicle properties is critical for the vehicle simulation. A list containing the value and description of each vehicle property needed for the vehicle simulation. The vehicle properties used for each vehicle are found in Appendix A. With the information in Appendix A and an accurate tire model, the vehicle simulation accurately reproduces the yaw and roll dynamics of passenger vehicles as will be shown in Chapter 3.

Figure 2.8. 2001 Chevrolet Blazer

2.7 Summary of Model Assumptions

Throughout the derivation of any model, assumptions are sometimes made in order to simplify the simulation. This is necessary due to computer processor power limitations, as assumptions and linearizations shorten the runtime of simulations. Some assumptions must be made due to unknown vehicle characteristics and properties such as suspension kinematics.

The bicycle model in this study was modified in order to include weight transfer and a non-linear tire model. It is effectively a four wheel bicycle model because it

includes weight transfer. The simplification that the tire slip angles are equal on the inside and outside of the front and rear axles is still assumed. This assumption is valid at highway traveling speeds [Gillespie, 1992].

In the roll dynamics derivation, both the front and rear roll centers are assumed to be constant throughout the suspension's range of motion. This approximation neglects the suspension kinematics. Therefore the simulation's runtime is decreased.

The un-sprung mass of the roll free body diagram seen in Figure 2.4 is assumed to be in steady state. The main information needed from the un-sprung mass is the tire's normal load, and the steady state equations provide this information. Just as the previous assumption, the purpose of this simplification is to decrease the simulation run time.

This model focuses on the roll and yaw dynamics alone, and neglects the longitudinal weight transfer effects of pitch. This assumption was made in order to simply the model. Neglecting the pitch dynamics is made possible by keeping the longitudinal acceleration and braking to a minimum in the simulation. Via simulation comparison with experimental data, it is shown in the following chapters that these assumptions are valid.

2.8 Summary and Conclusion

The derivation and intricacies of the vehicle model used in this study have been shown in this chapter. The governing equations of yaw and roll were derived using

Newton's method which included summing forces and moments on the sprung and un-sprung mass free body diagrams. The free body diagrams include the bicycle model for the yaw dynamics and sprung and un-sprung mass free body diagrams for the roll dynamics and lateral weight transfer. The "Magic Formula" tire model, developed by Hans Pacejka, was used for the vehicle model and shown. The non-linear tire model is a function of normal force and tire slip angle. It was chosen for its accuracy and ease of implementation in the vehicle simulation. Finally, the assumptions and simplification used in the model's derivation were shown and explained. This model is validated with experimental data in the next chapter.

CHAPTER 3

VEHICLE MODEL VALIDATION

3.1 Introduction

This chapter contains the validation of the vehicle model developed in the previous chapter. First, a comparison of the steady state roll model with the transient roll model is conducted. The purpose of this comparison is to see if the steady state response of the transient roll model matches the predicted steady state roll. After verifying that the steady state response is accurate for the transient roll model, the full transient dynamics response is validated. This validation is done by comparing data from the NHTSA Phase IV research with the transient roll model using a 2001 Chevy Blazer. The transient roll model is further validated using an experimental Blazer test vehicle at Auburn University. Once the validity of the transient model is shown, the lateral weight transfer dynamics of the transient roll model are explored and evaluated. The analysis in this chapter confirms the validity of the transient roll model such that the model can be used to conduct experimental simulations in later chapters.

3.2 Steady State Roll Analysis versus Transient Roll Analysis

A simple simulation was developed to determine the validity of the transient roll model that was developed in Chapter 2. The rationale behind this first test is to check the accuracy of the transient roll model by comparing it with the steady state roll analysis after the vehicle has reached steady state. The steady state roll model (SSRM) is well known and documented by previous research such that it can be considered as the "true" measurement of the vehicle states [Gillespie, 1992; Dixson, 1998]. Both vehicle models use the same transient yaw dynamics and vehicle properties. The only difference is how the roll dynamics are calculated. In order to correctly compare the transient roll model with the SSRM, the steady state values of the vehicle states are evaluated and compared at the end of the maneuver. For this test, a step steer at constant velocity is used as the maneuver to excite the vehicle.

The 2001 Blazer in the nominal configuration is the vehicle use for this analysis. The maneuver consists of a constant velocity held at 20 MPH and a step steer of 5 degrees that is filtered at 1.5 Hz. This maneuver is labeled as maneuver A for clarity in this chapter. The 1.5 Hz filter is implemented using a second order Butterworth filter. This filter is employed in order to better model a vehicle's true steering input. The simulation is updated every 0.001 second or 1000 Hz. Figure 3.1 shows the response of the Blazer using the SSRM.

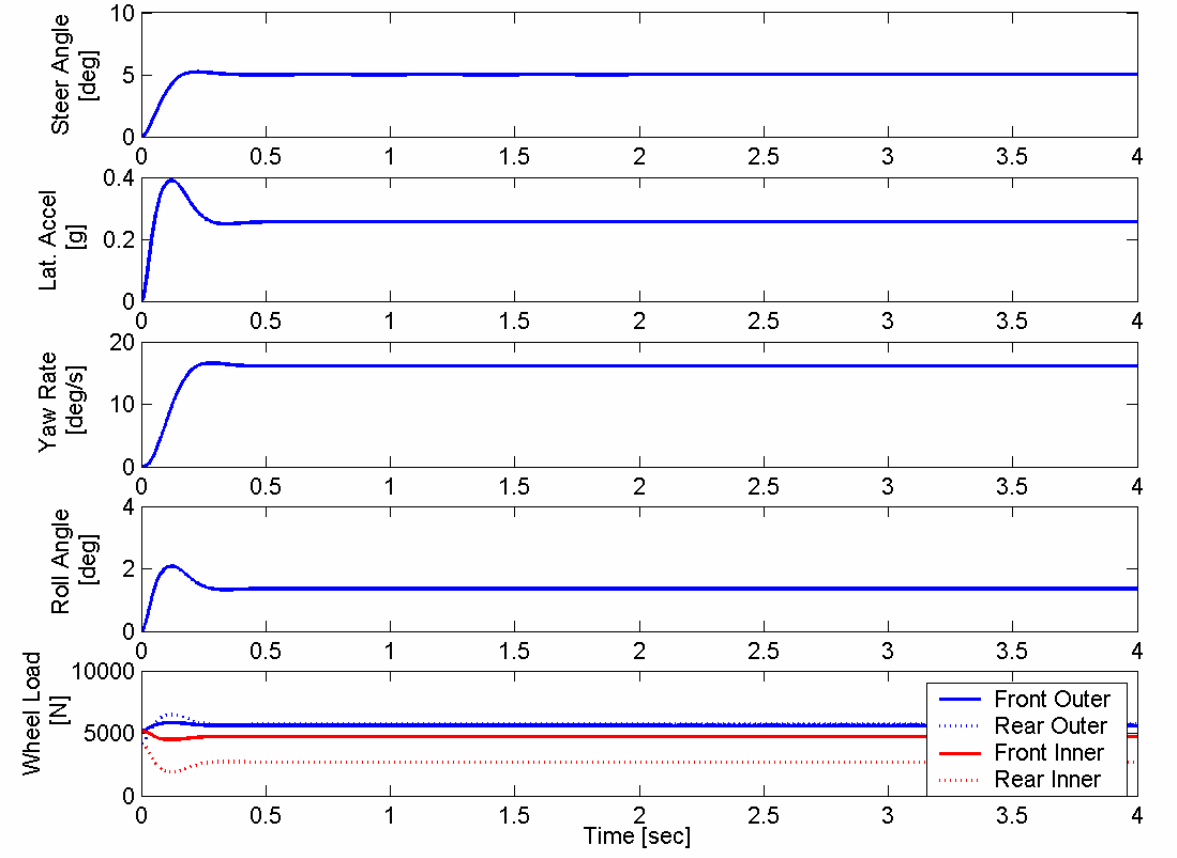

Figure 3.1. Maneuver A, S.S. Roll Model

Figure 3.2 uses the transient roll model with the same vehicle and maneuver as Figure 3.1. The difference between these models can be seen by comparing the roll angle and wheel loads within these figures. The transient roll model in Figure 3.2 contains an oscillation while the SSRM in Figure 3.1 does not. The reason for this is that the transient roll model derives the roll angle via the roll equation of motion which includes roll acceleration and damping, as was seen Equation (2.15), while the SSRM assumes roll acceleration and damping are zero thus making the SSRM roll angle a function of lateral acceleration, as was seen in Equation (2.13). The wheel loads are derived by calculating the lateral weight transfer on the front and rear axles, which was shown by Equation (2.22) in Chapter 2. The lateral weight transfer is calculated as a function of roll angle in

the SSRM and as a function of the roll dynamics in the transient roll model as seen in Equations (2.23 and 2.24). Since the roll dynamics are oscillatory in the transient roll model, the wheel loads are also oscillatory.

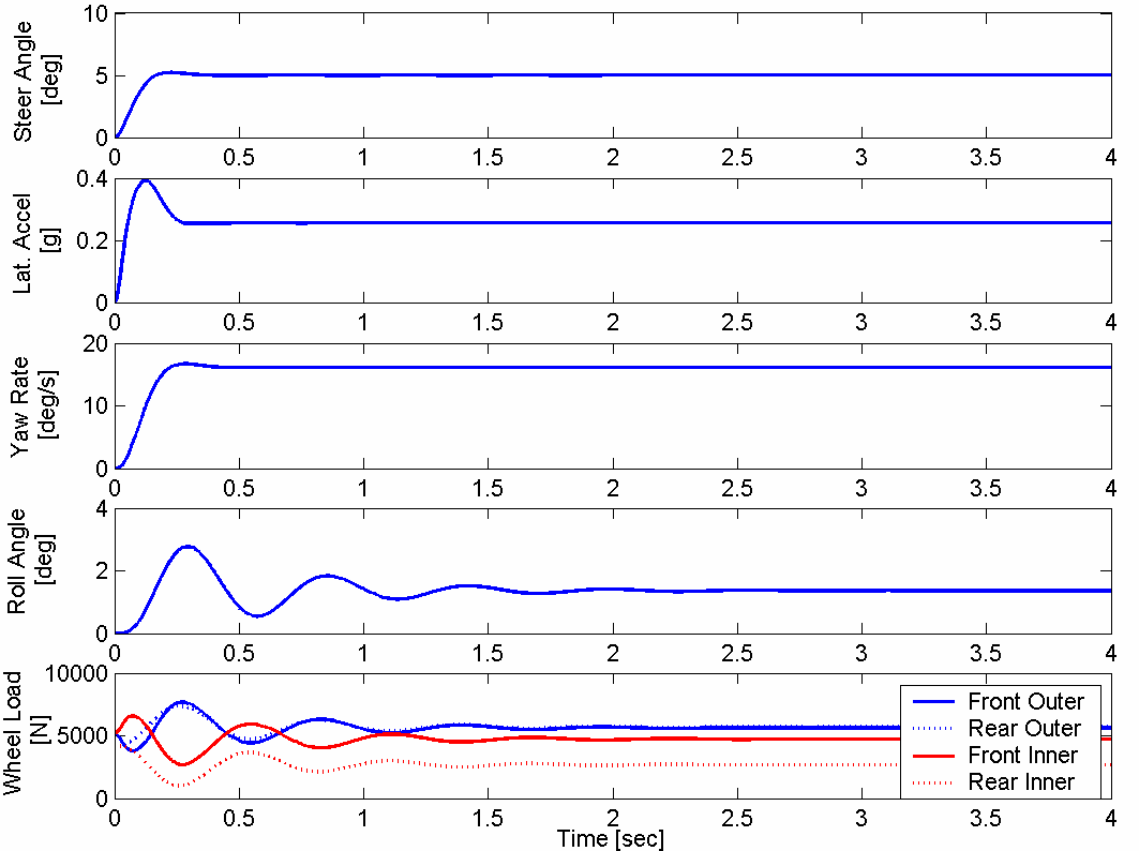

Figure 3.2. Maneuver A, Transient Roll Model

As stated earlier, in order to compare the different roll models, the dynamic states are compared once the simulations have reached steady state for each model. The steady state values are measured 10 seconds after the maneuver was started. The difference in the states are compared by computing the percent difference for the two models using Equation (3.1) where the SSRM measurement is used as the truth measurement.

$$\text{Percent Difference} = \left| \frac{\text{SS Roll - Transient Roll}}{\text{SS Roll}} \right| \times 100\% \qquad 3.1$$

Table 3.1 contains the steady state results for maneuver A. There is no wheel lift during this maneuver, and the steady state dynamic values for the two models are approximately the same as seen by the low percent difference between the two.

Table 3.1. Comparison of Models for Maneuver A

Dynamic State	S.S. Roll	Trans. Roll	% Difference	Units
Lateral Acceleration	.2554118	.2554118	0.0	[g]
Roll Angle	1.419507	1.419058	.0316307	[deg]
Side Slip	2.278848	2.278849	.0000439	[deg]
Yaw Rate	16.09942	16.09941	.0000621	[deg/s]
Front Weight Transfer	526.9914	526.3616	.1195085	[N]
Rear Weight Transfer	1,421.585	1,421.087	.0350313	[N]
Front Lateral Force	2,650.778	2,650.778	0.0	[N]
Rear Lateral Force	2,137.870	2,137.869	.0000468	[N]
Roll Rate	5.557720	5.55596	.0316676	[deg/g]

For the next test, the step steer of 5 degrees filtered at 1.5 Hz is used again. However, in this simulation (Maneuver B), the velocity is increased to 35 MPH. In this input scenario, the inside rear tire in both models lifts and remains un-weighted as the states are measured at the 10 second time interval. Figures 3.3 and 3.4 contain the response of the SSRM and the transient roll model, respectively, during maneuver B. In Figures 3.3 and 3.4, the rear inside wheel load is indicated by the dotted line. It is clear that the wheel load for this tire goes to zero, which indicated wheel lift.

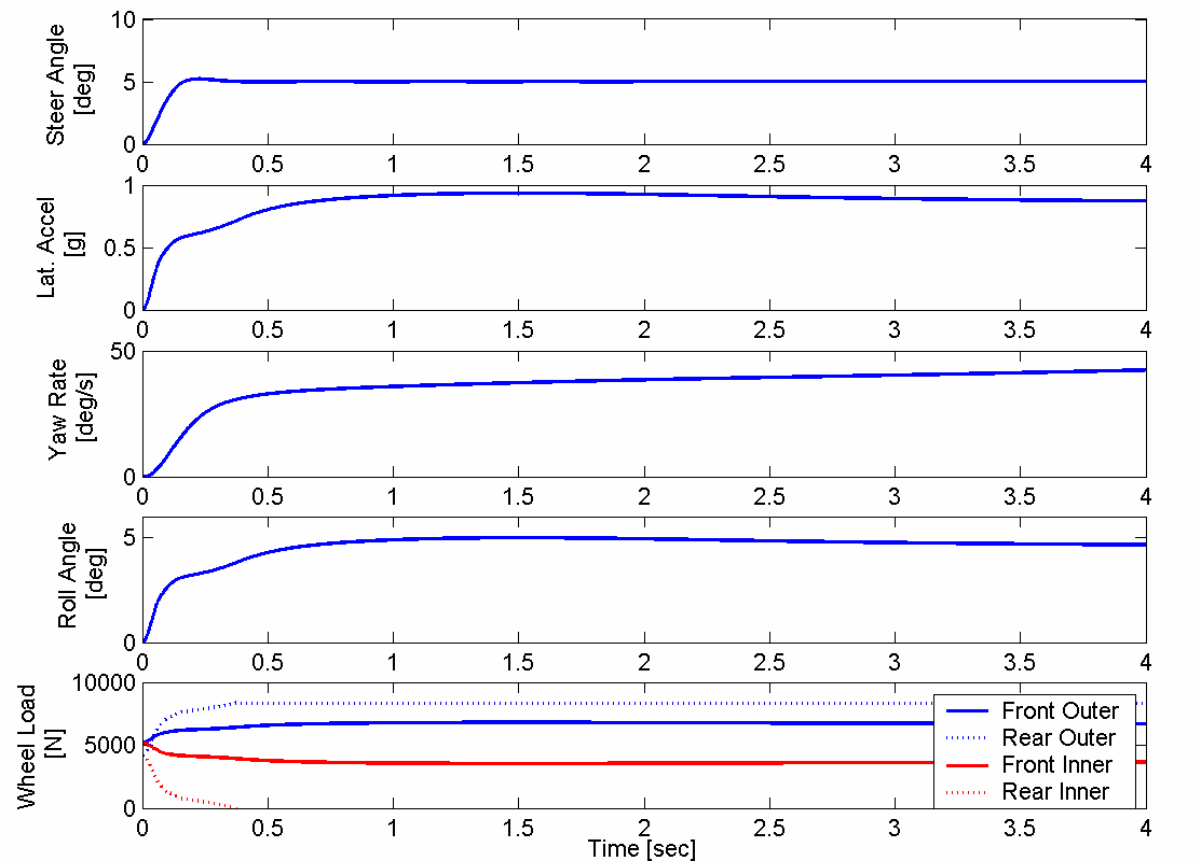

Figure 3.3. Maneuver B, S.S. Roll Model

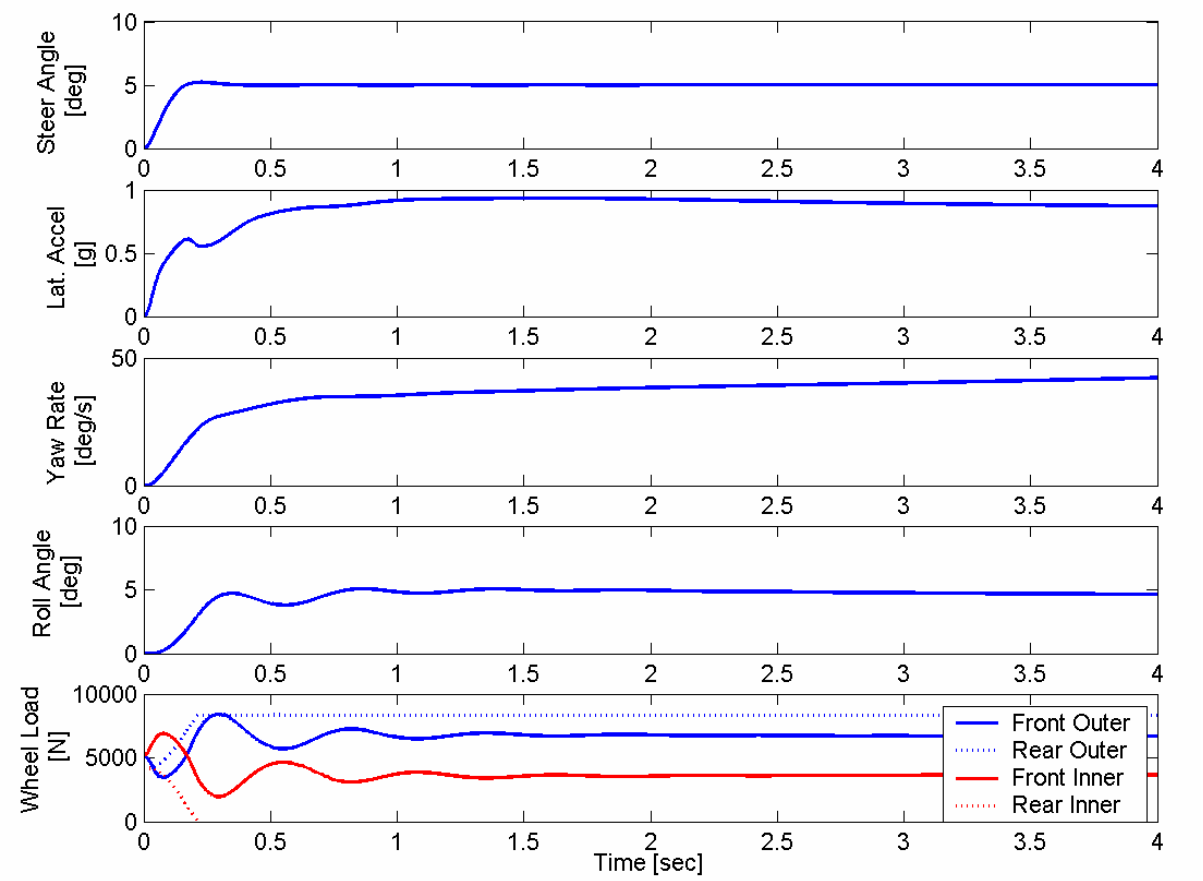

Figure 3.4. Maneuver B, Transient Roll Model

The comparison of the models' steady state dynamic states for maneuver B is recorded in Table 3.2.

Table 3.2. Comparison of Models for Maneuver B

Dynamic State	SS Roll	Trans. Roll	% Difference	Units
Lateral Acceleration	.8498721	.8499465	.008754	[g]
Roll Angle	4.723351	4.707426	.337154	[deg]
Side Slip	-54.79752	-54.74284	.099785	[deg]
Yaw Rate	56.05783	56.03894	.033697	[deg/s]
Front Weight Transfer	1,751.426	1,728.569	1.30505	[N]
Rear Weight Transfer	4,185.143	4,185.143	0	[N]
Front Lateral Force	8,894.704	8,895.999	.014559	[N]
Rear Lateral Force	7,040.835	7,040.957	.001733	[N]
Roll Rate	5.55772	5.538496	.345897	[deg/g]
Rear Inner Wheel Lift time	.373	.214	42.6273	[sec]

By examining Table 3.2, the greatest discrepancy between the two models is the time at which the rear inner wheel lifts. However, even during this maneuver, the percent difference between the two models is small enough that the models are still very comparable.

The SSRM takes an additional 0.159 seconds than the transient roll model to lift the inside rear wheel. This is explained by investigating the rear lateral weight transfer equation which dictates the rear wheel loads. Equation (3.2) describes the general weight transfer, while Equation (3.3) describes the full weight transfer for the rear axle.

$$dF_z = \left[F_{zo} - F_{zi}\right] \cdot \left[N\right] \tag{3.2}$$

$$dF_{zr} = \frac{2}{trk_r} \cdot \left[M_{arbr} + S_{kr} \cdot F_{kr} + S_{br} \cdot F_{br} + R_{yr} \cdot \left(h_{rcr} - h_{cgm}\right) + F_{yr} \cdot h_{cgm}\right] \cdot \left[N\right] \tag{3.3}$$

where:

F_{br}	Rear damper force	h_{rcr}	Rear roll center height
F_{kr}	Rear spring force	M_{arbr}	Rear anti-roll bar moment
F_{yr}	Rear axle lateral force	R_{yr}	Reaction force on the rear
F_{zi}	Axle inside tire wheel load	S_{br}	Length between rear shocks
F_{zo}	Axle outside tire wheel load	S_{kr}	Length between rear springs
h_{cgm}	Un-sprung mass CG height	trk_r	Rear track width

The lateral weight transfer equation, Equation (3.2), is calculated as the difference between inside and outside wheel loads on each axle. An increase in the rear, lateral weight transfer, dF_{zr}, causes a decrease in wheel load on the rear inside tire. For this simulation, the maximum value of dF_{zr} is one half of the weight on the rear axle, and at this maximum value, the rear inside wheel load is zero. The lateral weight transfer equation is identical for both roll models; however, the rear damper force (F_{br}) is zero in the SSRM, while it has a value in the transient roll model. The rear damper force is a function of roll velocity and the longitudinal distance between the CG and where the damper connects to the sprung mass (S_{br}). S_{br} and F_{br} are the variables in roll damping moment (RDM), as seen in Equation (2.19). The RDM value is positive when the roll angle velocity is positive. Note that increasing roll angle towards the outside of the vehicle is positive. For the step maneuver, the dF_{zr} increases faster in the transient roll model than in the SSRM due to the positive roll angle velocity. This causes the transient roll model to produce a wheel lift before the SSRM.

It is also important to note that while the transient roll model is the first to produce wheel lift, the wheel that lifted first, touches down again between time .515 and .543 seconds as seen in Figure 3.5. During this time, the roll angle velocity is negative which causes the RDM to be negative and results in the dF_{zr} decreasing from its maximum, thus causing touch down. Touch down does not occur with the SSRM because the roll dynamics are neglected. Therefore, once wheel lift occurs in this model, it does not regain normal wheel load.

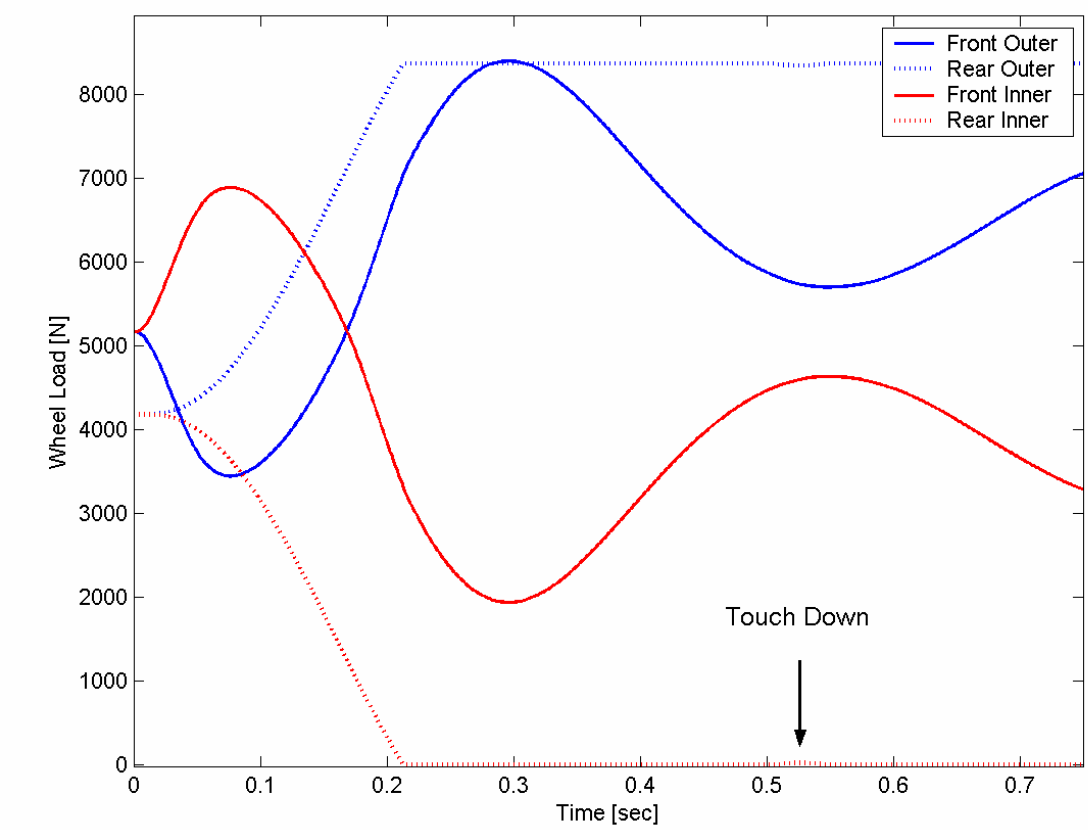

Figure 3.5. Zoom-In View of Test 2 Transient Model Wheel Load Response

With the minimal percent difference between the two models in the two maneuvers found in Tables 3.1 and 3.2, the transient roll is considered accurate at steady

state for the dynamic states analyzed. Although, this analysis of the SSRM and the transient roll model is successful in capturing the steady state response of the transient roll model, further analysis of the transient model is needed to verify the full transient response of the model.

3.3 NHTSA Phase IV Comparison

Due to the increasing fatality rate caused by rollover crashes (especially in SUVs) Congress charged NHTSA to conduct dynamic rollover resistance rating tests. For the purposes of a dynamic rollover resistance rating test, NHTSA selected the Fishhook steering maneuver as a primary candidate, which was refined in the Phase IV of the TREAD act investigation. During the TREAD act, NHTSA took exhaustive data measurements of the vehicle dynamics from the vehicles they tested. This data was made available to the general public and is used in this chapter to further validate the vehicle model.

In order to validate the vehicle model described in Chapter 2, simulation results were compared to the NHTSA Phase IV experimental data for the Fishhook 1a maneuver (also known as the Fixed Timing Fishhook). The Fishhook 1a maneuver uses a steering input consisting of an initial steer followed by a counter steer at a set entrance velocity. The velocity profile of this maneuver is characterized by the vehicle reaching a desired steady state speed, known as the entrance speed, and coasting through the rest of the

maneuver once the initial steer is begun. The steer angle input for the Fishhook 1a maneuver is shown in Figure 3.6. The steer angle initially starts at zero degrees and then commanded to steer angle 'A' at a rate of 720 degrees per second at the hand wheel. In the Fishhook 1a maneuver, the steer angle 'A' is held constant for 0.250 seconds then a counter steer to '-A' at the same rate occurs. The steer angle '-A' is held constant for 3 seconds, after which it returns to zero, completing the maneuver. The value 'A' is specific to each vehicle configuration, and is defined by multiplying 6.5 by the steer angle of the handwheel at which the vehicle experiences 0.3 g of lateral acceleration in the Slowly Increasing Steer (SIS) maneuver. The SIS maneuver is performed at a constant velocity of 50 mph with a continually increasing steer input of 13.5 degrees per second at the hand wheel.

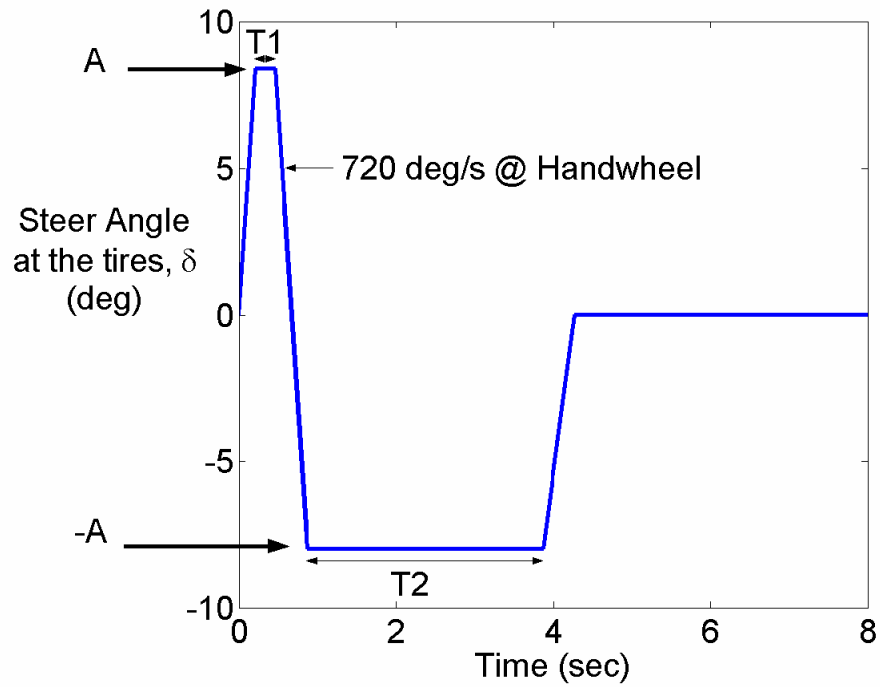

Figure 3.6. Steer Angle Input for the Fishhook 1a Maneuver

To accurately simulate the vehicle, there are three parameters of the Blazer that must be quantified. These parameters are the suspension stiffness, damping, and the front-to-rear roll stiffness ratio. However, ranges for these values are known. Therefore a method to approximate a value for each of these properties without 'tuning' the properties for a specific maneuver was used. NHTSA evaluated the Blazer using multiple maneuvers such as the J-Turn, Fishhook 1a, and Fishhook 1b. Since the maneuver of most dynamic interest, the Fishhook 1a, is used later for model validation, the J-Turn maneuver is compared with the simulation in order to back out the approximate unknown properties. The frequency and damping of the suspension's roll dynamics are seen in the roll data in Figure 3.7. With this information, the suspension roll stiffness and roll damping are varied to match the roll angle frequency and damping. Since the differences between the front and rear roll stiffness and roll damping are not known at this point, they are kept equal to one another.

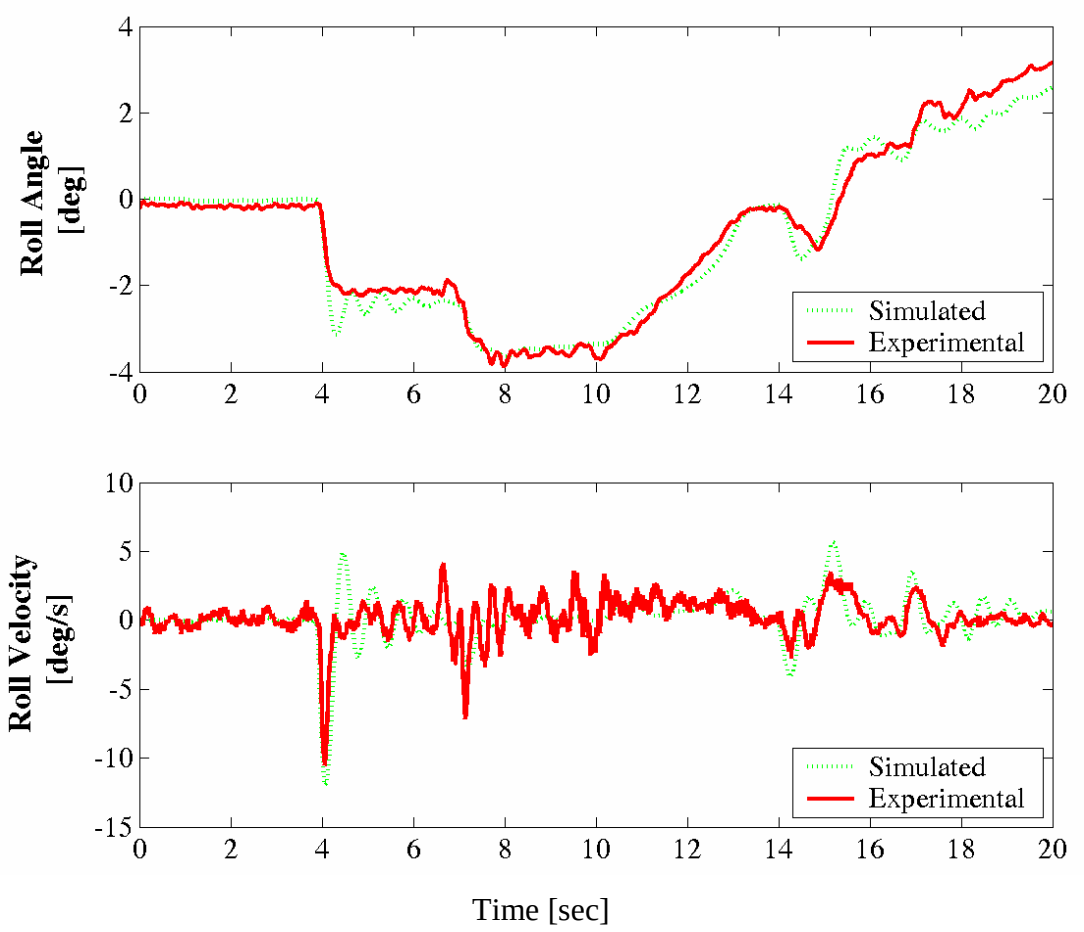

Figure 3.7. J-Turn Maneuver Roll Dynamics for Experimental and Simulation Data

With the suspension roll stiffness and roll damping approximated, there still exists an error between the experiment and simulation yaw data. The simulation showed tire saturation while the experiment did not. In order to minimize this error, the vehicle's front to rear roll stiffness was changed to match the yaw rate. However, the total roll stiffness was held constant to retain the roll dynamic response. Changing the front to rear roll stiffness changes the understeer gradient which dictates the maximum yaw rate a vehicle can attain for a given maneuver. The yaw dynamics for the experimental data and the simulation are shown in Figure 3.8. With the roll stiffness, roll damping, and

front to rear roll stiffness ratio approximated for the J-Turn maneuver, the comparison of the simulation with the experimental data for a Fishhook maneuver can be performed with confidence that the parameters are not 'tuned' specifically for the Fishhook maneuver.

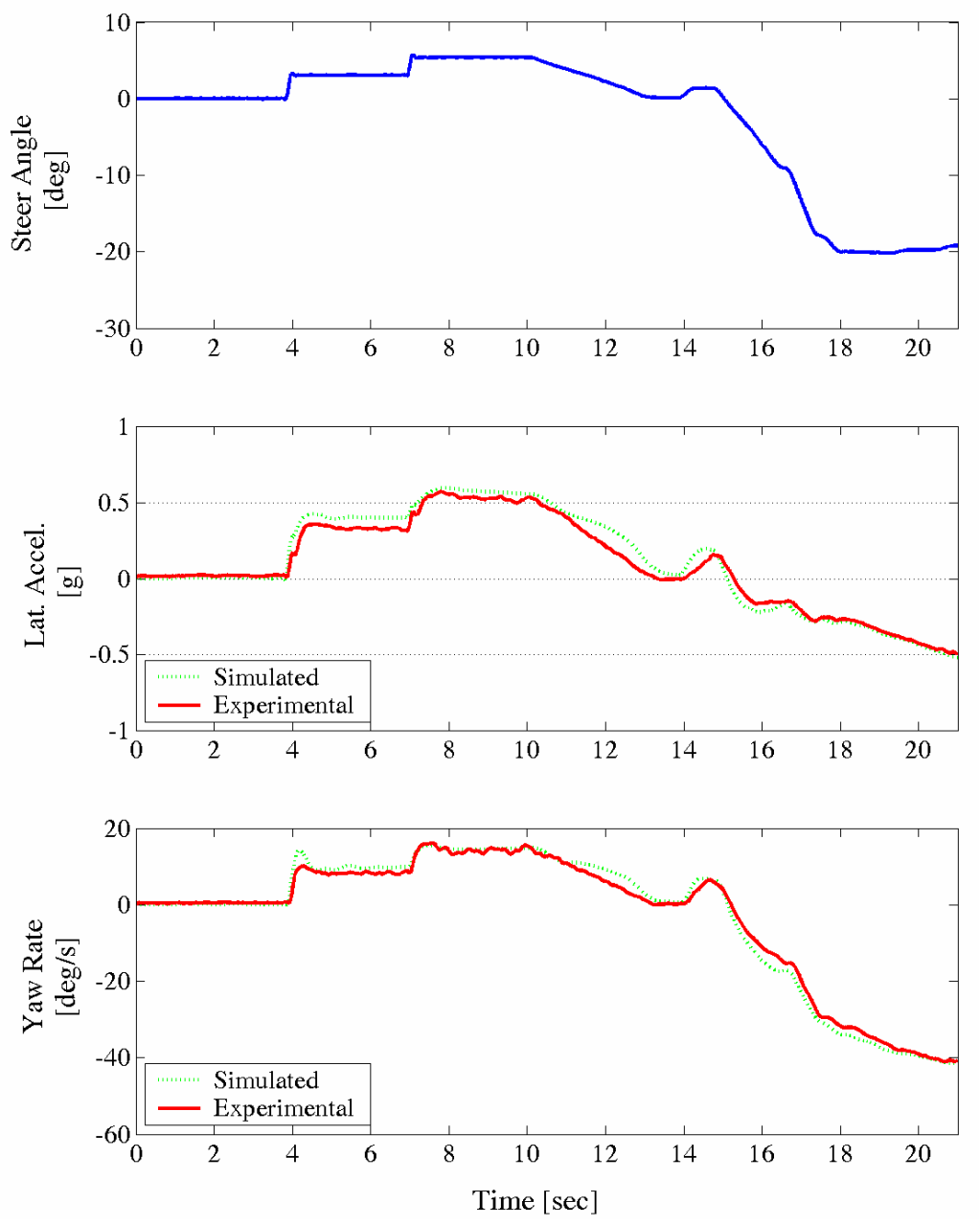

Figure 3.8. J-Turn Maneuver Yaw Dynamics for Experimental and Simulation Data

The vehicle used for comparison in this study is a 2001 Chevy Blazer 4x2. NHTSA's Phase IV experiments recorded data for the Blazer in three different configurations: Nominal, Reduced Rollover Resistance (RRR), and Rear Mounted Ballast (RMB). The Nominal configuration is the Blazer equipped with a driver, data acquisition, and outriggers on board. It has a weight distribution of 55:45 (front to rear), CG height of 26.3 inches, and a track width of 56.89 inches. These parameters result in a static stability factor (SSF) of 1.048 (Equation 1.1). Complete property values of each vehicle can be found in Appendix A. Figure 3.7 shows the Nominal configuration center of gravity drawn on the Auburn University GAVLAB Blazer.

Figure 3.9. Auburn University GAVLAB Blazer
Center of Gravity drawn in the Nominal Configuration

Figure 3.10 shows the Nominal Blazer experimental data and simulation data during a Fishhook 1a maneuver. Both the yaw and roll dynamics of the transient yaw and roll model closely match to dynamic states measured in the actual vehicle.

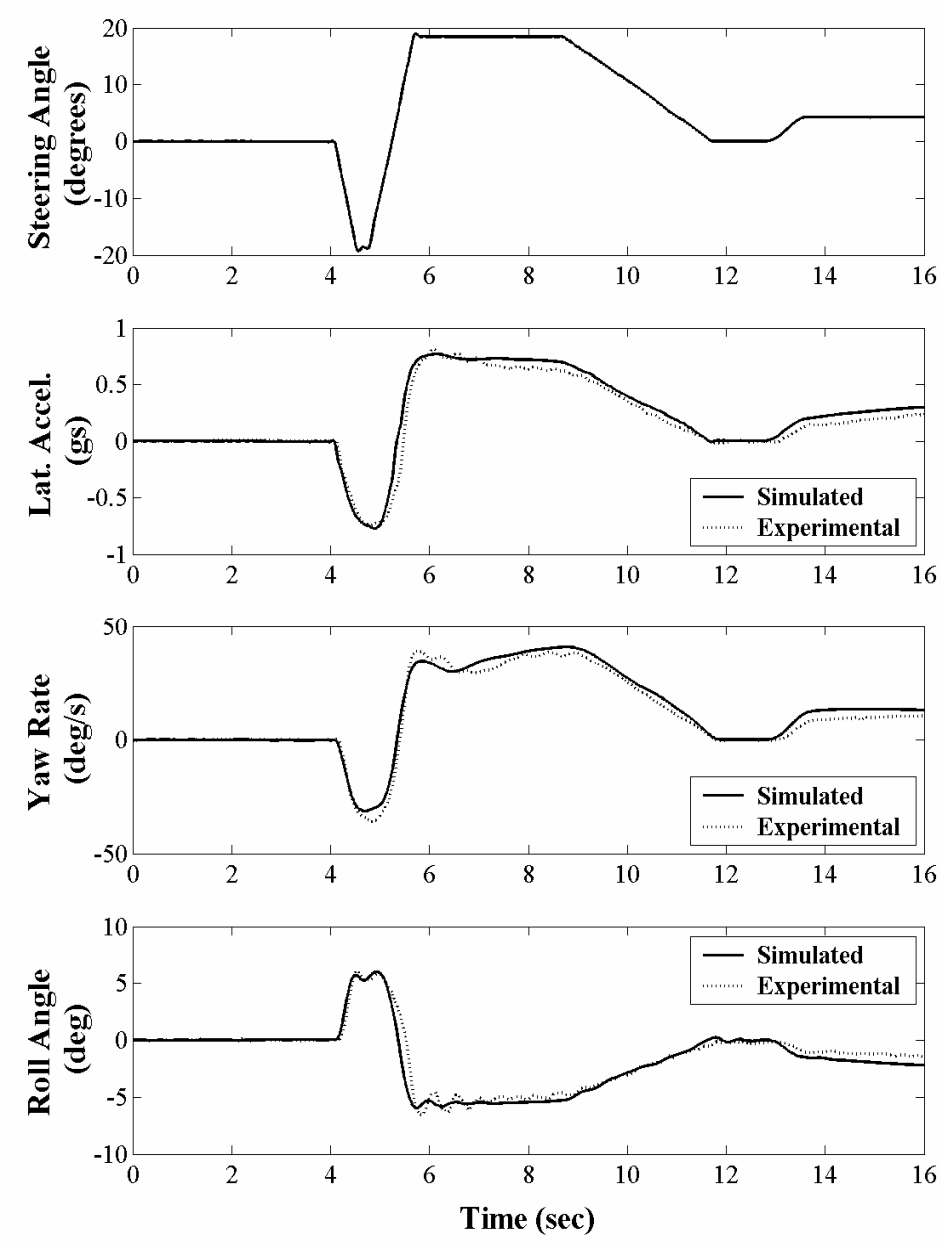

Figure 3.10. Nominal Blazer Dynamics for a Fishhook 1a Maneuver

The RRR configuration is the vehicle in the Nominal configuration with a 181 lbs roof ballast added on the top of the vehicle and shown in Figure 3.11. This serves to raise the CG vertically by 5% from the Nominal configuration to 27.6 inches. This results in a new SSF of 0.989, while maintaining the same vehicle longitudinal weight split as the Nominal configuration.

Figure 3.11. Auburn University GAVLAB Blazer
Center of Gravity drawn in the RRR Configuration

In order to conduct this simulation, the CG height, roll inertia, and yaw rate were the only parameters that were changed in the garage when converting the Nominal Blazer to the RRR Blazer. The changes of these properties were recorded in the NHTSA study and are shown in Table 3.3.

Table 3.3. Nominal vs. RRR Blazer Configuration [Forkenbrock, 2002]

	Weight (lbs)	CG Height (inches)	Roll Inertia (ft-lbs-sec^2)	Yaw Inertia (ft-lbs-sec^2)	Pitch Inertia (ft-lbs-sec^2)
Nom. Blazer	4154	26.3	520	2765	2573
RRR Blazer	4335	27.6	579	2766	2637

The roll inertia for the RRR configuration is 11.3 percent higher than the Nominal configuration. However, since the placement of the roof ballast is near the CG in the x and y axes, the yaw inertia changes by less than 0.04 percent. Though pitch inertia is neglected in vehicle model, thus not needed, it is interesting to note the roof mounted ballast causes it to increase by 2.49 percent. The increase in the pitch inertia will cause an increase in understeer during heavy breaking with the Blazer.

In Figure 3.12, the experimental and simulated RRR Blazer configuration data is compared. Again, the vehicle model follows the actual RRR Blazer Fishhook 1a experiment data. The largest discrepancy between the simulation and experimental data is in the roll angle. This is most likely due to wheel lift of the inside tires.

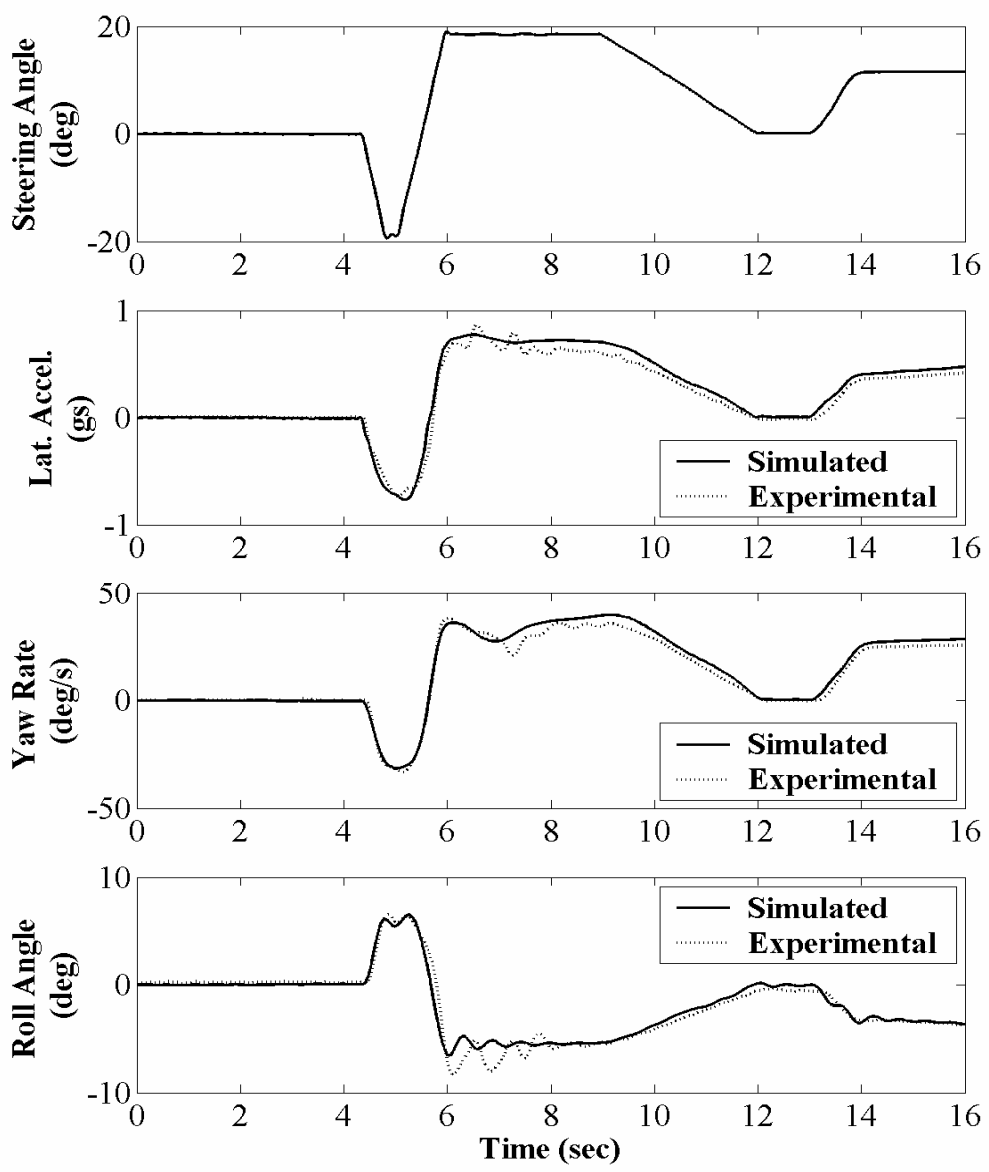

Figure 3.12. RRR Configuration Blazer Dynamics for a Fishhook 1a Maneuver

The RMB configuration is the vehicle in the Nominal configuration with weight added to the rear of the vehicle, which moves the CG longitudinally by 10.5 inches toward the rear, but retains the same SSF. This center of gravity shift is illustrated in Figure 3.13. The RMB has a front to rear weight distribution of 44:56, but maintains the SSF of 1.048. For the Nominal and RRR configurations, experimental data for a

Fishhook 1a maneuver is available. However, for the RMB configuration, only experimental data for a Fishhook 1b maneuver is available. The Fishhook 1b maneuver is similar to the Fishhook 1a, but does have some subtle differences [Forkenbrock, 2002; NHTSA, 2002].

Figure 3.13. Auburn University GAVLAB Blazer
Center of Gravity drawn in the RMB Configuration

Table 3.4 reveals the change in vehicle properties between the Nominal and RMB Blazer configurations.

Table 3.4. Nominal vs. RMB Blazer Configuration [Forkenbrock, 2002]

	Weight Split Front:Rear	CG Height (inches)	Roll Inertia (ft-lbs-sec^2)	Yaw Inertia (ft-lbs-sec^2)	Pitch Inertia (ft-lbs-sec^2)
Nom. Blazer	55:45	26.3	520	2765	2573
RMB Blazer	44:56	26.1	567.9	3604	3368.3

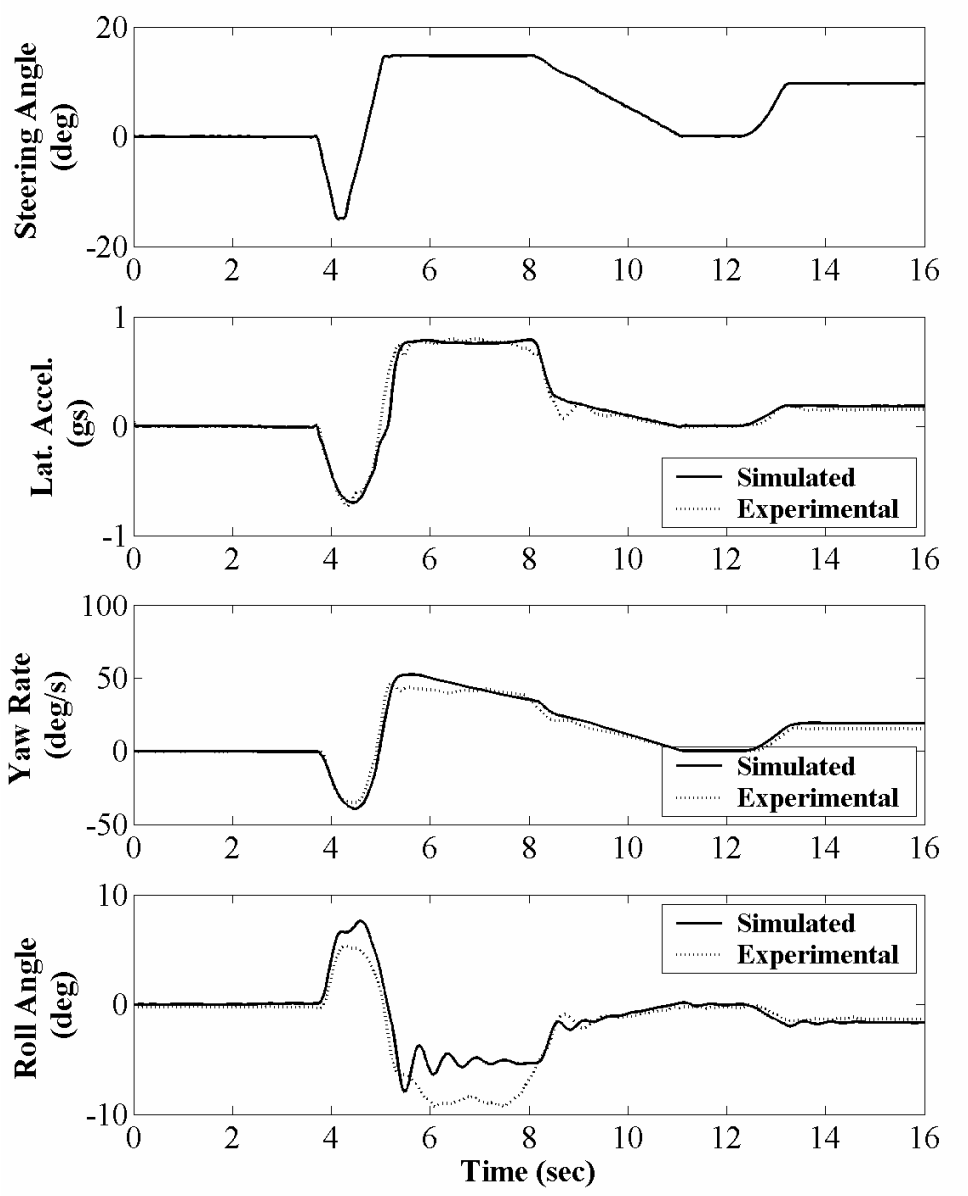

Figure 3.14. RMB Configuration Blazer Dynamics for a Fishhook 1b Maneuver

Figure 3.14 shows experimental and simulation results from Fishhook 1b for the RMB configuration. The largest discrepancy between the simulation results and the experiment data is again in the roll angle. The experimental data reveals that two-wheel lift occurs. This is seen in the roll angle measurement along with the NHTSA notes for

this experiment. However, the simulation result predicts only one-wheel lift with the second wheel approaching wheel lift. This is seen from the normal forces for each tire, as shown in Figure 3.15. This difference is most likely due to limitations of the simulation model. Some of the model's assumptions discussed in Chapter 2 may not be valid for all scenarios the vehicle encounters. For example, the roll stiffness is more than likely not linear in the real Blazer. Also, the assumption of the un-sprung mass being in steady state is no longer accurate after one wheel lift occurs for the roll dynamics (yet it appears to remain valid for the yaw dynamics). Also note that this discrepancy is small and it occurs only in the Fishhook 1b RMB data.

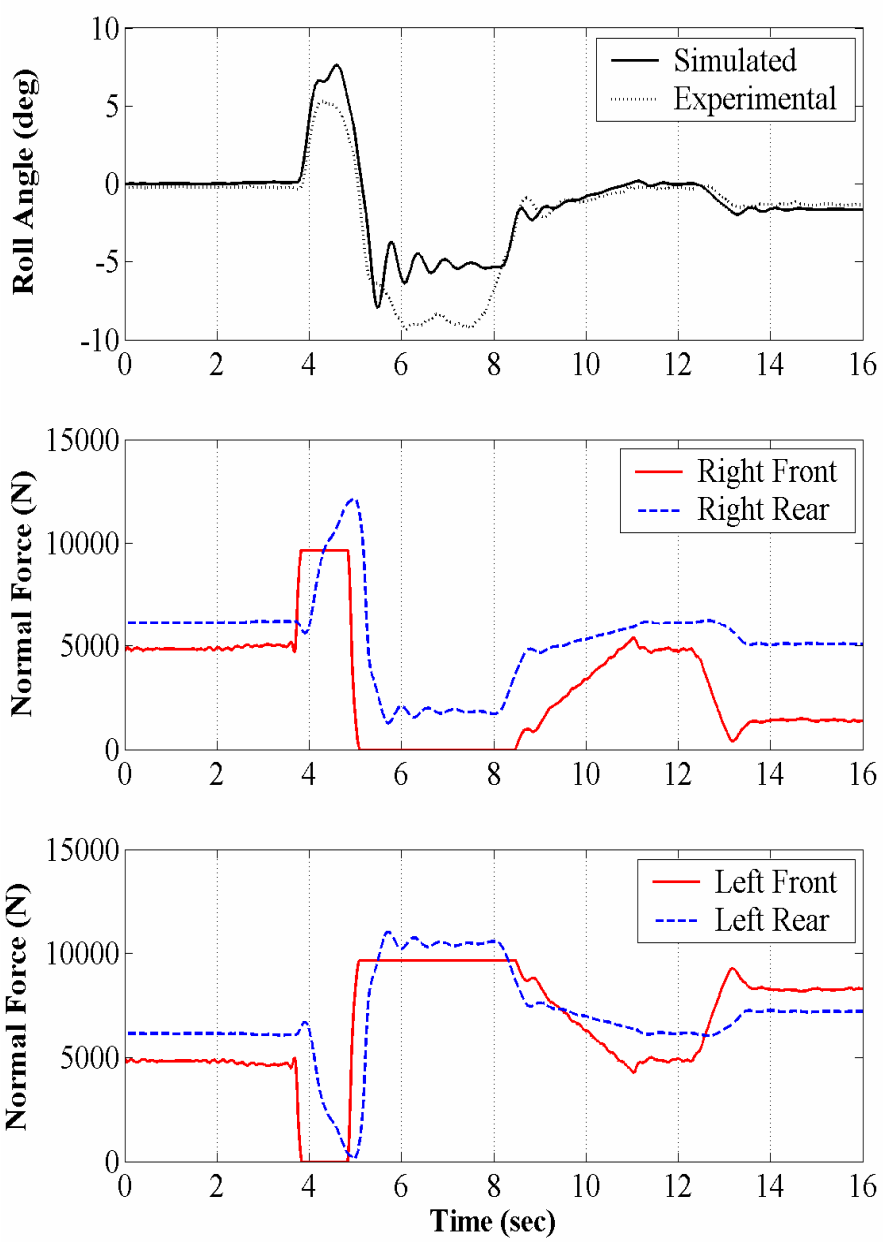

Figure 3.15. RMB Configuration Blazer Wheel Loads for a Fishhook 1b Maneuver

3.4 Auburn University GAVLAB Blazer

The GPS and Vehicle Dynamics Lab in the Department of Mechanical Engineering at Auburn has performed maneuvers with an instrumented Chevrolet Blazer. These tests were conducted at Auburn's NCAT facility, shown in Figure 3.16.

Figure 3.16. Auburn University NCAT Test Track Facility

The experimental data was again compared with simulation results using the Nominal configuration of the Blazer. In these tests, the velocity and steer angle were recorded and used as inputs in the simulation. The test track limits maneuvers to either single or double lane-change maneuvers. Figure 3.17 shows a comparison of the Auburn experimental data with results from the simulation model during lane-change maneuvers.

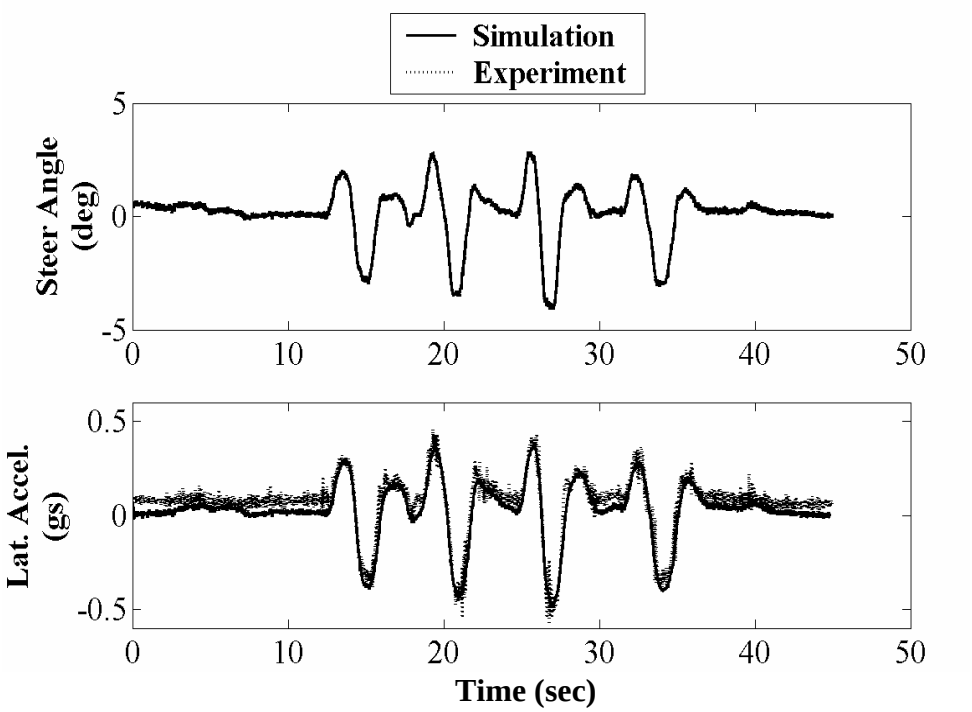

Figure 3.17. Lane Change Maneuver Data for the GAVLAB Blazer

Though the yaw dynamics of the experiment and simulation data closely match each other, differences between the simulation and experiment roll angles can be clearly seen in Figure 3.18. This is caused by a change in the bank angle of 4 degrees during the lane change maneuver, commonly known as the road crown (which aids in water drainage).

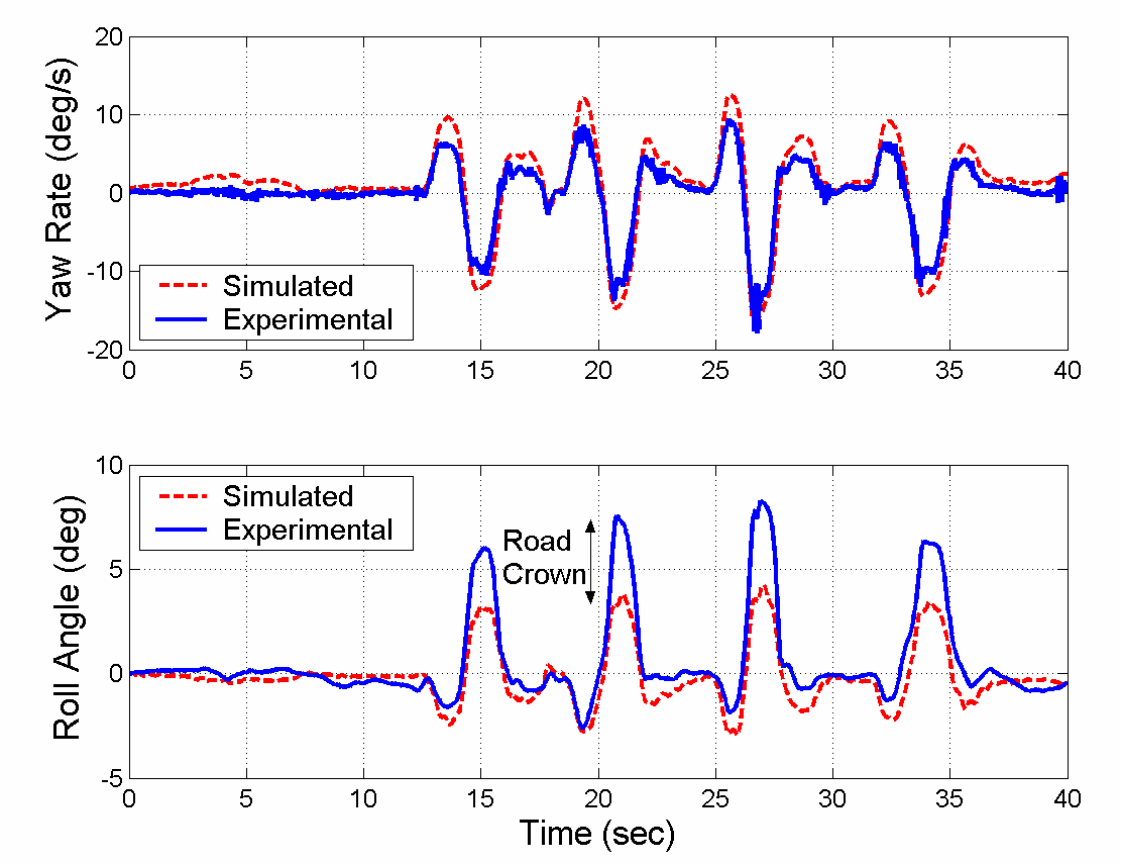

Figure 3.18. Lane Change Maneuver Yaw and Roll Angle Data for the GAVLAB Blazer

The parameters used in this simulation are the ones used for the Nominal Blazer which were tuned with the NHTSA experimental data for the J-Turn maneuver. The similarity of the dynamic behavior in the simulation and the various experiments provide much confidence in the vehicle model.

3.5 Lateral Weight Transfer Simulation

In the some of the simulation maneuvers, the vehicle exhibits an initial counter weight transfer, analogous to a non-minimum phase system. In other words, during a maneuver, the weight transfer is initially in opposite direction of steady state weight transfer as seen in Figure 3.5. The steady state values for the dynamic states reveal that the outside wheel loads are higher than the inside wheel loads, as seen in Figure 3.4. However, at the beginning of a step maneuver, the front inside wheel load increases and the front outside decreases, as seen in Figure 3.5. Closer analysis shows that during the first 0.1685 seconds of the maneuver the weight transfer on the front axle is negative. This increases the inside wheel load. For the normal force on the inside wheel to increase during a turn is counter intuitive. In steady state, the normal force on an axle's inside wheel decreases and the normal force on the outside wheel of the same axle increases as expected.

In order to understand this phenomenon, the weight transfer equation must be further examined. The weight transfer equation for the front axle and rear axle are the same. However, vehicle parameters for the front and rear axles are different. The equation of the front weight transfer from Chapter 2 is shown again here as Equation (3.4).

$$dF_{zf} = \frac{2}{trk_f} \cdot \left[M_{arbf} + S_{kf} \cdot F_{kf} + S_{bf} \cdot F_{bf} + R_{yf} \cdot \left(h_{rcf} - h_{cgm} \right) + F_{yf} \cdot h_{cgm} \right] \cdot [N] \qquad 3.4$$

During the initial 0.1685 seconds of the step maneuver, the roll angle and velocity are positive and therefore the moments from the anti-roll bar (M_{arbf}), springs ($S_{kf} \cdot F_{kf}$) and dampers ($S_{bf} \cdot F_{bf}$) are all positive. By investigating the un-sprung mass free body diagram in Figure 3.19, it is seen that the tire lateral forces are also positive for this left steer, step steer maneuver.

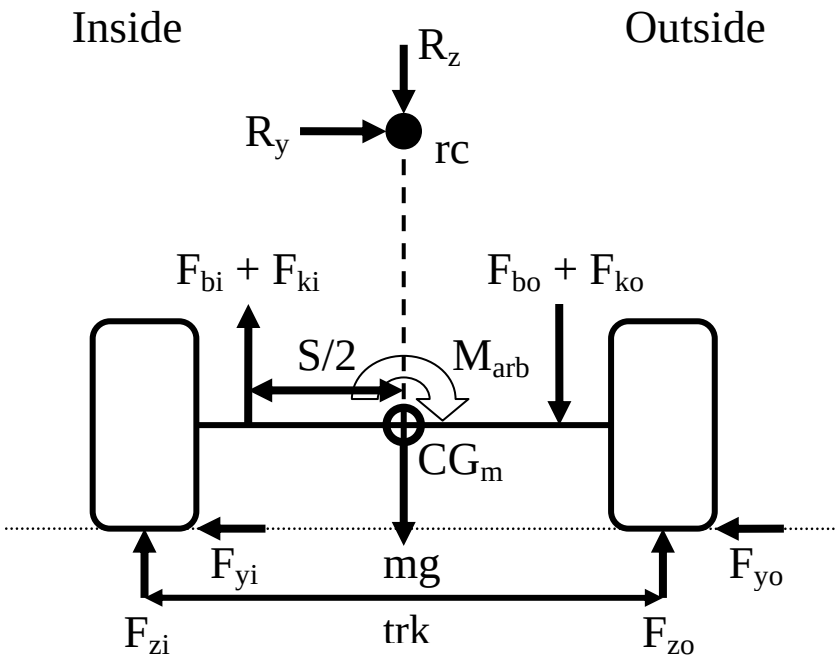

Figure 3.19. Roll FBD Un-Sprung Mass

The only variable remaining in the weight transfer equation that could be negative and cause dF_{zf} to be negative is the term $R_{yf} \cdot \left(h_{rcf} - h_{cgm}\right)$. For the step maneuver, the lateral reaction force is always positive. Therefore, the variables causing the initial counter weight transfer are the un-sprung mass CG height and the roll center height. When the roll center height is below the un-sprung mass CG height, the moment arm becomes negative and is multiplied by a positive lateral reaction force, thus causing the

dF_{zf} to be negative at the beginning of this maneuver. On the Blazer vehicle model, the front roll center height is below the un-sprung mass CG height and the rear un-sprung mass height is equal to the un-sprung mass height. Because the rear weight transfer is never negative, note that the inside rear wheel load is never greater than the outside rear in Figure 3.5. This is due to the fact that the un-sprung mass CG height and the roll center height are the same; the moment arm of the $R_{yf} \cdot \left(h_{rcf} - h_{cgm}\right)$ term is zero. To clarify which variable or variables is causing the weight transfer to be negative, three terms of the front lateral weight transfer are analyzed separately. These terms include the total front weight transfer, the front weight transfer without the $\frac{2}{trk_f} \cdot R_{yf} \cdot \left(h_{rcf} - h_{cgm}\right)$ term, and the $\frac{2}{trk_f} \cdot R_{yf} \cdot \left(h_{rcf} - h_{cgm}\right)$ term. Figure 3.16 shows these terms during a step maneuver.

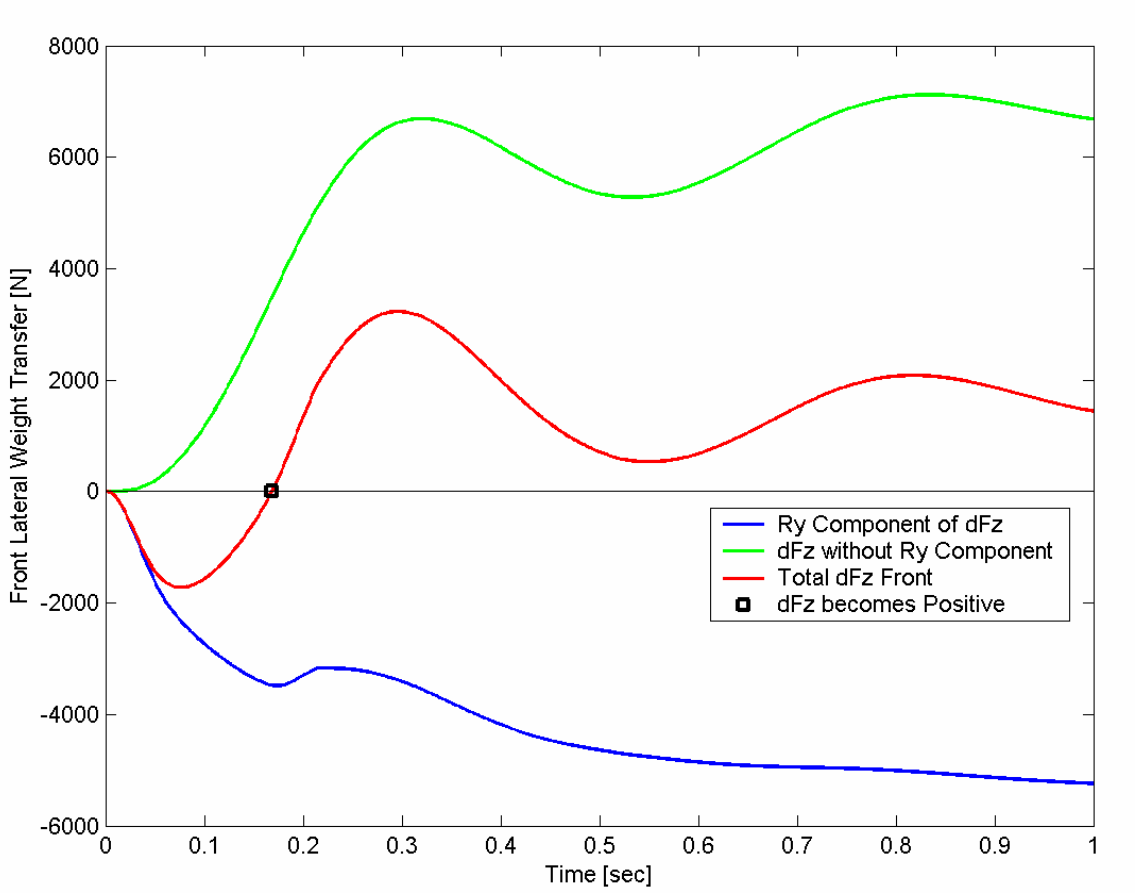

Figure 3.20. Maneuver B, Transient Roll, Front Lateral Weight Transfer

It can see in Figure 3.20 that the dF_{zf} is negative before time 0.1685 seconds. This is because the R_{yf} component is greater than the other terms of Equation (3.4). This narrows the possible vehicle properties that cause the counter weight transfer down to two: the roll center height and the un-sprung mass CG height.

To further explore the counter weight transfer on the front axle, a simulation of a step steer input is performed with both front and rear roll center heights equal to the un-sprung mass CG height. The response is shown in Figure 3.21.

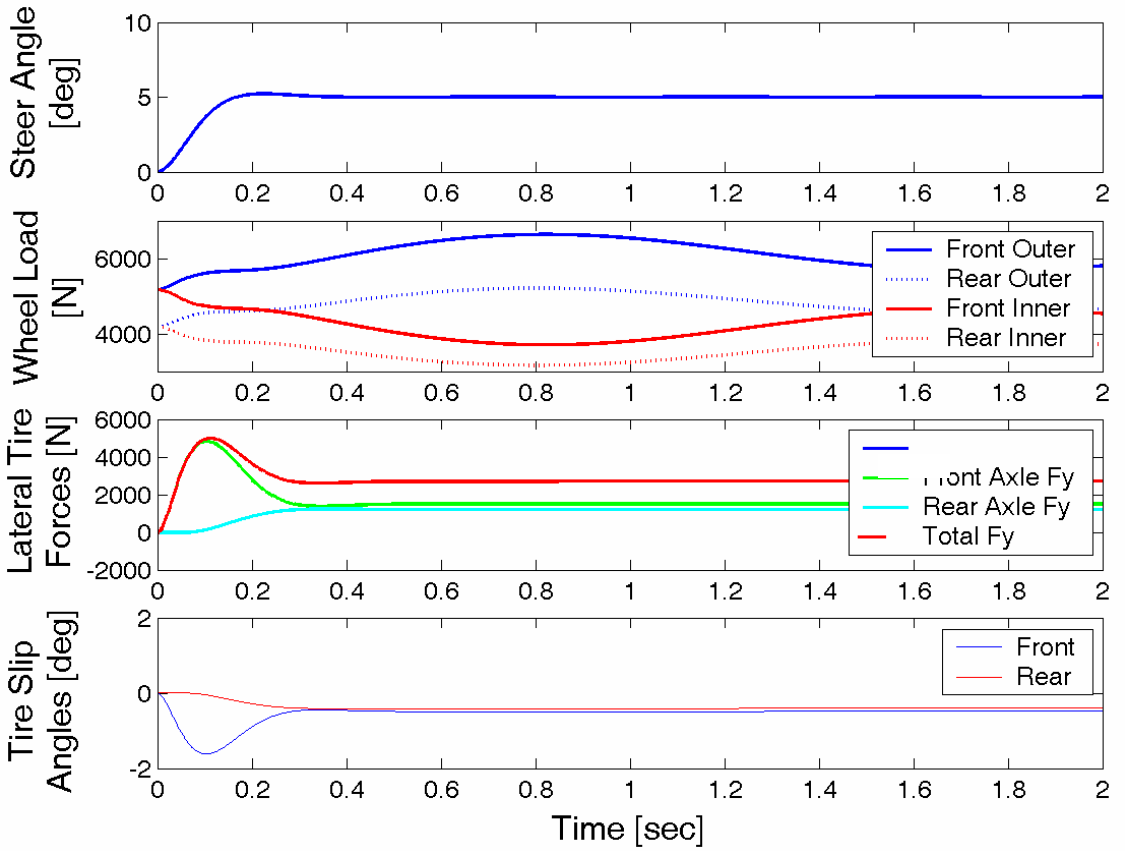

Figure 3.21. Step Maneuver with Roll Center Height equal to Un-Sprung Mass CG Height

It is shown that the counter weight transfer does not exist when the roll center height is equal to the un-sprung mass CG height. Also note the convention of the negative tire slip angles producing positive lateral tire forces. The conclusion is that a roll center height below the un-sprung mass CG height creates an initial counter weight transfer.

3.6 Summary and Conclusion

In this chapter, the accuracy and validity of the transient roll model has been demonstrated. The transient roll model was shown to produce the same steady state results as the steady state roll model. Experimental vehicle data acquired from NHTSA's Phase IV rollover research was used to determine unknown vehicle properties. Additional data from the Phase IV testing was then used to validate that the transient roll model matches the transient dynamics of the experimental data. It has also been shown that the vehicle model accurately captures the dynamics of the vehicle when properties are changed, as shown by the RRR and RMB Blazer configurations. Experimental data produced by the Auburn University GAVLAB was used to provide further validation that the vehicle model matches experimental data for a lane change maneuver. An initial counter weight transfer was seen in the wheel load data during the simulation maneuvers. This phenomenon was examined and ultimately produced more confidence in the simulation's accuracy. This wide range of validation of the model developed in Chapter 2 allows for confidence in the vehicle dynamics analysis in the following chapters.

CHAPTER 4

ANALYSIS OF VEHICLE ROLLOVER STABILITY LIMIT

4.1 Introduction

This chapter investigates the effect of various vehicle parameters on rollover propensity using computer simulation. The vehicle model used in the simulation was developed in Chapter 2. The computer simulation's accuracy was verified in Chapter 3 by comparing the simulation data to experimental data from NHTSA's Phase IV testing on rollover of passenger vehicles. In this chapter, the vehicle model is subjected to a specific steering input defined by NHTSA, called the Fishhook 1a. An analysis of the vehicle loading condition and its influence on rollover propensity is conducted using the validated vehicle simulation.

4.2 NHTSA Phase IV Analysis

As discussed previously, NHTSA performed the Phase IV of TREAD rollover analysis in 2002. Chapter 3 showed data for a 2001 Blazer in various configurations that were tested, and this data was used to validate the vehicle simulation. In the NHTSA tests, the vehicle's loading condition was changed to three specific locations. The Nominal, Reduced Rollover Resistance (RRR), and Rear Mounted Ballast (RMB) configurations represent these loading condition changes, which are shown in Table 4.1.

Table 4.1. NHTSA Phase IV Vehicle Load Configurations [Forkenbrock, 2002]

	Nominal	RRR	RMB
CG Height [inches]	26.3	27.6	26.1
Weight Split Front : Rear	55:45	55:45	44:56

NHTSA performed a Fishhook 1b maneuver with the Blazer in each of these configurations. To determine vehicle rollover, the Blazer was equipped with outriggers to allow the vehicle to lift both wheels of one side of the vehicle. Entrance speeds of the maneuver were increased until two-wheel-lift (TWL) was detected. TWL was defined as both wheels on one side of the vehicle being two inches off the ground. Table 4.2 contains the NHTSA Phase IV data which shows the Blazer lowest entrance speed at which TWL was detected.

Table 4.2. Blazer TWL Velocity in Fishhook 1b Maneuver [Forkenbrock, 2002]

	Nominal	RRR	RMB
TWL Velocity [mph]	40.1	36.2	34.9

The results of this experiment show that the Blazer's tendency to rollover increases as the CG height is increased. The RRR configuration has a CG height 1.3 inches higher than the Nominal configuration and experiences TWL at 36.2 mph while the Nominal configuration requires 3.9 mph more velocity before TWL is achieved. This follows intuition and the results of the SSF explained previously.

The RMB configuration, like the RRR, increases the Blazer's tendency to rollover. However, the CG height of the RMB is 0.2 inches lower than the Nominal CG height. The physical difference between these two configurations causing the TWL velocity variation is the weight split. The Nominal and RMB have approximately the same SSF, and weight splits of 55:45 and 44:56, respectively. NHTSA performed a Fishhook 1b maneuver on both of these configurations, and the Nominal configuration experienced TWL at 40.2 mph, while the RMB had TWL at 34.9 mph.

In order to better quantify the difference between the Nominal and RMB configurations, the vehicle model is used to simulate and duplicate NHTSA's Phase IV data for the Blazer. The vehicle's weight split and CG height are varied to assess their affect on rollover propensity. The front to rear weight split is varied from 30:70 to 70:30, while holding the SSF constant. The Nominal configuration of the Blazer is also modified so that the roll center, suspension stiffness and damping are the same on the front and rear. With these changes to the suspension, the effects of changing the weight split are isolated from other factors. The parameters varied in this simulation test are the lengths 'a' and 'b', while their sum, the wheelbase, is held constant. The Slowly Increasing Steer (SIS) maneuver and constant are used and adopted from the NHTSA Fishhook 1a test. The change in weight distribution caused the SIS constant to also

change for each different weight split. For each parametric variation of the vehicle load condition, a new SIS constant is determined as described in Chapter 3. The SIS constant varied from 0.675 to 1.827 degrees at the tire for the splits of 30:70 to 70:30 respectively as shown in Figure 4.1.

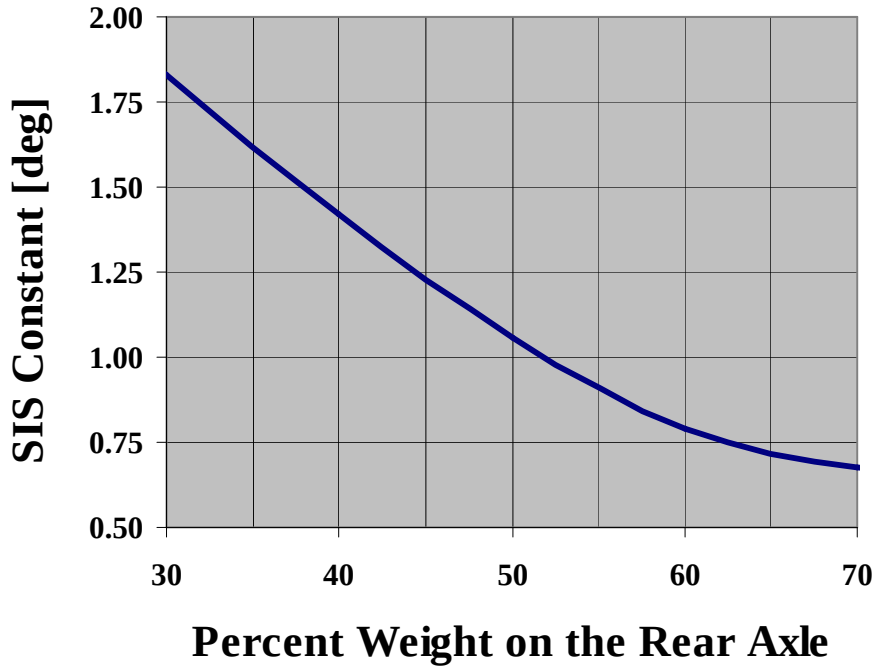

Figure 4.1. SIS Constant Change for Weight Split Variation

The dynamic test used to determine the effects of these property changes is the Fishhook 1a maneuver. The Fishhook 1a is a highly repeatable maneuver as cited by NHTSA's Phase IV research and is an easily programmed open loop input (unlike its the Fishhook 1b, which requires roll velocity data in a closed loop feedback control) [Forkenbrock, 2003].

As in the NHTSA study, rollover velocity is calculated by determining the vehicle speed at which the steering maneuver causes TWL. As previously described, NHTSA determines TWL as both wheels on one side of the vehicle being lifted 2 inches off the

ground. However, TWL for the simulation is defined as the instant that the normal forces on both tires on one side of the vehicle go to zero. This definition is due to the fact that the simulation is not able to measure the height of each wheel after wheel lift since the un-sprung mass dynamics are not modeled. The simulation is still accurate until the point where wheel lift occurs. The difference in the definition of TWL between the simulation and experiment results in a discrepancy in the velocity that TWL occurs. Since the simulation rollover is defined as the instant that TWL occurs and not after both wheels have lifted 2 inches, the rollover velocity for the simulation is lower than the NHTSA experiment data. Figure 4.2 shows the simulation of TWL velocity across a range of vehicle weight splits. NHTSA's Nominal and RMB configurations for the Blazer are also shown in Figure 4.2.

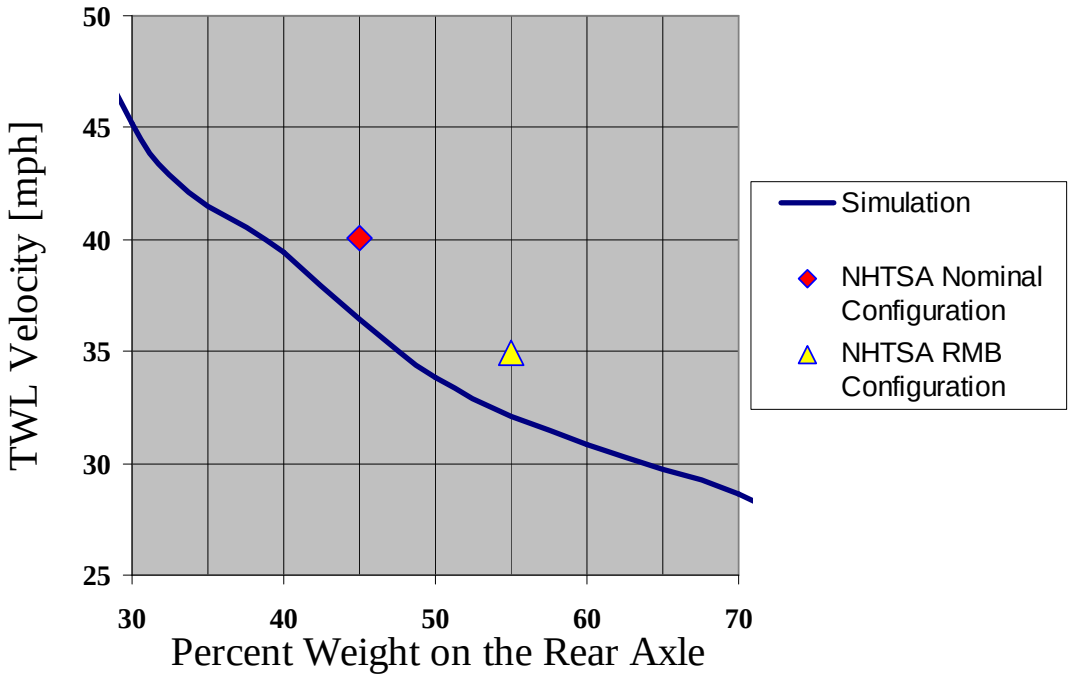

Figure 4.2. TWL Velocity for Weight Split Variation

Figure 4.3 shows the corresponding understeer curve. Inspection of Figures 4.2 and 4.3 reveals a correlation between understeer and rollover propensity. As the Blazer's weight is shifted toward the rear, the vehicle begins to oversteer as well as roll at a lower velocity than when the weight is shifted toward the front axle. Also note that as the weight is shifted toward the front axle, the corresponding SIS increases causing the Fishhook 1a to become a more severe maneuver. However, the TWL velocity continues to increase as the weight is moved to the front axle. NHTSA's Phase IV experiments reveal this same correlation between weight split and rollover propensity, as seen in Figure 4.2.

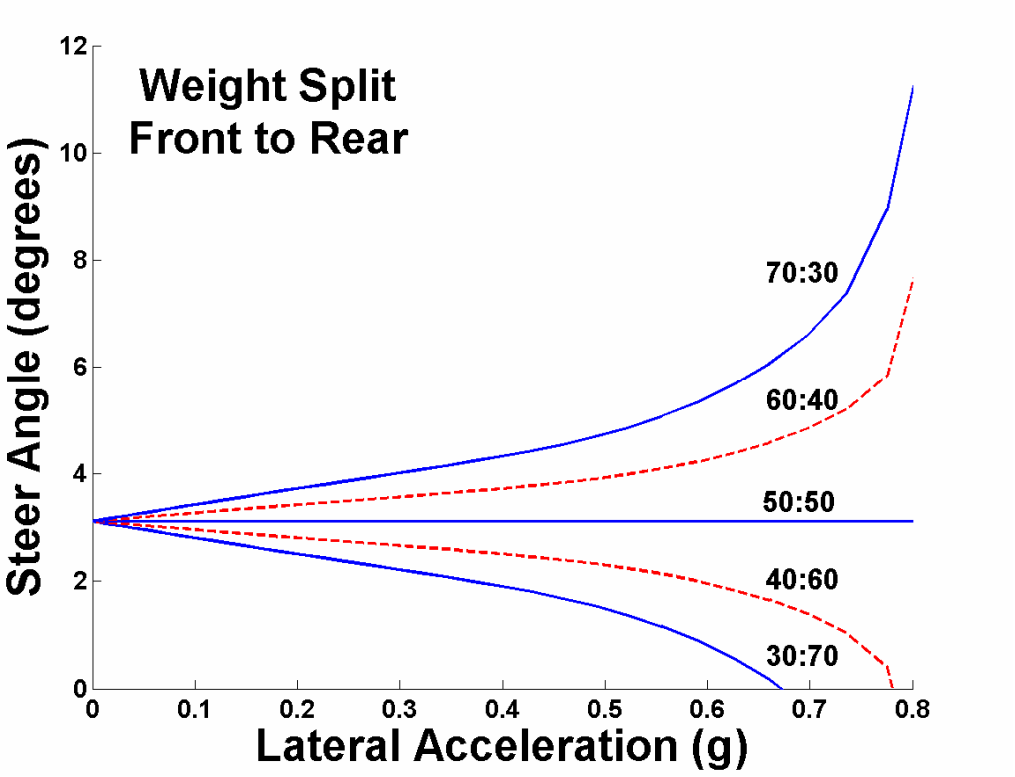

Figure 4.3. Vehicle Understeer Gradient for a Variation of Weight Splits

Another interesting observation from the simulation data was seen for two vehicle configurations with a SSF equal to 1.048. One vehicle configuration experiences TWL at

28.6 mph and the other experiences TWL at 45.2 mph. These speeds were recorded for various weight distributions of 30:70 through 70:30 front to rear, respectively. Although the SSF is considered the most important measurement of a vehicle's rollover propensity, two vehicles with the same SSF may experience a difference in rollover velocity for the same maneuver. This clearly demonstrates that there are other vehicle parameters that play an important role with regard to rollover propensity besides center of gravity height and track width (SSF parameters).

The simulation was also configured to vary the CG height on the Blazer to assess its effect on rollover propensity. The Blazer configuration used was the Nominal case, and the only parameter varied was the CG height. This results in a constant SIS of 1.268 degrees measured at the tire. Figure 4.4 shows the corresponding Blazer simulation results. Also shown in the Figure are the Nominal and RRR TWL velocities.

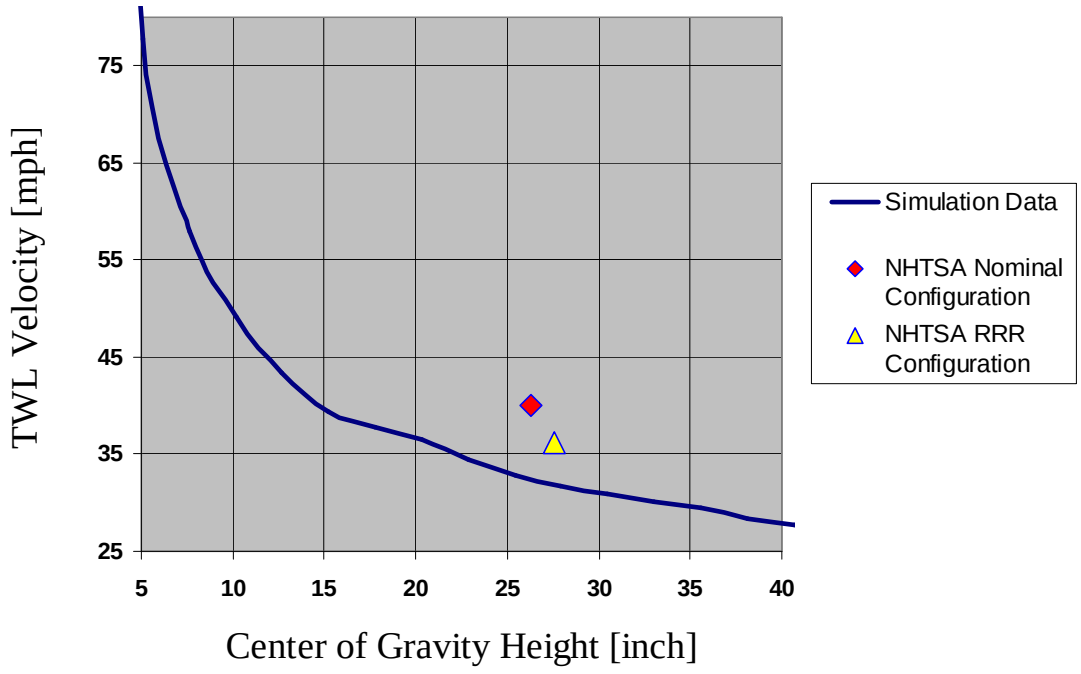

Figure 4.4. TWL Velocity for Various CG Heights

With the track width is held constant, the SSF varies from 3.467 to 0.2774 with change in CG height. The Nominal configuration has a SSF of 1.048, which corresponds to a CG height of 16.76 inches. The TWL velocity for the Nominal configuration as determined by the simulation is 38.8 mph. NHTSA documented TWL for the same configuration and maneuver as being 40.2 mph. Again, the difference in the TWL velocities is caused by the different definition of TWL between the simulation and experiment. The observed trend of the data is not surprising since it is well known that a vehicle will roll at a lower velocity if the CG is raised or the SSF is decreased.

4.3 Stability Limit Development

From Section 4.2, it can be seen that a vehicle's rollover threshold varies not only with CG height, but also the CG longitudinal location, otherwise known as the vehicle's weight split. In this section, vehicle states other than rollover velocity are measured to further develop an understanding of how the vehicle's dynamic states at rollover vary with the vehicle's load condition.

Vehicle simulations are again used to determine the stability threshold for different vehicle load conditions. This is done by independently varying the vehicle's center of gravity height and weight split. The maximum value of the each of the following states is recorded when rollover is detected: maneuver entrance velocity, lateral acceleration, yaw rate, roll angle, roll rate, side slip angle, and side slip rate. For the general Fishhook maneuver, rollover is consistently measured slightly after the maximum

counter steer. The Fishhook maneuver used is different than the NHTSA Fishhook 1a because the maneuver's steer angle magnitude is independent of the SIS constant described in Chapter 3. Therefore, the maneuver is unchanged for variations of vehicle properties, thus allowing for a more concise comparison between the property variations.

For these simulations, a Fishhook steering profile was chosen with a maximum steer angle of 5 degrees and a maximum steering rate of 40 deg/s, both measured at the tires. This profile was filtered by a second order 0.75 Hz Butterworth filter to remove the abrupt changes in the simulation's steer angle.

The first property varied was the CG height. The Nominal Blazer configuration was used as the baseline. The CG height was varied between 65 and 160 percent of the baseline CG height. The rollover velocity, lateral acceleration and yaw rate are shown in Figure 4.5. As shown in the previous section, the vehicle will roll at lower velocities as the CG height is raised. Also, note that as the CG height is raised, the lateral acceleration and yaw rate that the vehicle can achieve before experiencing a rollover event is decreased. These results confirm those of the SSF, which states that the vehicle is more prone to rollover as the CG height is increased.

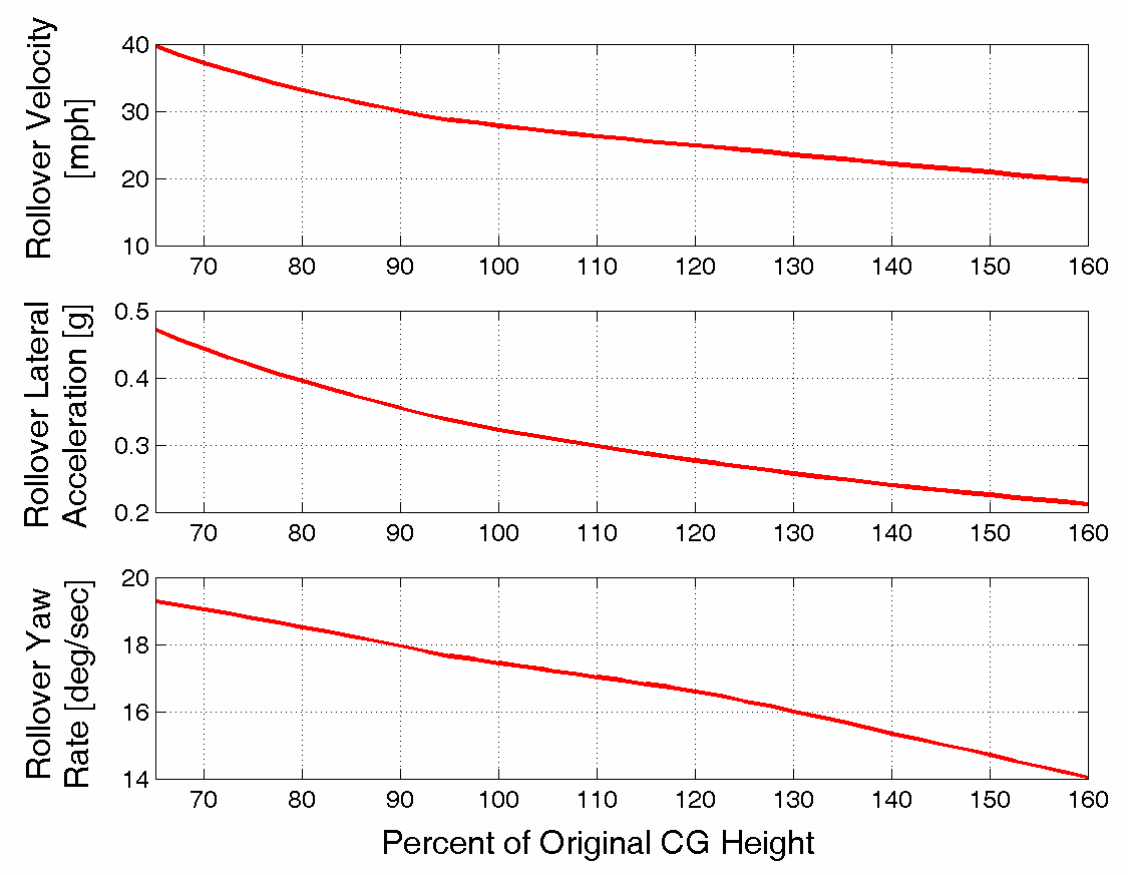

Figure 4.5. Velocity and Yaw Dynamics at Rollover for CG Height Variation

The roll angle and roll rate along with the side slip angle and the side slip rate are important states when determining rollover [Hac, 2004]. Currently, Ford utilizes the roll rate dynamic state in its electronic stability control system for SUVs, and much research is ongoing to use the side slip rate state in vehicle stability control systems. The following states at rollover are shown in Figure 4.6: roll angle, roll rate, side slip, and side slip rate.

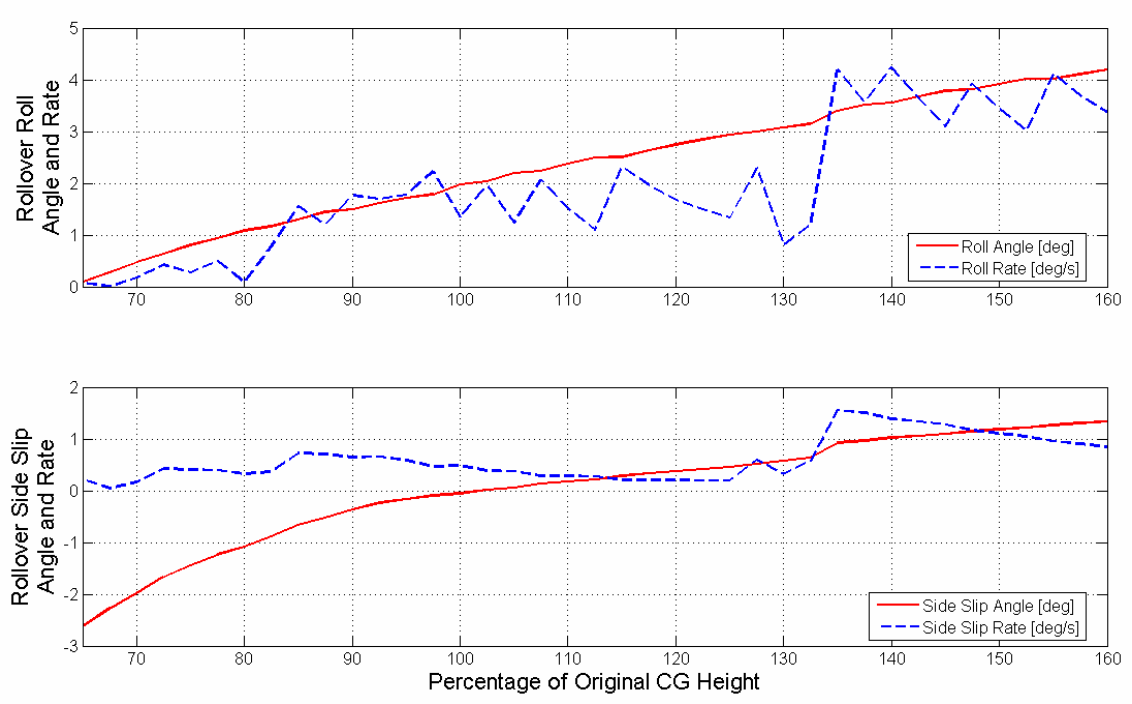

Figure 4.6. Roll and Side Slip States at Rollover for CG Height Variation

As the CG height is increased, the roll angle and roll rate at rollover increase. This increase in roll angle and roll rate is caused by the increase in the vertical distance (d_1) between the roll center axis and the CG height as the CG height is raised. The angle of roll per lateral acceleration is known as the Roll Rate property (not to be confused with the roll rate [deg/s] state), as seen in Equation (4.1) [Gillespie, 1992] and Figure 4.7 shows the change in Roll Rate as the CG height is varied.

$$\text{Roll Rate} = \frac{-M \cdot g \cdot d_1}{-k_{\phi_t} + M \cdot g \cdot d_1} \cdot \frac{180}{\pi} \cdot \left[\frac{\text{deg}}{g}\right] \tag{4.1}$$

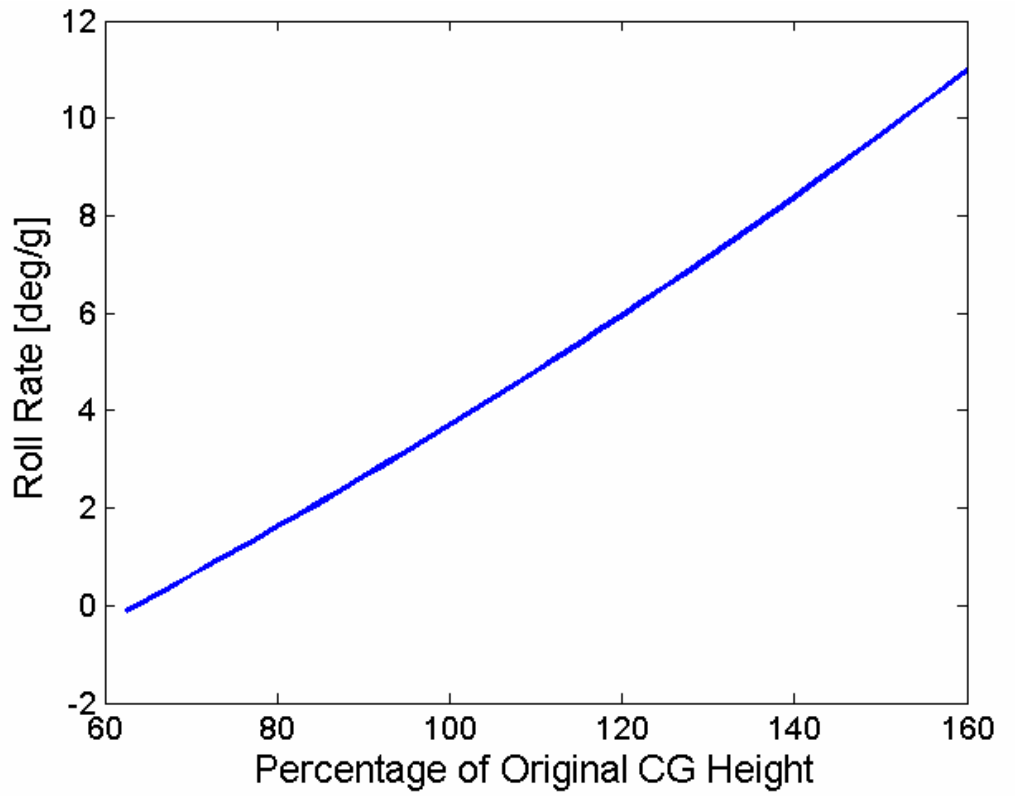

Figure 4.7. Roll Rate for CG Height Variation

The lateral force on the front and rear axles for the CG height variation is shown in Figure 4.8. It can be seen that as the CG height increases, the lateral force at vehicle rollover is decreased.

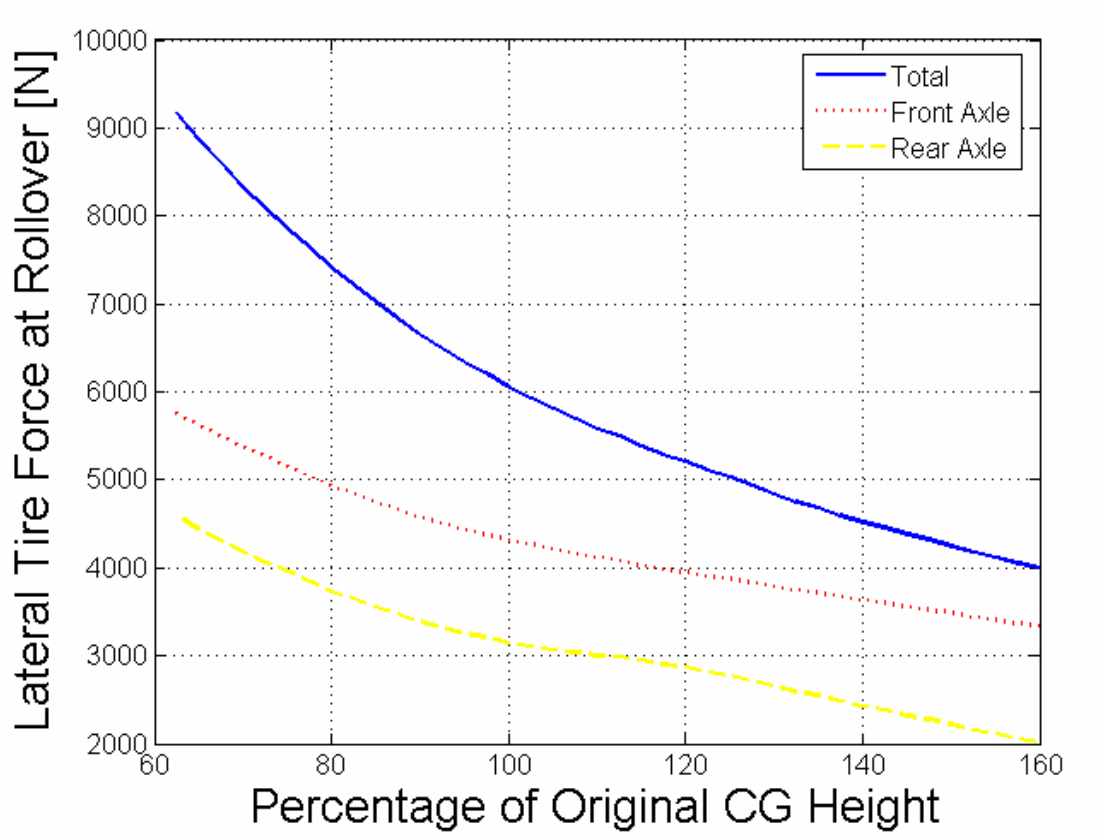

Figure 4.8. Lateral Tire Force at Rollover for CG Height Variation

The second property which was varied on the Nominal Blazer is the vehicle's weight split. The vehicle weight split was varied from a weight ratio of 70:30 (front axle to rear axle) to a ratio of 30:70. The same maneuver and vehicle from the CG height variation simulation were used. Figure 4.9 shows the velocity, lateral acceleration, and yaw rate at rollover for the weight split variation simulations.

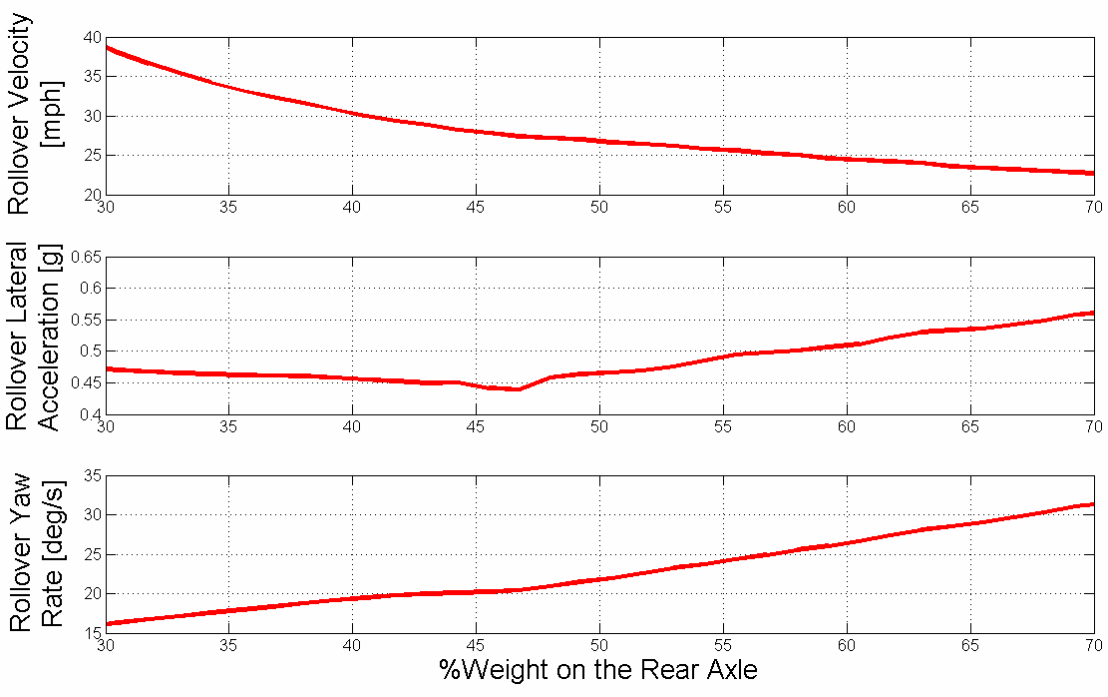

Figure 4.9. Velocity and Yaw Dynamics at Rollover for Weight Split Variation

As noted in Section 4.2, the maximum speed the Blazer can safely negotiate the Fishhook maneuver without rollover decreases as the weight is shifted towards the rear axle. However, the yaw rate at which the vehicle rolls increases as the weight is moved toward the rear axle [Gillespie, 1992]. This is explained by the change in the vehicle's weight transfer causing limit oversteer as the weight split is shifted rearward. As weight is shifted toward the rear axle, the weight transfer on the rear axle increases and saturates the rear tires faster than the front tires and this causes limit oversteer [Milliken, 1995]. If the vehicle's velocity is increased, the limit oversteer will cause the yaw rate to approach infinity. The vehicle's understeer gradient is also decreased as the weight is shifted to the rear as shown previously in Figure 4.3. For the same steering input and velocity, a vehicle with a lower understeer gradient will have a greater yaw rate than one with a higher understeer gradient [Gillespie, 1992].

The maximum lateral acceleration that Blazer can achieve before rollover also increases as the weight split is moved rearward. The lateral acceleration at rollover as the weight is shifted to the rear mimics the yaw rate at rollover. Although Equation (4.2) is only true at steady state, it does explain why the lateral acceleration at rollover trend follows the yaw rate at rollover trend.

$$a_y = V \cdot r^2 \tag{4.2}$$

Figure 4.10 shows the maximum roll angle, roll rate, side slip angle, and side slip rate achieved at rollover. The rollover roll angle remains nearly constant as weight split is varied. However, the rollover roll angle rate decreases as the vehicle's weight is shifted to the rear axle. The side slip rate varies from 0 to 0.5 deg/s at rollover yet the side slip angle decreases at the weight split is shifted toward the rear.

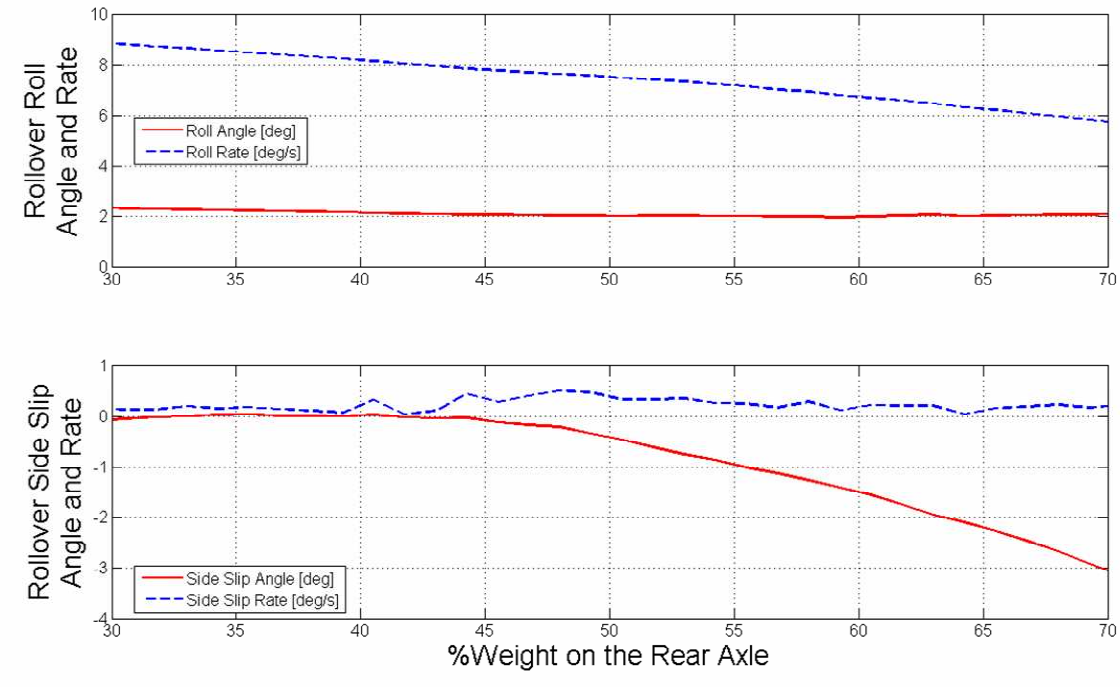

Figure 4.10. Roll and Side Slip Thresholds for Weight Split Variation

4.4 Tire Property Variation

As noted in Chapter 2, the non-linear, 'Magic Formula' tire model can be easily modified. In this section, the tire's cornering stiffness and peak lateral force are varied to see how they affect rollover propensity. Again, a Fishhook maneuver of 5 degrees is used to study this effect.

To examine how peak lateral tire force influences rollover, three different tires were used. The three different tires are modeled in Figure 4.11 with the tire normal force set at 5 kN. As seen in Figure 4.11, the cornering stiffness is held constant at 2400 N/deg for each tire, but each tire has a different peak lateral force.

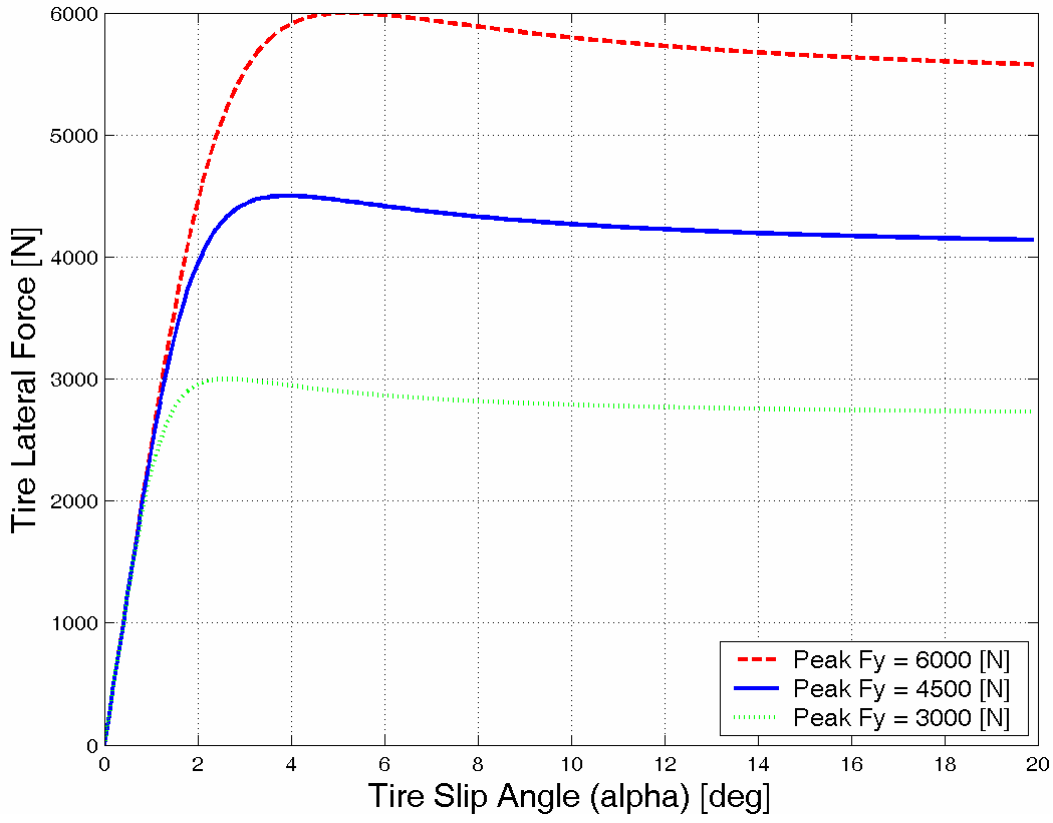

Figure 4.11. Tire Curves for Variation of Peak Lateral Tire Force (F_z =5 kN)

The limits of each state at rollover for the three different tires models during the Fishhook maneuver are given in Table 4.3. It can be seen that the tire with the lower peak lateral tire force has a higher rollover velocity for this maneuver. Additionally, the tire with the lowest peak lateral force requires a higher velocity to produce the required lateral force for rollover on each axle than the other tires.

Table 4.3. Peak Lateral Tire Force Variation Results

	Peak Lateral Forces		
Dynamic States at Rollover	6000 [N]	4500 [N]	3000 [N]
Velocity [mph]	26.0	26.0	26.5
Yaw Rate [deg/s]	18.256	18.204	17.8839
Lateral Acceleration [g]	0.3512	0.3509	0.3463
Roll Angle [deg]	2.191	2.178	2.131
Roll Rate [deg/s]	16.268	16.104	15.026
Side Slip Angle [deg]	1.449	1.443	1.344
Side Slip Rate [deg/s]	6.485	6.356	5.907

The tire cornering stiffness was also varied to determine its effect on rollover propensity. Four different cornering stiffnesses are evaluated. The tire curve for each tire with a normal load of 5 kN is shown in Figure 4.12. The peak lateral tire force was held constant at 4500 N, as seen in Figure 4.12.

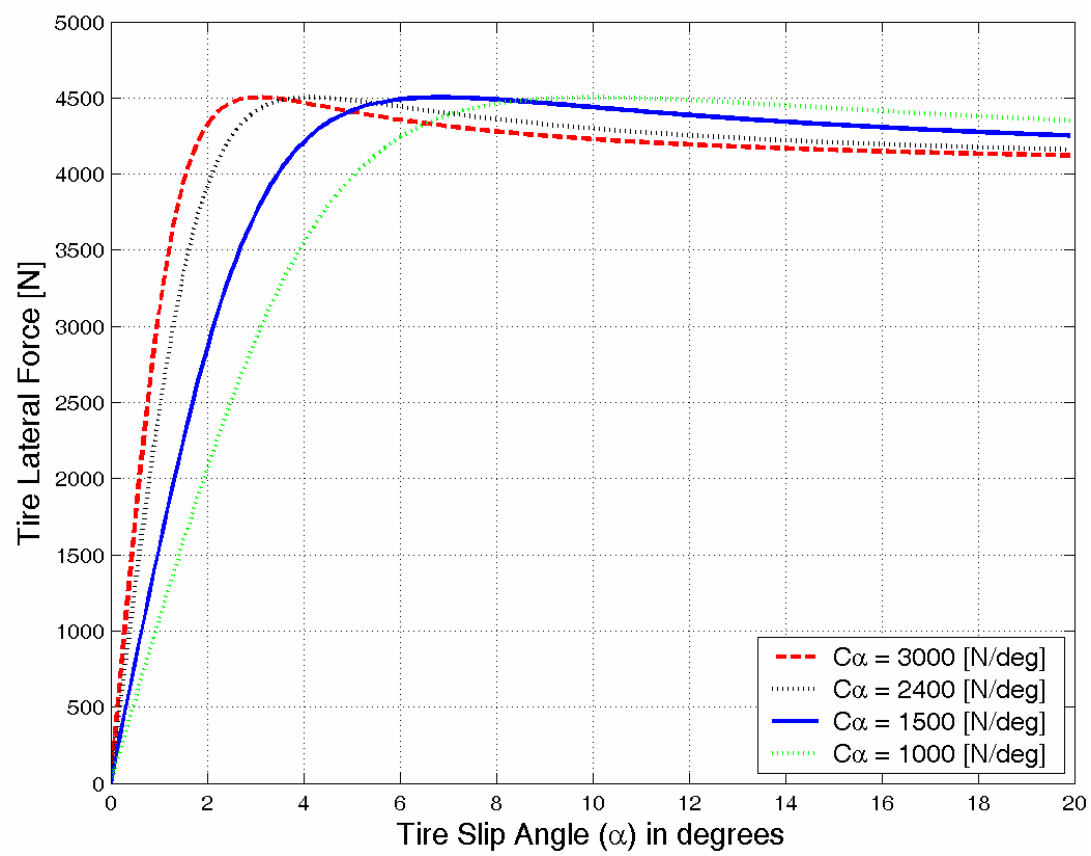

Figure 4.12. Tire Curves for Variation of Tire Cornering Stiffness (F_z =5 kN)

The limits of each state at rollover for the tire models with the tire cornering stiffness variation are seen in Table 4.4. The tire with the lowest cornering stiffness requires the highest velocity in the Fishhook maneuver to rollover. The rollover velocity is higher in the tire with the lowest cornering stiffness because a higher velocity is required to produce the same lateral force that the other tire models rollover.

Table 4.4. Tire Cornering Stiffness Variation Results

	Tire Cornering Stiffness [N/deg]			
Dynamic States at Rollover	3000	2400	1500	1000
Velocity [mph]	25.25	26.0	28.0	29.25
Yaw Rate [deg/s]	18.574	18.214	17.50	16.604
Lateral Acceleration [g]	0.3651	0.3511	0.3245	0.2934
Roll Angle [deg]	2.282	2.180	1.985	1.773
Roll Rate [deg/s]	18.801	16.154	11.523	8.1247
Side Slip Angle [deg]	1.710	1.444	0.9541	1.381
Side Slip Rate [deg/s]	7.214	6.369	4.769	5.472

4.5 Summary and Conclusion

In this chapter, simulation data along with NHTSA experimental data were used to evaluate how two vehicle properties, CG height and weight split, affect a vehicle's rollover limit. The simulations were also used to explore how the cornering stiffness and peak lateral force of the tire affect a vehicle's rollover propensity. It was shown that the SSF is not the sole determinate of a vehicle's rollover propensity, and that there are vehicle properties other than SSF, such as weight distribution and tire properties, that can significantly influence rollover propensity. It was also shown that there is a correlation between the understeer gradient and rollover propensity. As the vehicle understeer increases, the TWL velocity tends to increase.

Finally, rollover stability limits were developed in this chapter. The stability threshold consisted of many vehicle dynamics states: velocity, lateral acceleration, yaw

rate, roll angle, roll angle rate, side slip angle, and side slip rate. Those were the states used to express the rollover stability limits. These stability limits will be used with an ESC in the following chapters.

CHAPTER 5

ELECTRONIC STABILITY CONTROL DEVELOPMENT

5.1 Introduction

As was stated in Chapter 1, vehicle rollover accidents have received much attention in the past decade. There is high demand for SUVs (vehicles with low SSFs) in the automobile market despite their high rollover propensity. The automotive engineering world's solution to making these vehicles safer is electronic stability control (ESC). As was shown in the previous chapters, the foundation of ESC begins with an understanding of how vehicle dynamics and vehicle properties affect rollover. These principles are used to develop the stability controller in this chapter.

The first generation ESCs implemented yaw control by limiting yaw rates with differential braking [Tseng, 1999]. These ESCs used yaw rate gyros, wheel speed sensors, and lateral accelerometers and the pre-existing anti-lock braking actuator. Although differential braking is still the most common actuator used in ESCs, others such as active suspensions and steer-by-wire, are being developed to enter the market [Vilaplana, 2004; Amberkar, 2004]. Although yaw control has been shown to reduce rollover, Ford utilizes an ESC that couples the yaw and roll dynamics for control and therefore equips their SUVs with a roll rate gyro [van Zanten, 2000].

In this chapter, a simple ESC is developed and implemented on a Blazer in simulation. It uses steer angle and braking to control the vehicle's stability and to track the driver's intended path.

5.2 Electronic Stability Control

The ESC developed and used in this thesis is a proportional and integral (PI) yaw controller. It uses the vehicle's brakes to control velocity and controls the steer angle of the front tires. Controller limits are given from the stability threshold derived in Chapter 4. The ESC takes these limits into account and adjusts the steer angle and velocity to keep the vehicle within the stability region.

In order to implement the P-I controller, the vehicle model must first be linearized. Placing the linearized equation of the bicycle model into the state space form is shown in Equation (5.1).

$$\begin{bmatrix} \dot{\beta} \\ \dot{r} \end{bmatrix} = \begin{bmatrix} \frac{-C_1}{MT \cdot V} & \frac{-C_2}{MT \cdot V^2} - 1 \\ \frac{-C_2}{I_z} & \frac{-C_3}{I_z \cdot V} \end{bmatrix} \cdot \begin{bmatrix} \beta \\ r \end{bmatrix} + \begin{bmatrix} \frac{C_{\alpha f}}{MT \cdot V} \\ \frac{a \cdot C_{\alpha f}}{I_z} \end{bmatrix} \cdot [\delta] \tag{5.1}$$

Equations (5.2 – 5.4) provide the definitions of the constants C_1, C_2, and C_3.

$$C_1 = C_{af} + C_{ar} \tag{5.2}$$

$$C_2 = a \cdot C_{af} - b \cdot C_{ar} \quad 5.3$$

$$C_3 = a^2 \cdot C_{af} + b^2 \cdot C_{ar} \quad 5.4$$

The tire cornering stiffnesses $C_{\alpha f}$ and $C_{\alpha r}$ represent the total axle cornering stiffness of the front and rear axles, respectively. The axle cornering stiffness is found by adding the cornering stiffness of each tire for that axle.

The yaw dynamics are controlled with a PI controller. The transfer function for the PI controller is given in Equation (5.5).

$$\frac{Output}{Input} = \frac{k_p \cdot s + k_i}{s} \quad 5.5$$

Where:

k_p = Proportional Gain

k_i = Integral Gain

The controller gains were chosen by imputing the desired response frequency of 1 Hz and desired damping of 0.707 into the MATLAB ‘place’ command. The ‘place’ command sets the controller’s eigenvalues to achieve the desired output. The proportional gain was 1.0, and the integral gain was -0.5.

The Nominal Blazer configuration is simulated with and without the ESC activated. The Fishhook 1a steering profile is once again used. The maneuver velocity was set at 35 mph, yet the vehicle can only negotiate this maneuver with a maximum speed of 32 mph. The ESC response is shown in Figure 5.1. The ESC effectively keeps

the vehicle within the stability threshold. It is also seen that as the velocity is decreased, the steer angle is decreased in order to limit the driver the maximum yaw rate to the rollover limit yaw rate.

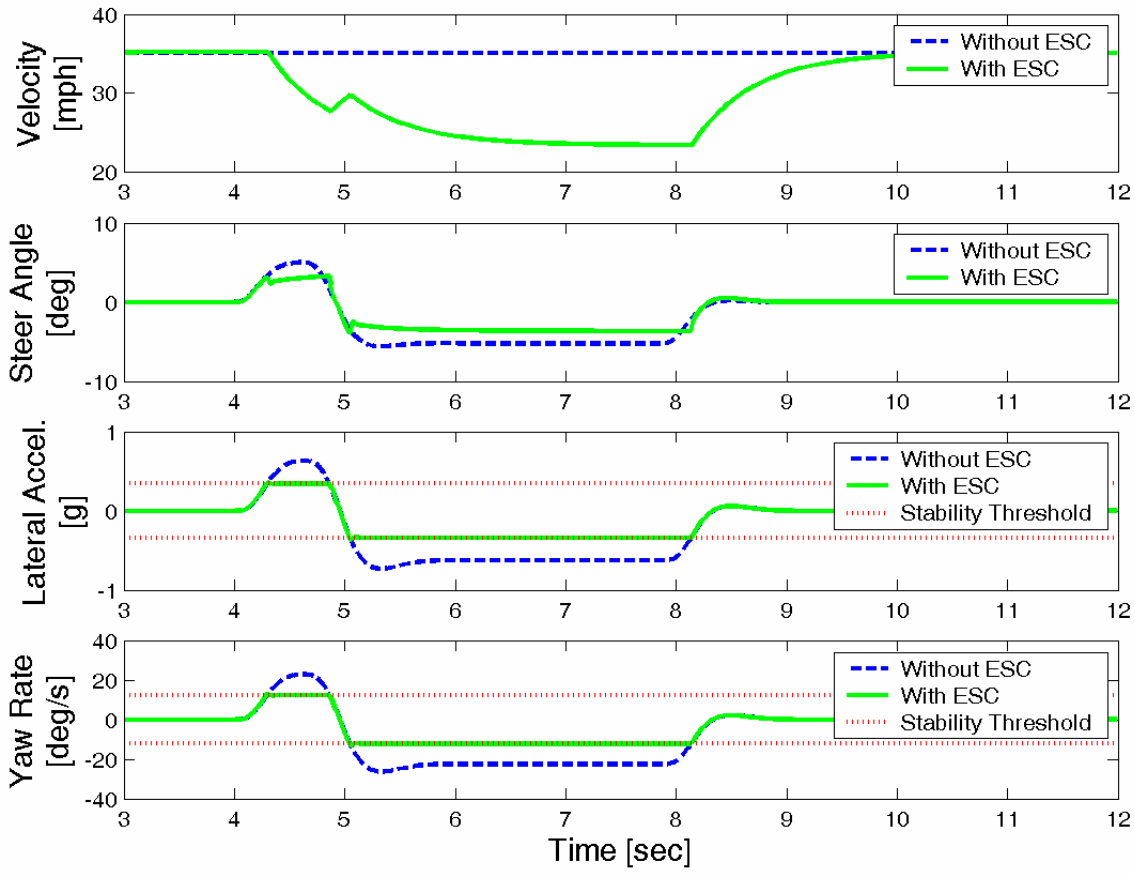

Figure 5.1. ESC Simulated on the Nominal Blazer Configuration

5.3 Intelligent Vehicle Model

Although statistics were shown in Chapter 1 that ESC's ability to prevent single vehicle rollover is high, there is room for improvement by using an intelligent vehicle model (IVM) that modifies the ESC's vehicle model and controller limits. Vehicle payload variation is the most common vehicle property varied. The ESC with the IVM is different from a regular ESC where the vehicle model does not change, and only one stability limit is known. The purpose of the IVM is to update the ESC controller limits as the vehicle's load condition changes. The IVM utilizes the stability limit for a range of load conditions to know the vehicle's changing rollover limit. Although not developed in this thesis, sensors and estimation can be used to inform the IVM of weight split and CG height changes.

Simulations were conducted to determine how the IVM could serve to increase the effectiveness of ESC in reducing vehicle rollover. Simply adding a full load of passengers to the Blazer can change the CG height by as much as 10%. With this information, the Nominal Blazer was simulated driving through a Fishhook maneuver with a maximum steer angle of 5 degrees at 24 mph. The Nominal Blazer can navigate this maneuver without crossing the stability threshold. However, the Blazer with the driver and four passengers has a CG height 10% higher than the Nominal configuration. This raises the CG height from 0.663 to 0.73 meters. The Blazer with the passengers can only negotiate the Fishhook maneuver at 22 mph. In Figure 5.2, simulation results are seen of the Blazer with the passengers implemented with ESC. Two configurations are

shown, the Blazer with and without the IVM. The stability threshold for the Blazer with the passengers is also shown.

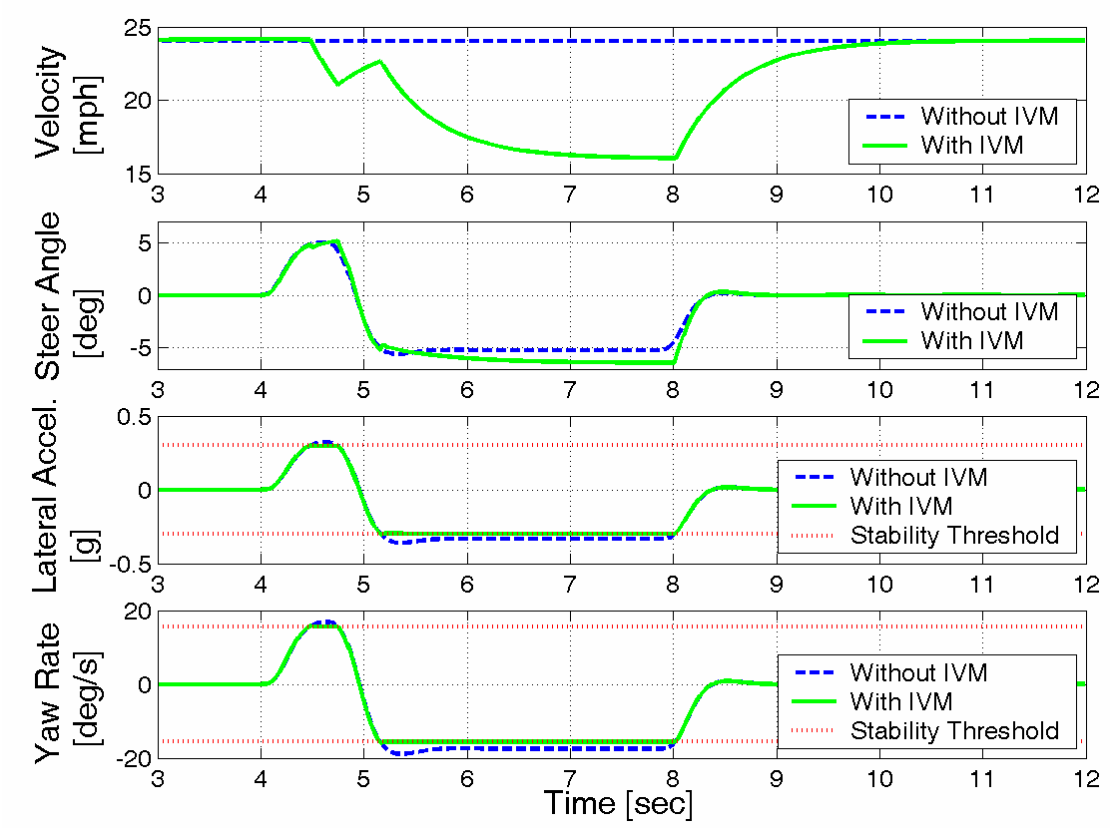

Figure 5.2. ESC with and without IVM for CG Height Variation

The Blazer with the IVM updates the stability threshold from the Nominal configuration of 0.33 g for lateral acceleration and 17.5 deg/s of yaw rate to the new configuration that has the CG height 10% higher. The stability threshold for the loaded condition is 0.295 g for lateral acceleration and 17.0 deg/s for yaw rate. It is seen in Figure 5.2 that without the IVM, the vehicle never activates its ESC because the nominal stability threshold is never breached. Therefore, the vehicle without IVM rolls as seen in Figure 5.3.

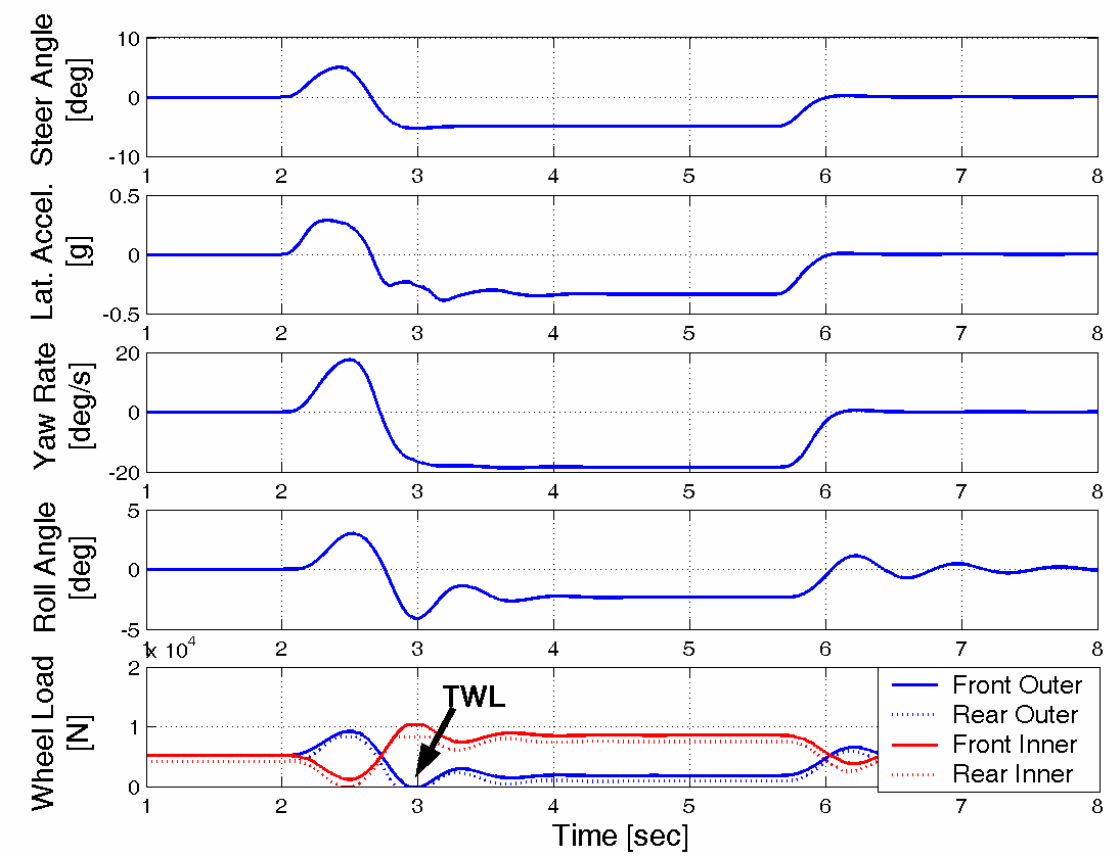

Figure 5.3. Effect on Dynamic Behavior due to CG Height Move without IVM

However, the vehicle with IVM updates the ESC limit for yaw rate and lateral acceleration which causes the ESC to activate. With the IVM, the vehicle never exceeds the stability threshold and does not roll over. Table 5.1 contains the stability thresholds for both vehicle configurations and the maximum yaw rate and lateral acceleration achieved during the maneuver.

Table 5.1. ESC with and without IVM for CG Height Change

	CG Height		
	0.663 [m]	0.73 [m]	0.73 [m]
IVM	No	No	Yes
ESC	Enabled	Enabled	Engaged
Rollover Incident	No	Yes	No
Maneuver Maximum Lateral Acceleration	0.32g	0.32g	0.295g
Maneuver Maximum Yaw Rate	17.3 deg/sec	17.3 deg/sec	17.0 deg/sec
Stability Threshold Lateral Acceleration	0.33g	0.295g	0.295g
Stability Threshold Yaw Rate	17.5 deg/sec	17.5 deg/sec	17.0 deg/sec

Utilizing the IVM during CG Height changes appears to have merit, yet there is difficulty in using the IVM during weight split variations. Table 5.2 shows the stability threshold for the Blazer at two different weight splits, 60:40 and 40:60.

Table 5.2. Blazer Stability Threshold for Two Weight Splits

	Weight Split Front:Rear	
Dynamic States at Rollover	60:40	40:60
Velocity [mph]	30.9 [mph]	24.4 [mph]
Yaw Rate [deg/s]	19.2 [deg/s]	26.1 [deg/s]
Lateral Acceleration [g]	0.46 [g]	0.51 [g]
Roll Angle [deg]	8.10 [deg]	6.84 [deg]
Roll Rate [deg/s]	1.4 [deg/s]	1.5 [deg/s]
Side Slip Angle [deg]	-0.05 [deg]	0.2 [deg]
Side Slip Rate [deg/s]	0.5 [deg/s]	0.3 [deg/s]

Assuming that an ESC is implemented for the 60:40 weight split, it will use a stability threshold of 19.2 deg/s for yaw rate and 0.46 g of lateral acceleration. The maximum velocity that the 60:40 weight split can safely navigate the Fishhook maneuver is 30.9 mph. After a change in weight split to 40:60, the maximum safe velocity that the vehicle can achieve is lowered to 24.4 mph. However, the maximum yaw rate is

increased to 26.1 deg/s and the maximum lateral acceleration is increased to 0.51 g. As was shown in Chapter 4, the vehicle's understeer gradient decreases as the weight split is shifted rearward. This causes the vehicle to oversteer more as the weight is shifted rearward. For a oversteer vehicle, the maximum lateral acceleration and yaw rate increase for the same maneuver velocity as an understeer vehicle. The use of an IVM in this case of changing weight split is redundant. The ESC limit is set at 19.2 deg/s for yaw rate and 0.46 g for lateral acceleration to start out with. Since a shift of the weight split toward the rear only increases the maximum yaw rate and lateral acceleration, as shown in Figure 5.4, the initial controller limit will suffice to keep the vehicle stable. However, if the weight split is shifted towards the front axle of the vehicle, the rollover limit decreases and the IVM is effective. In this case, the IVM would update the ESC's stability limit and cause the ESC to engage before rollover occurred. Also, note that as the weight split deviated from the nominal configuration by being shifted to the rear, the nominal controller limit becomes more conservative. As the controller's limit becomes more conservative, the vehicle's response potential is not meet. By utilizing the IVM, the controller limit can be updated to avoid the ESC limit from becoming ultra conservative, and causes the vehicle's response to be maximized. The rollover limits for the weight split variation is shown in Figure 5.4.

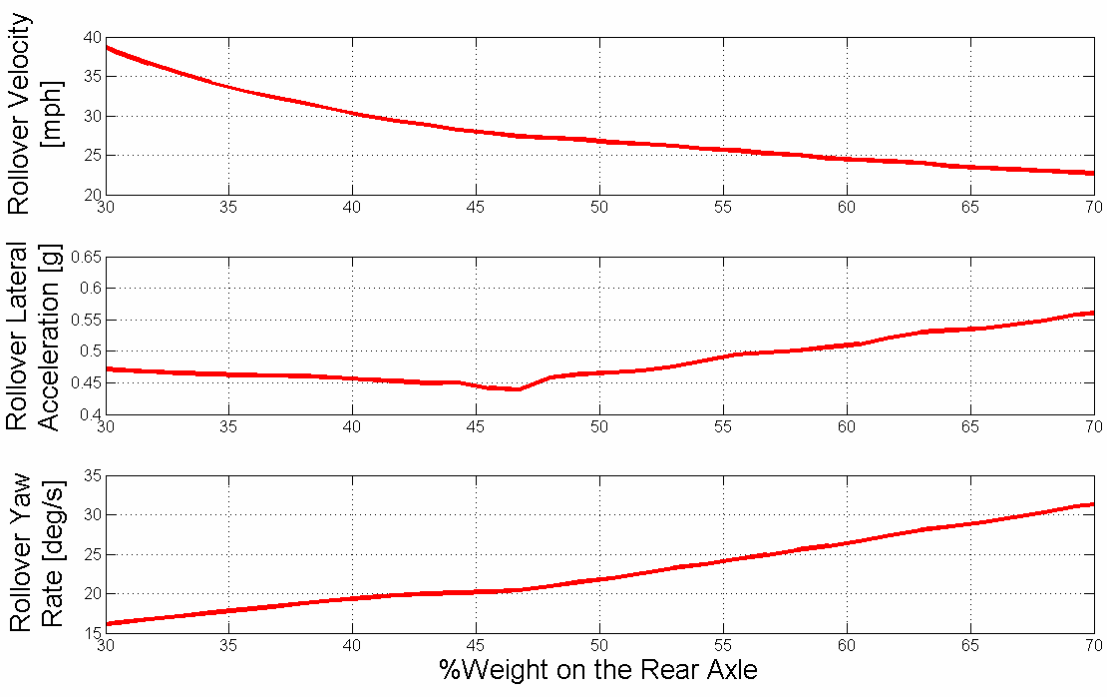

Figure 5.4. Stability Limits for Weight Split Variation

5.4 Summary and Conclusion

In this chapter, a simple ESC was developed and implemented in simulation. The vehicle's stability threshold for changes in load conditions was used in coordination with the ESC to increase the ESC's ability to prevent rollover. The use of the stability threshold to change the ESC's limits is called an Intelligent Vehicle Model since it updates changes to the vehicle's parameters and stability limit. The significance of the IVM was seen in simulation when the vehicle CG location was modified. The IVM

proved to be valuable for changes in CG height. However, the IVM was shown to be redundant in cases where the vehicle's weight split is shifted rear of the nominal configuration, but useful in keeping the controller limit from being ultra conservative.

CHAPTER 6

IMPLEMENTATION ON A SCALED VEHICLE

6.1 Introduction

Rollover testing using full-size vehicles is an expensive and somewhat dangerous endeavor. However, if dynamic behavior from the scaled vehicle tested in a controlled environment can predict the dynamic behavior of full-size vehicles, then scaled vehicles offer an alternative safe approach to investigate rollover. In this chapter, an analysis of vehicle rollover is performed on a scaled vehicle. Details of the scaled vehicle and its modifications are given, including development and implementation of a wireless IMU for providing critical vehicle measurements. Simulation data and experimental data of the scaled vehicle are compared to validate the dynamic similarity of the scaled vehicle with a passenger vehicle. Stability limits for the scaled vehicle with variation of the CG height and weight split are then derived using the vehicle simulation. Finally, a stability control system is developed for the scaled vehicle and the stability threshold is used in conjunction with an intelligent vehicle model to increase the stability controller's effectiveness.

6.2 Motivation for using Scaled Vehicles

Scaled vehicles have proven to be reliable test beds for a variety of applications such as yaw controller development and tire testing [Brennan, 2000; Burns, 2002; Hallowell, 2003]. Scaled vehicles also provide several advantages when testing and designing. For example, costs associated with a scale model vehicle are significantly lower and modifications are easier to make on a scale vehicle than a full-scale passenger vehicle. Most radio control cars are purchased for less than five hundred dollars, while it is difficult to purchase the cheapest of new passenger vehicle for fewer than ten thousand dollars. The cost of modification and maintenance is also much less expensive on a scaled vehicle than a passenger vehicle. The testing area required for scaled vehicles is much smaller, allowing the testing environment to be more accurately controlled. Compared with the Honda owned vehicle test facility in East Liberty, Ohio, where many vehicle tests are conducted, a scaled test center is much easier to acquire and maintain. Simple, low-cost road simulations have been built for testing scaled vehicles [Brennan 1998]. And pushing the vehicle to its limits in order to observe what happens in the non-linear regions of the vehicle is much safer with a scale vehicle than with a full-sized vehicle [Yih, 2000].

6.3 Scaled Vehicle Description

A 1:10 scale radio controlled (RC) car was used as a test bed in order to validate the rollover experiments done in the simulation. The vehicle was modified in order to allow the CG location, spring stiffness, and roll center height to be easily modified. Changing the CG location provides the opportunity to view dynamics occurring at different weight splits. It also provides a means to adjust the distance between CG height and roll center height, which is a crucial parameter when assessing steady state roll [Hac, 2002].

There are two generations of $1/10^{th}$ scale vehicles which were used to validate simulation results. The first generation test vehicle was configured with a rear wheel drive and front wheel steer configuration to better emulate many of today's RWD SUVs. Figure 6.1 shows the first generation scaled vehicle.

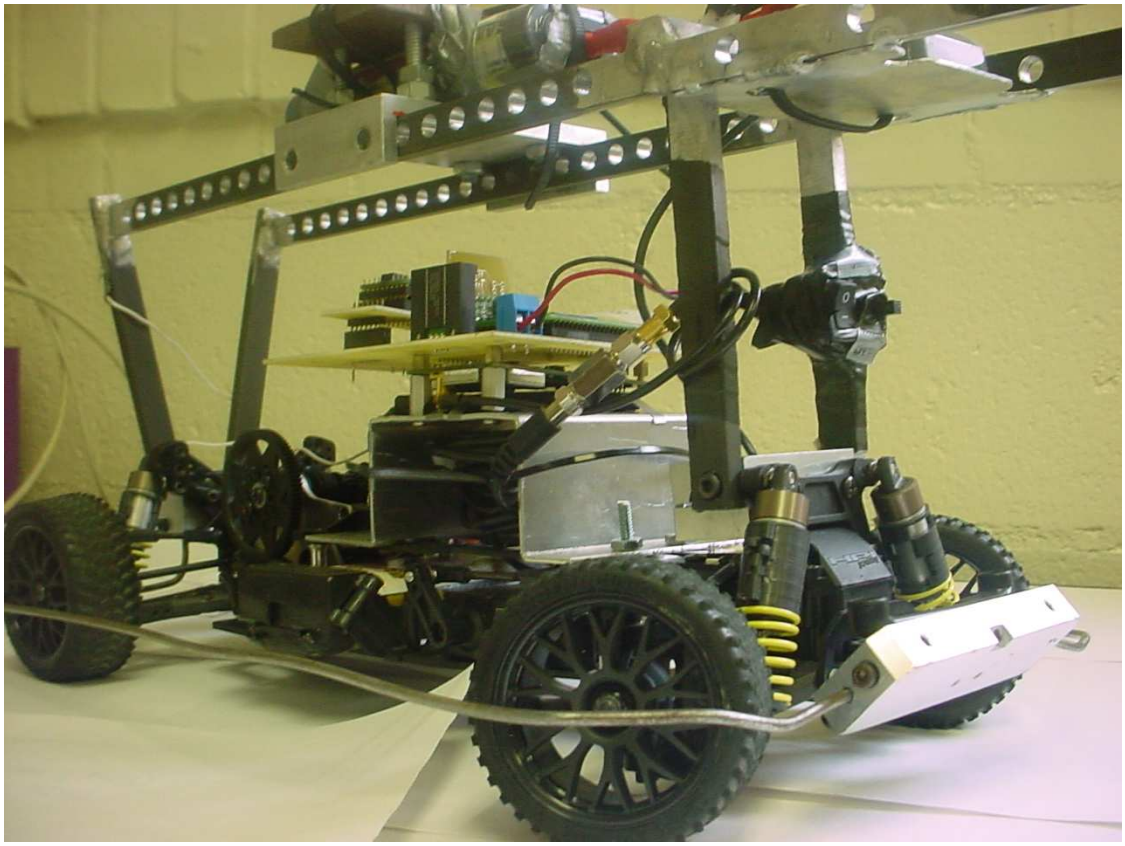

Figure 6.1. First Generation Scale Vehicle Test bed

Other notable aspects of the vehicle's setup include off-road tires, a CG relocator, and IMU board. Scaled vehicle street tires have a relatively high cornering stiffness in comparison with full size vehicles. Therefore, in order to compensate for this effect, knobby tires are used to help scale the cornering stiffness as suggested in [Brennan, 1999]. The steering servo used was a Futaba 3003 which has a response time of 240 deg/s. The CG relocator was created to move the CG in both the longitudinal and vertical directions. It also served as a roll cage that protects the vehicle's servos, motor and IMU. The first generation test bed was primarily used to record data during fishhook maneuvers and to study how changing the loading condition effects rollover. During the research, several drawbacks were noticed with this test bed. A tennis court was used as a

test area for experiments, which provided a small area for testing. Therefore a hard acceleration was needed in order to reach the maneuver speed, which caused major wheel spin on the two-wheel drive vehicle and led to rapid tire wear. A lack of repeatability and measurement of the vehicle's true velocity were some other faults of the first generation test bed. During testing, radio disturbances would disrupt a maneuver causing the scaled vehicle to frequently veer off its desired course and collide with surrounding objects during experiments, which made testing long and tedious. Additionally, the same vehicle configuration would not consistently cause rollover at the same programmed velocity. Other limitations included a weak roll cage, which was easily bent during rollover events, and a CG relocator design that raised the center of gravity too high when weight split changes were needed.

A second generation scaled vehicle was built to compete in NHTSA's first annual Enhanced Safety Vehicle Competition (ESV). Despite the vehicle being designed with the intention to show a scaled safety technology for the ESV competition it also became a vehicle dynamics and ESC test bed to study rollover. This second generation scaled vehicle is shown in Figure 6.2.

Figure 6.2. Second Generation Scale Vehicle Test bed

The second generation test bed was also a 1/10th scale vehicle. However, this vehicle was equipped with four-wheel-drive. The four-wheel-drive allowed rear wheel spin to be eliminated during acceleration before entering a maneuver. This vehicle was equipped with a more elaborate CG relocator, which enables the weight split to be changed while retaining a low center of gravity. A 0.3 kg weight is positioned fore or aft to change weight split, and risen up or down along four pieces of ¼”aluminum all-thread to change the CG height. The weight split can also be changed by adding weights to rods that are bolted into aluminum blocks attached fore and aft of the front and rear axles. The roll cage is stronger than the previous generation in order to better protect the data acquisition system. The black box in Figure 6.2 contains the wireless data acquisition

system which enabled improved telemetry. It was both small, and allowed wireless feedback control to be implemented on the test bed.

The wireless feedback control system is implemented by sending driver inputs via a steering wheel and pedal assembly. Similar to the ESC described in Chapter 5, the ESC is preset with the yaw rate at the stability limit and decides if the driver's inputs are outside the vehicle's stability region. An inertial navigation system monitors the vehicle states and informs the ESC through a wireless connection. If the driver is within the stability threshold, the ESC simply passes the driver's commands to the radio transmitter. If the driver's inputs bring the vehicle to the stability threshold, then the controller modifies the inputs accordingly to keep the vehicle from rolling over while maintaining the driver's intended path as close as possible. The inputs of the driver or the adjusted inputs from the ESC are sent to the radio transmitter which sends commands to the vehicle actuators. The wireless feedback control schematic is shown in Figure 6.3.

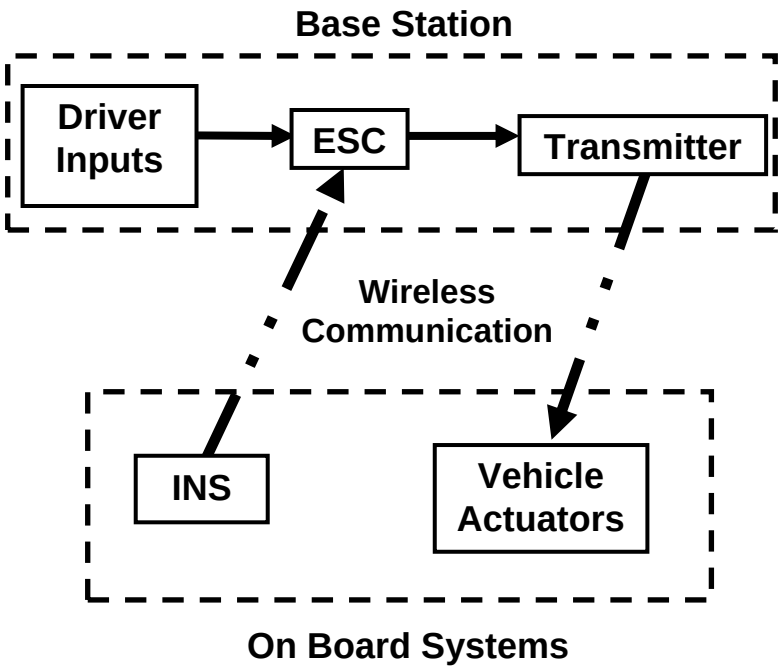

Figure 6.3. Vehicle Control Schematic

6.4 Data Acquisition

The first generation data acquisition system consisted of an inertial sensing module and was constructed to meet the basic dimensional requirements of fitting on a scaled vehicle. The system contained two gyroscopes capable of measuring 150 deg/s at a bandwidth of 40 Hz, one two-axis accelerometer capable of measuring ±2g at 50Hz, a GPS receiver, and a Rabbit microprocessor. The gyroscopes were oriented to obtain roll rate and yaw rate on the scale car. The accelerometer was placed in the horizontal plane to obtain longitudinal and lateral accelerations. The GPS unit provided vehicle position,

velocity, and course measurements, and when used in conjunction with accelerometers and gyroscopes, can also provide measurements of vehicle sideslip [Bevly, 2001]. The Rabbit was set up to record the inertial sensors at 100 Hz and the GPS receiver at 1 Hz for a duration of 45 seconds at a time. After each 40 second sample period, the data must be uploaded to a computer and the unit must be reset. This first generation data acquisition system is shown in Figure 6.4.

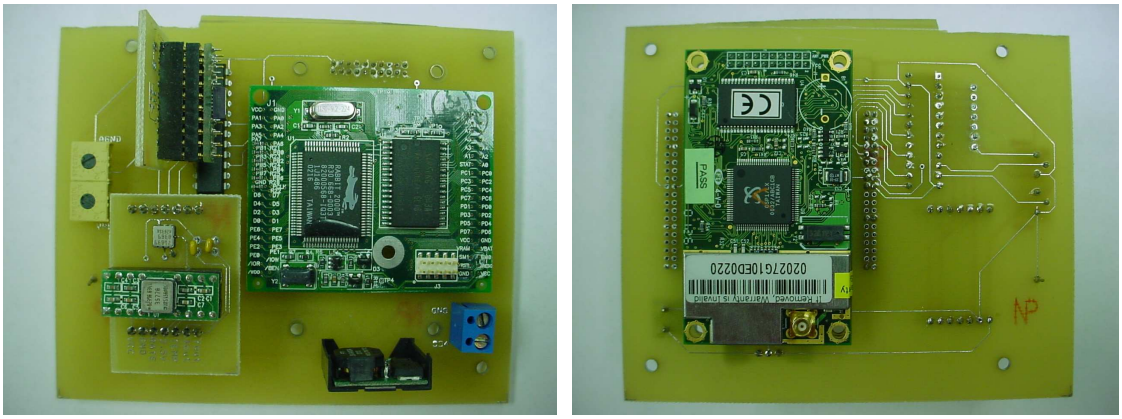

Figure 6.4. First Generation IMU

The second generation data acquisition system consists of an inertial measurement unit (IMU) that uses the same accelerometers and gyros as the first generation IMU. The IMU board that is mounted on the second generation scaled vehicle and includes a six-axis accelerometer/gyroscope package (3 accelerometers and 3 gyros), a GPS receiver, a wireless transmitter, a Rabbit 2000 microprocessor, and power management components. The wireless transmitter is a radio modem. It is used to collect inertial and position data and send it to the base station where the ESC analyzes the vehicle's dynamics. The components are mounted on a printed circuit board and placed in a protective box which is then mounted to the vehicle. The second generation data acquisition package can be seen in Figures 6.5 and 6.6.

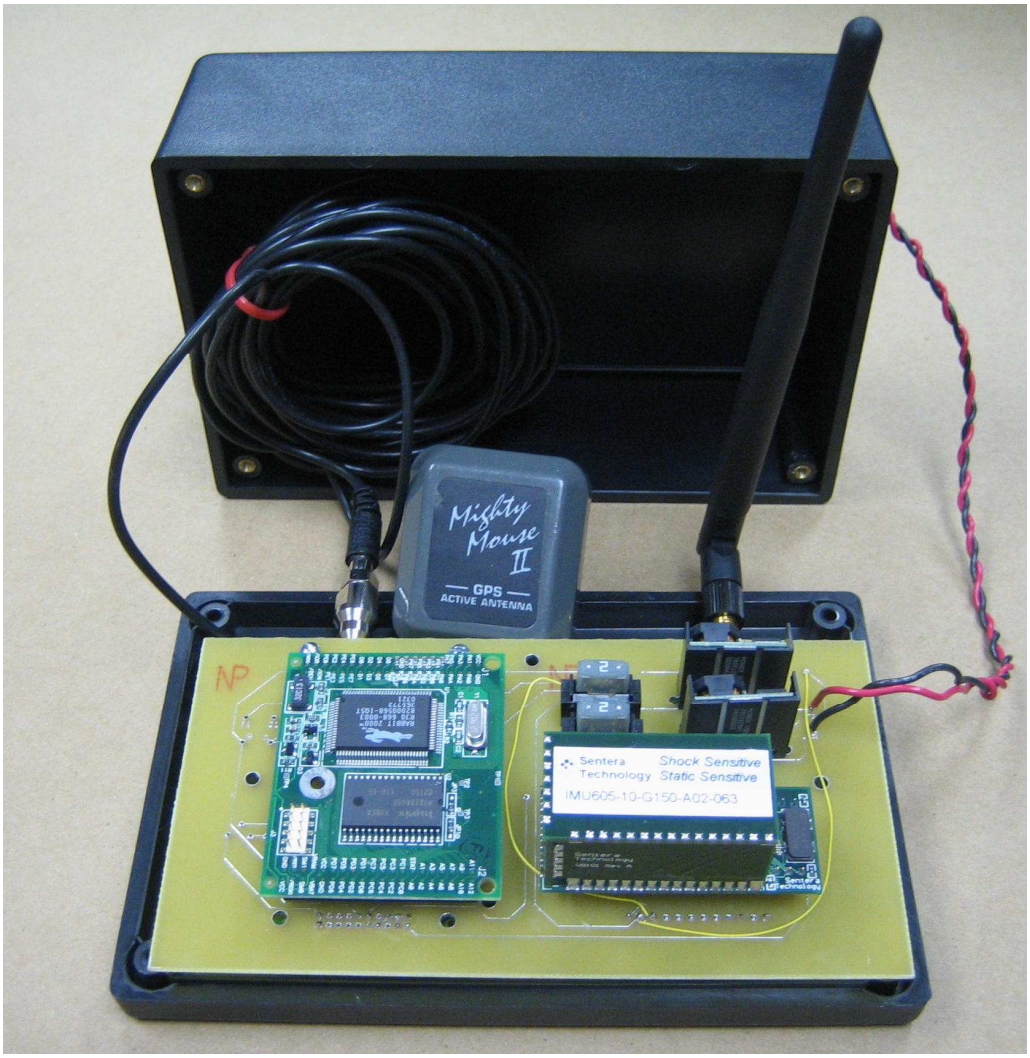

Figure 6.5. Wireless Data Acquisition Package

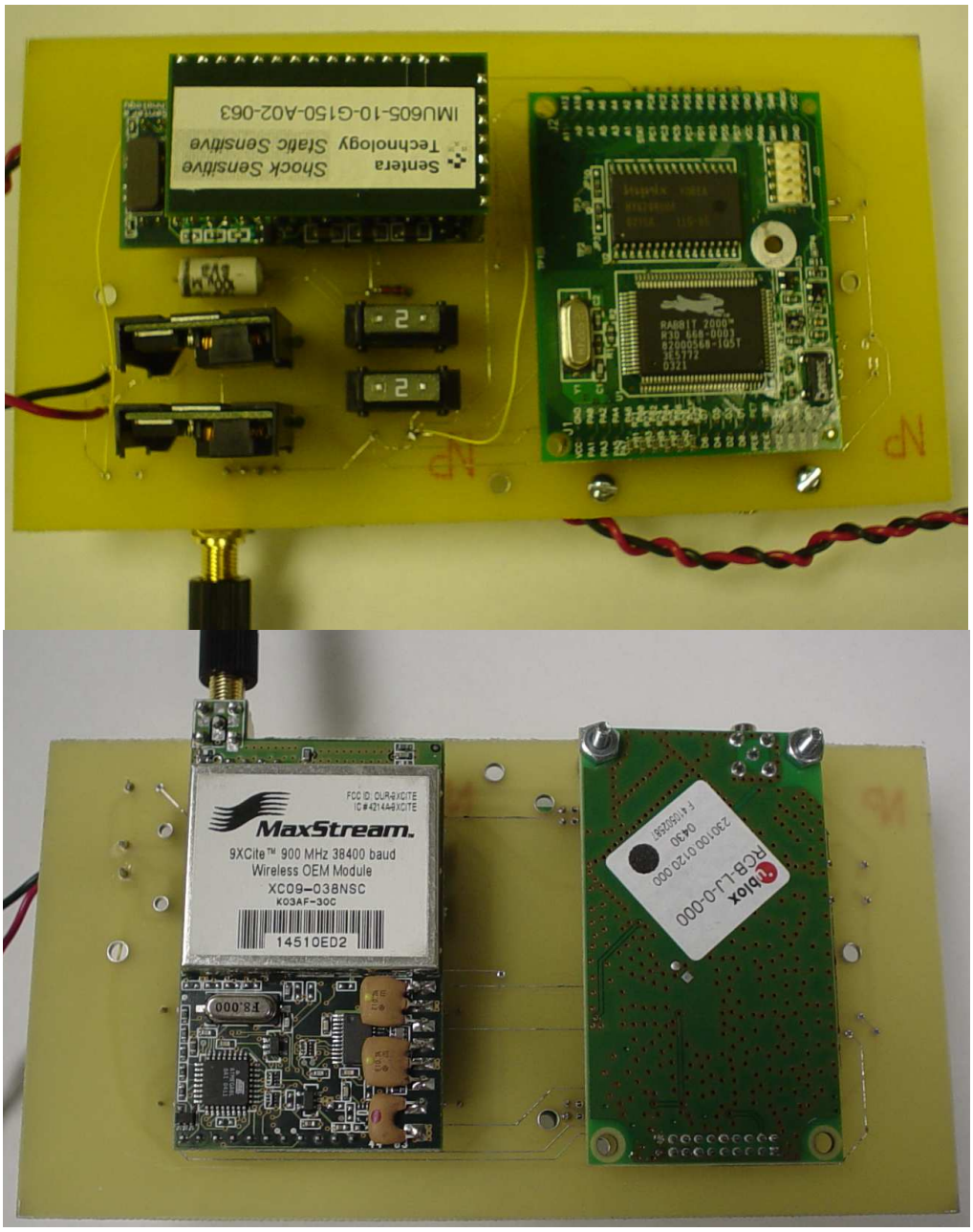

Figure 6.6. Second Generation Data Acquisition PCB Board. IMU and Microprocessor shown on top, GPS Receiver and Radio Modem shown on bottom

All data sampling is controlled by the Rabbit 2000 microprocessor which uses C code to log and transmit data. The microprocessor begins by collecting GPS and IMU data to be sent to the base station. It then prepares a packet of data to be sent through the wireless transmitter/receiver (MaxStream Xcite 9) which sends the data to the base

station. This data packet can be either literal data received from the GPS and IMU units or raw data parsed from their messages and processed onboard. The data is received by a wireless receiver plugged into the base station and is further processed by the ESC to determine the vehicle's stability. The dimensions of the INS box are 6.75" x 4.25" x 2.5". Table 6.1 includes the specifications of the IMU.

Table 6.1 IMU Specifications

Component	IMU605 - Accelerometer	IMU605 – Gyroscope	RCB-LJ– GPS
Update Rate (Hz)	Up to 256 (default 60)	Up to 256 (default 60)	4
Range	+/- 2g	+/- 150 deg/sec	n/a
Output format	Digital UART	Digital UART	Digital UART

6.5 Scaled Vehicle Simulation and Experiment Comparison

Simulations of the scaled vehicle and scaled vehicle experiments were used to compare scaled vehicle dynamics with passenger vehicle dynamics. The simulations and experiments were also used to verify the load dependant stability limits that were discussed in Chapter 4.

Vehicle simulations were compared with real experimental data in order to determine if scaled vehicle dynamics correlate with passenger vehicle dynamics. If the vehicle model derived for the passenger vehicle (which was verified in Chapter 3) also matches experiment data for the scaled vehicle, then scaled vehicles are valid tools for

researching the vehicle dynamics that effect passenger vehicle rollover. Figure 6.7 shows experimental and simulation data, which has not been filtered, of the first generation scaled vehicle during a maneuver.

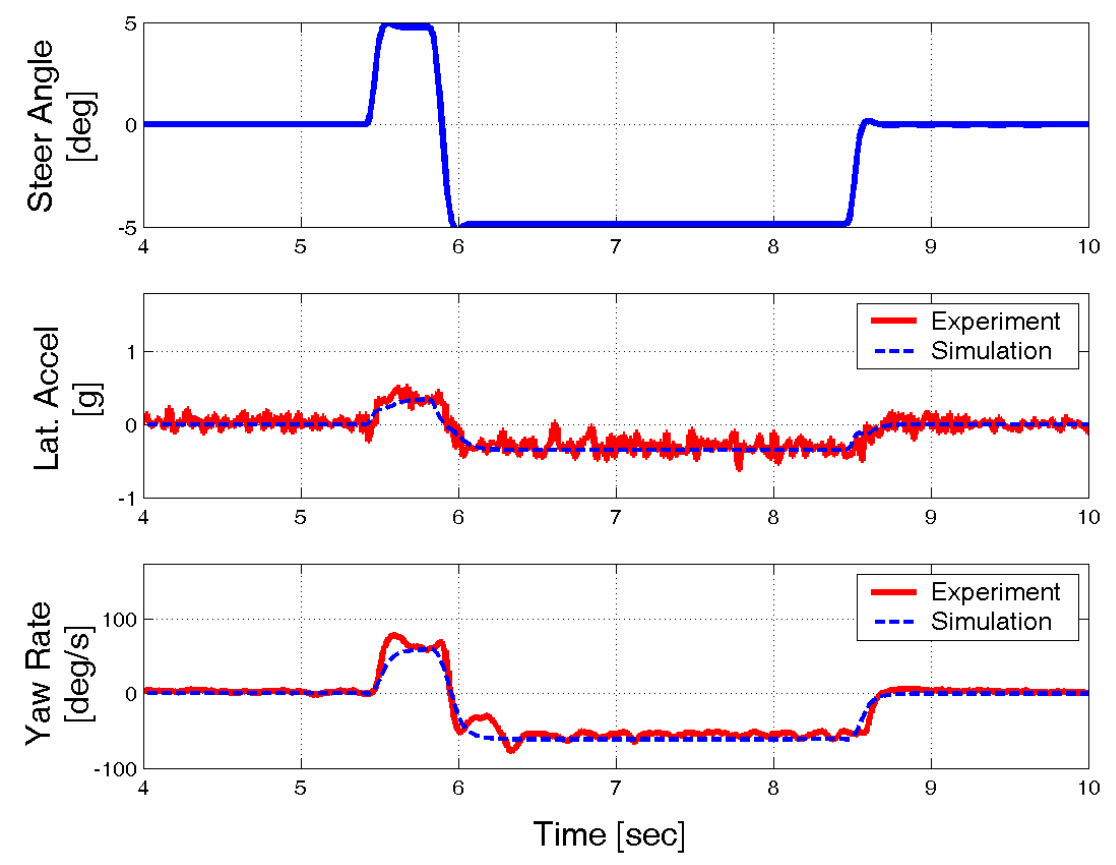

Figure 6.7. First Generation Scaled Vehicle Experimental versus Simulation Data

Note that the same governing equations used for the Blazer's dynamics also accurately capture the dynamics of the scaled vehicle.

6.6 Stability Limit Development

The stability limit developed for the Blazer in Chapter 4 was also developed for the scaled vehicle and tested with experiments in order to assess its validity. The simulation was limited to developing stability thresholds by changing only one vehicle property at a time. Therefore, two separate stability thresholds were developed for the load condition: CG height variation and weight split variation.

Vehicle simulations were used to determine the stability threshold for different vehicle loading conditions. This was done by varying individual parameters such as the CG height, and recording the velocity, lateral acceleration, yaw rate, and roll angle at which rollover is detected. For these simulation experiments, a Fishhook steering profile was chosen with a maximum steer angle of 5 degrees and a maximum steering rate of 40 degrees per second, both measured at the wheels. This profile, shown in Figure 6.8, was filtered using a 2^{nd} order Butterworth filter with a 1 Hz bandwidth. The velocity profile for the maneuver was set to a constant in order to simplify the results.

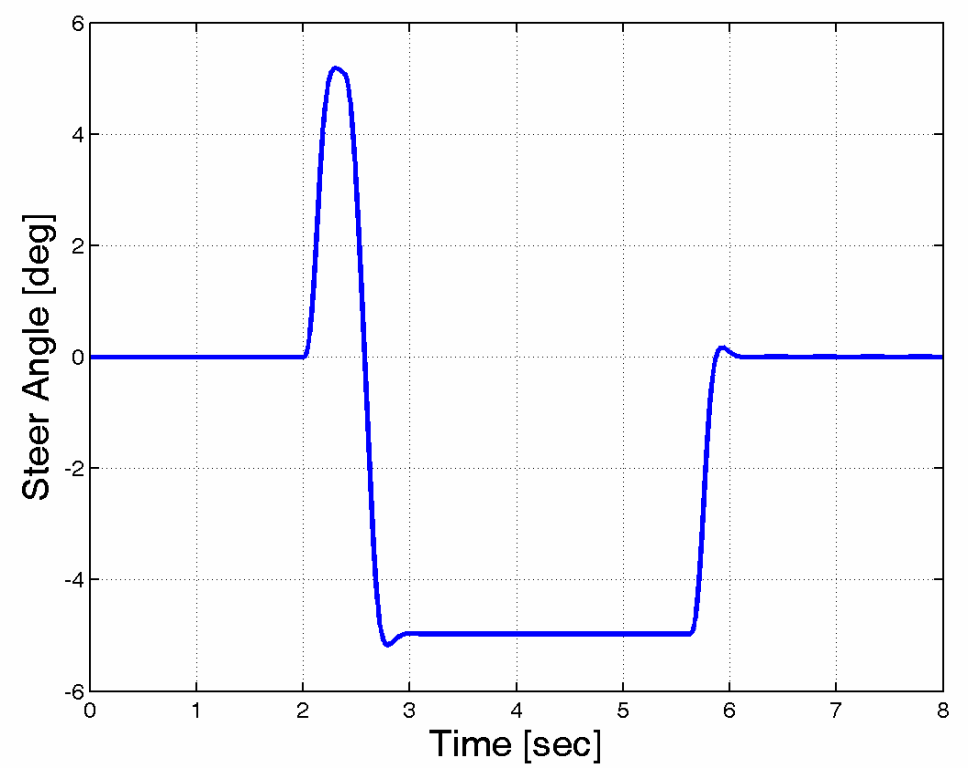

Figure 6.8. Fishhook Steering Profile for Stability Limit Development

The second generation scaled vehicle was used to determine the stability limit since it is the vehicle that was used in the experiments. For a given configuration, the test maneuver was repeated with the velocity being increased by 0.1 MPH increments until rollover occurred. NHTSA defines rollover to be the point at which both tires on one side of the vehicle are lifted by two inches [Forkenbrock, 2003]. For this simulation experiment, TWL over the duration of 0.4 seconds was declared to be a rollover event since the simulation cannot determine the height of tire lift. For the simulation, TWL is defined as the instance that wheel loads on one side of the vehicle go to zero. The stability limit was defined as the lateral acceleration, yaw rate, and roll angle at which a rollover event occurs. This stability limit was calculated for a variety of different vehicle properties [Whitehead, 2004].

The first scaled vehicle experiment varied the CG height with a neutral suspension setup (i.e. the weight split was set to 50:50, and the front and rear springs were the same stiffness). Figure 6.9 shows the stability threshold for the vehicle test bed as a function of CG height. The vehicle requires a higher lateral acceleration to rollover as the CG height is lowered, which follows intuition and the results of the static stability factor. The yaw rate required for rollover in this maneuver also increases as the CG height is lowered. Once the CG height is below a certain height, the vehicle no longer experiences rollover but begins to slide. This is due to the fact that at low CG heights, the moment created by the un-sprung mass height and the tire lateral force does not provide enough moment to roll the vehicle before the tires saturate. The vehicle no longer rolls over because of a decrease in the moment in the lateral weight transfer equation caused by the spring and damper loads, and their distance from the vehicle's centerline, S. This decrease in the spring and damper loads is caused by the decrease of the moment caused by the lateral acceleration of the sprung mass and the distance between the roll center and the CG height. The springs and dampers transfer this moment to the wheels, and since this moment is decreased by the lowering of the CG height, the lateral weight transfer is decreased as well.

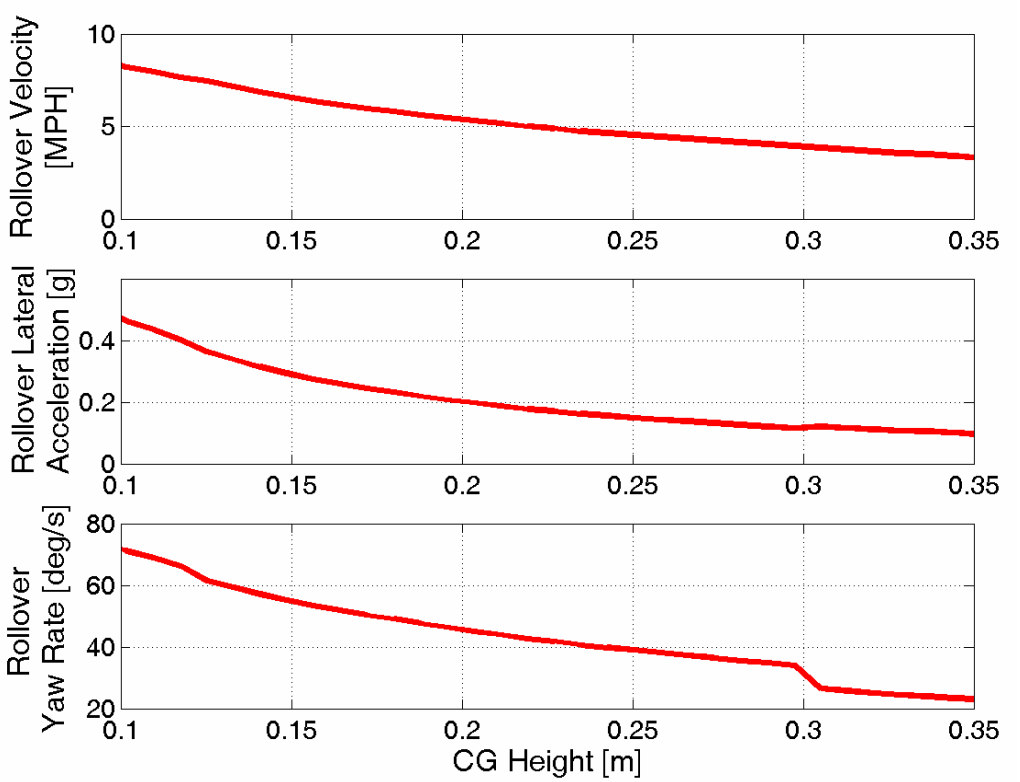

Figure 6.9. Stability Limits for CG Height Variation

Note that there is a difference of 0.375 g in the lateral acceleration rollover limit. The vehicle requires 0.472g of lateral acceleration to roll at a CG height of 0.1m, while .097g will roll the vehicle with a CG height of 0.35m. There is also a difference of 40.3 deg/sec in the yaw rate limit for rollover. The rollover yaw rate threshold is 71.8 deg/sec and 23.0 deg/sec for the CG heights of 0.1m and 0.35m respectively.

In order to develop the stability threshold for the longitudinal CG variation in the simulation, the vehicle's weight split was varied from 30:70 to 70:30, front to rear axle weights, respectively, and the CG height was held constant at 0.15 meters. The results of this simulation are shown in Figure 6.10.

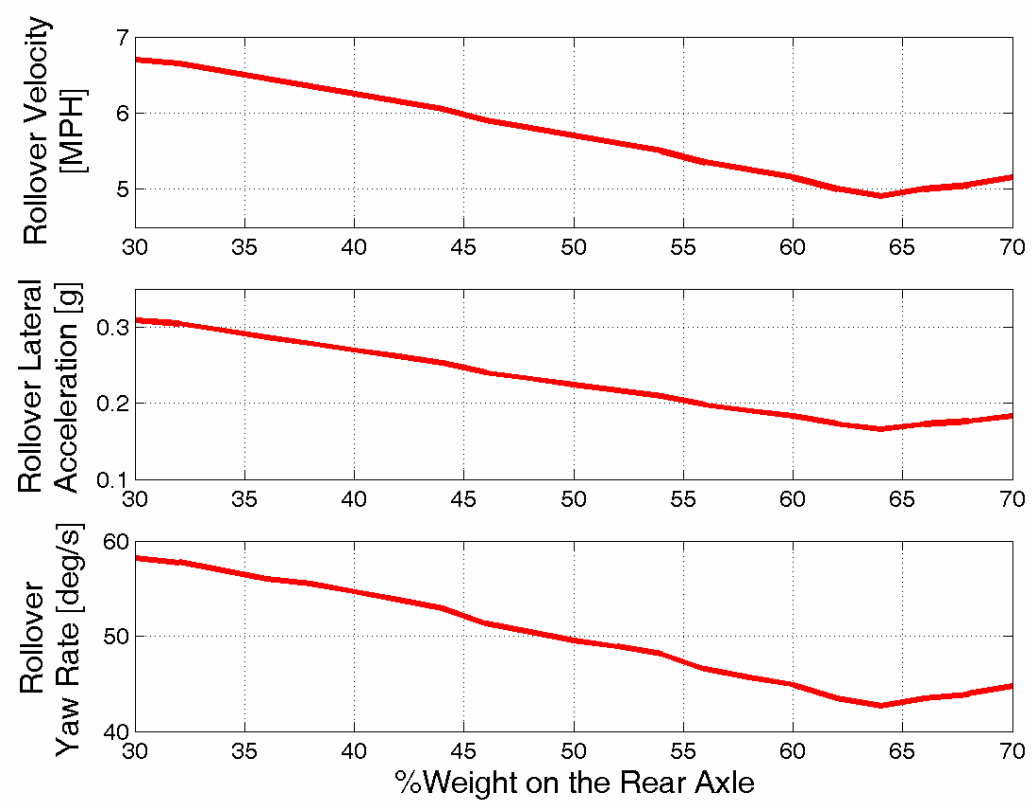

Figure 6.10. Stability Limits for the Weight Split Variation

Both the yaw rate and lateral acceleration stability limits decrease as weight is shifted from 30:70 to 36:64. The stability limits for the 30:70 weight split are 0.183 g and 44.8 deg/s. The rollover limits of the scaled vehicle for the weight split simulation vary by 0.186 g for lateral acceleration and 15.6 deg/s for yaw rate. Stability limits are 0.309g and 58.2 deg/s for a 70:30 weight split, and 0.166 g and 42.6 deg/s for a 36:64 weight split. A higher lateral acceleration and yaw rate is required for vehicle rollover as the weight is shifted towards the front axle. It is interesting to note that the vehicle understeer gradient also increases as the weight split is shifted to the front. Therefore, a generalization can be made that an understeer vehicle has a higher stability threshold than an oversteer vehicle, although this trend is not always followed.

The change in the stability threshold during these experiments shows how important vehicle loading data is to the ESC. For example, the stability limit changes from 0.270 g to 0.183 g and 54.6 deg/s to 44.9 deg/s as the vehicle's weight split is changed 60:40 to 40:60. Therefore, if the ESC model is not updated it will use 0.270 g and 54.6 deg/s as the stability limit, which are .087g and 9.7 deg/s more than the actual stability limit. This may not seem like much, but the stability threshold is actually off by 32.22% for lateral acceleration and 17.77% for the yaw rate. Knowing the stability threshold as a function of loading condition gives the ESC better ability to keep the vehicle stable by taking out errors in the controller's reference limits.

6.7 Stability Limit Validation

To validate the stability limits derived from the simulations, experiments which varied the properties center of gravity height and weight split were conducted with the scaled vehicle test bed. The first generation scale vehicle test bed operating on a concrete tennis court was used for these experiments. This environment was preferred over a parking lot due to the smoothness of the surface, and lack of gravel, and minimal grade. Lack of gravel is important because gravel is perceived by the scaled vehicle test bed as a basketball sized rock. The grade of the test environment used a constant value of 2 degrees. The size of the test area was small for high speed maneuvers, and radio frequency disturbances frequently disrupted experiments.

The Fishhook maneuver used in the simulation was also used in the experimental tests. The vehicle was driven by a computer in order to make the maneuver accurate and repeatable. The computer was programmed to accelerate the vehicle for four seconds in order to reach the desired velocity before the maneuver was initiated. Unlike the NHTSA study, where the vehicle begins to coast once the maneuver is entered, the velocity for the experiment was held constant throughout the maneuver.

Figure 6.11 shows the experiment results of the CG height variation for the stability threshold, which follows the static stability factor and the simulation results. The CG height was varied from 0.128 to 0.195 meters which corresponds a SSF variation of 0.4564 to 0.6138. The results of the experiment closely match the simulation. For a center of gravity height of 0.16 meters, the simulation shows the vehicle rolling over at a velocity of 6.25 MPH while the rollover velocity of the experiment was recorded at approximately 6.5 MPH. The proximity of these results provides validity gives value to the developed stability limits. Additionally, it is important to note that the same trend is evident in both experiment and simulation.

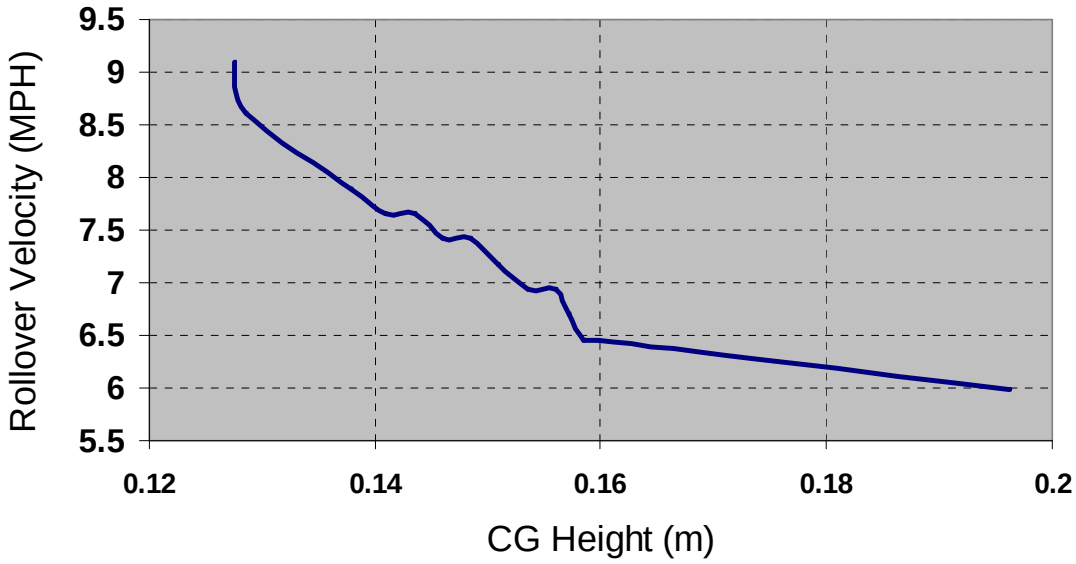

Figure 6.11. Experimental Stability Limit for Variations in the CG Height

The second set of experiments varied the longitudinal weight distribution. The first generation test bed was again used at the tennis court to perform this test. The maneuver and computer controls were kept the same as in the previous CG height variation experiments.

Figure 6.12 shows the experimental stability limit for rollover. It can be seen that the experimental results validate the simulation shown previously in Figure 6.10. Although weight split variation in the simulation and experiment follow the same derived trend, their rollover velocities do not match. This is due to the center of gravity height being higher in the simulation than the experiment. With the CG height setup in the experiment, the vehicle will not roll at weight splits favored to the front because of tire saturation. Qualitatively, the experimental results do follow the simulation trend which acknowledges that the vehicle is less prone to rollover as the weight split is shifted towards the front of the vehicle.

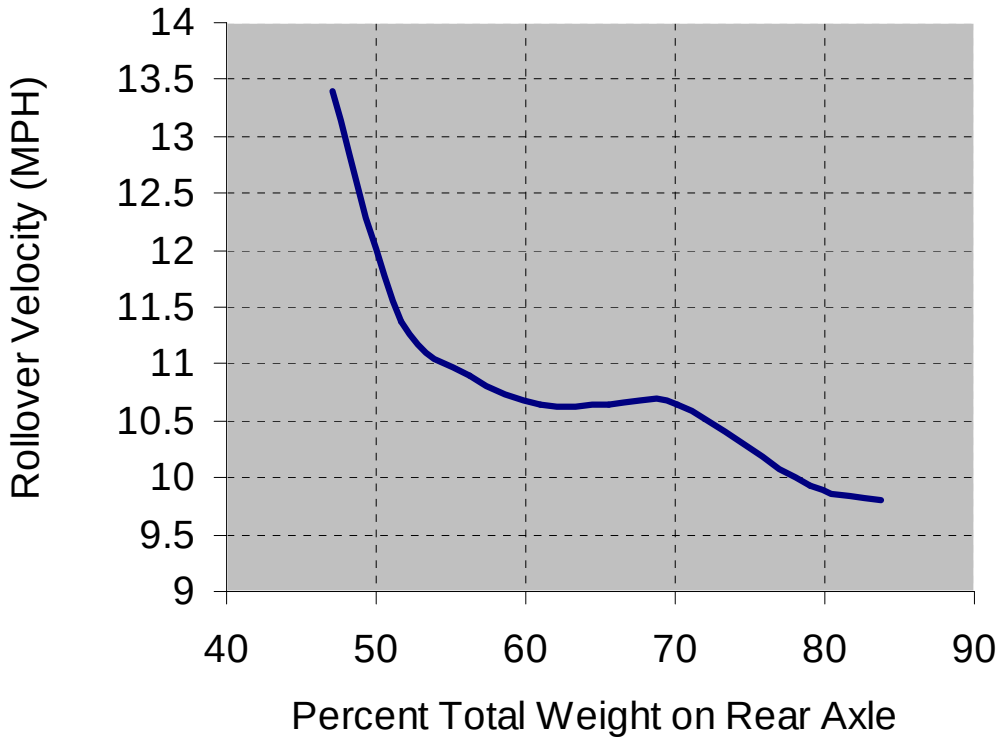

Figure 6.12. Weight Split Variation Experiment Stability Limit

6.8 Electronic Stability Control

As described in Chapter 5, the ESC is implemented as a PI controller via MATLAB simulation. The ESC's purpose is to keep the vehicle within the stability threshold. The stability limit is defined as the lateral acceleration and yaw rate at which the vehicle will experience TWL during a fishhook maneuver. The ESC monitors these two states and when the stability threshold is approached, the controller adjusts steer angle and velocity to maintain stability. When the ESC enabled vehicle is below the

stability limits, the ESC does not modify with the driver's inputs. However, once the driver's inputs exceed the stability limit, the ESC adjusts the steer angle and velocity to limit the yaw rate to the yaw rate stability limit and limit the lateral acceleration to the lateral acceleration stability limit. Since the scaled vehicle used was an off-the-shelf radio control vehicle, the only actuators available to the ESC on the scaled vehicle testbed were the steering servo and velocity control unit which brakes and accelerates the rear wheels. Figure 6.13 shows a simulated scaled vehicle with and without the ESC enabled. The maneuver that the vehicle is attempting to negotiate is a Fishhook maneuver at a maximum steer angle of 5 degrees with a maximum steer rate of 40 degrees per second at the tires. The driver's desired velocity is 8 MPH.

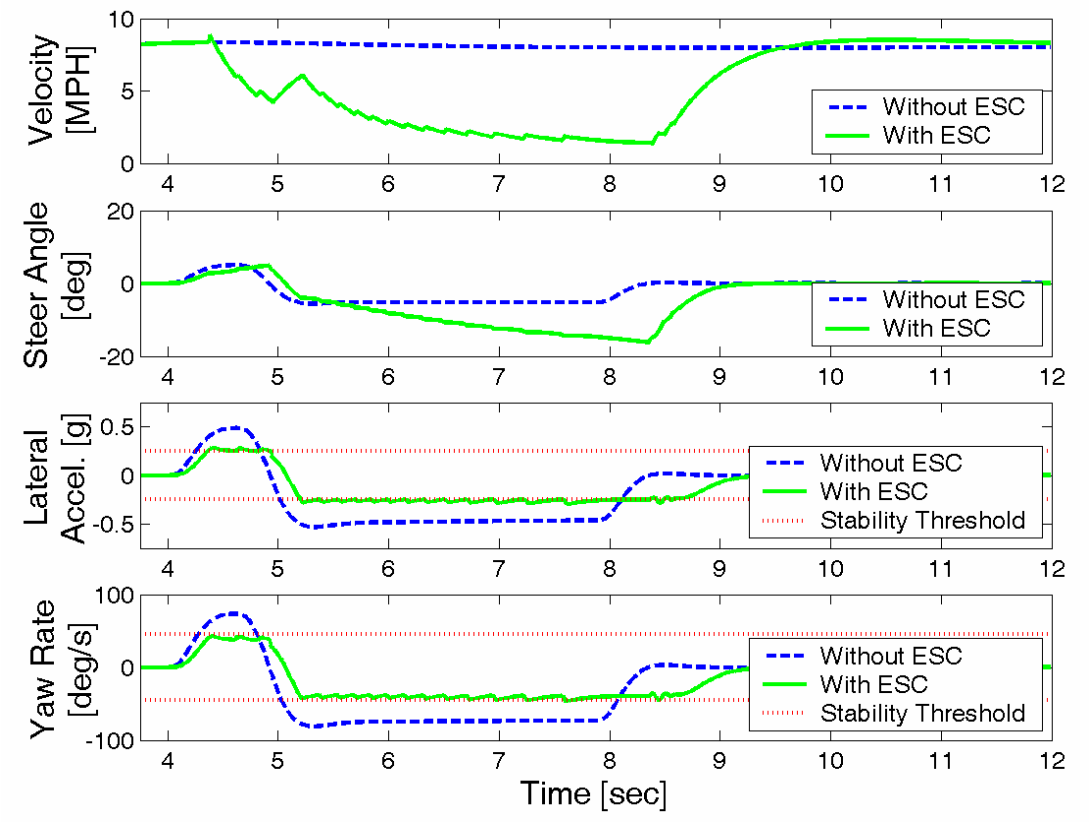

Figure 6.13. Results for the Fishhook Maneuver with and without ESC enabled

In order to maintain stability in this maneuver, the ESC adjusts the steering angle and actuates the brakes in order to not exceed the lateral acceleration and yaw rate limit. However, the ESC still tries to follow the driver's desired path by calculating the desired radius of the turn. The lateral acceleration stability threshold for this particular vehicle setup is 0.25g and the yaw rate stability threshold is 53.6 deg/sec. Figure 6.13 reveals how the ESC keeps the vehicle within the stability threshold when it would otherwise become unstable.

6.9 Intelligent Vehicle Model (IVM)

As a vehicle's payload changes, the Intelligent Vehicle Model (IVM) gives the controller knowledge of the change in the stability limit and adjusts the controller limits accordingly. Sensors, in conjunction with vehicle parameter estimation techniques would constantly monitor the vehicle weight split and CG height. The stability limit for the load condition would then be used as the controller's limit in the ESC.

In order to see how the IVM can improve the ESC effectiveness, a simulation was performed with the scaled vehicle model using a 60:40 and 40:60 weight split (front to rear axle weights, respectively). The CG height and static stability factor were held constant for this property variation. Again, a Fishhook maneuver with a maximum steer angle of 5 deg and maximum steer rate of 40 deg/s was used for the simulation. The

vehicle longitudinal velocity was set to 6 MPH and held constant throughout the maneuver.

In the initial configuration, the scaled vehicle had a weight split of 60:40 front to rear. The stability limit for this load condition is 0.270 g for lateral acceleration and 53.6 deg/sec for yaw rate. The ESC vehicle model is initially programmed to use these state limits in order to maintain stability. Since the vehicle does not exceed this limit during the maneuver, the ESC is never activated. It can be seen from the wheel loads in Figure 6.14 that the vehicle does not roll, but one wheel lift does occur.

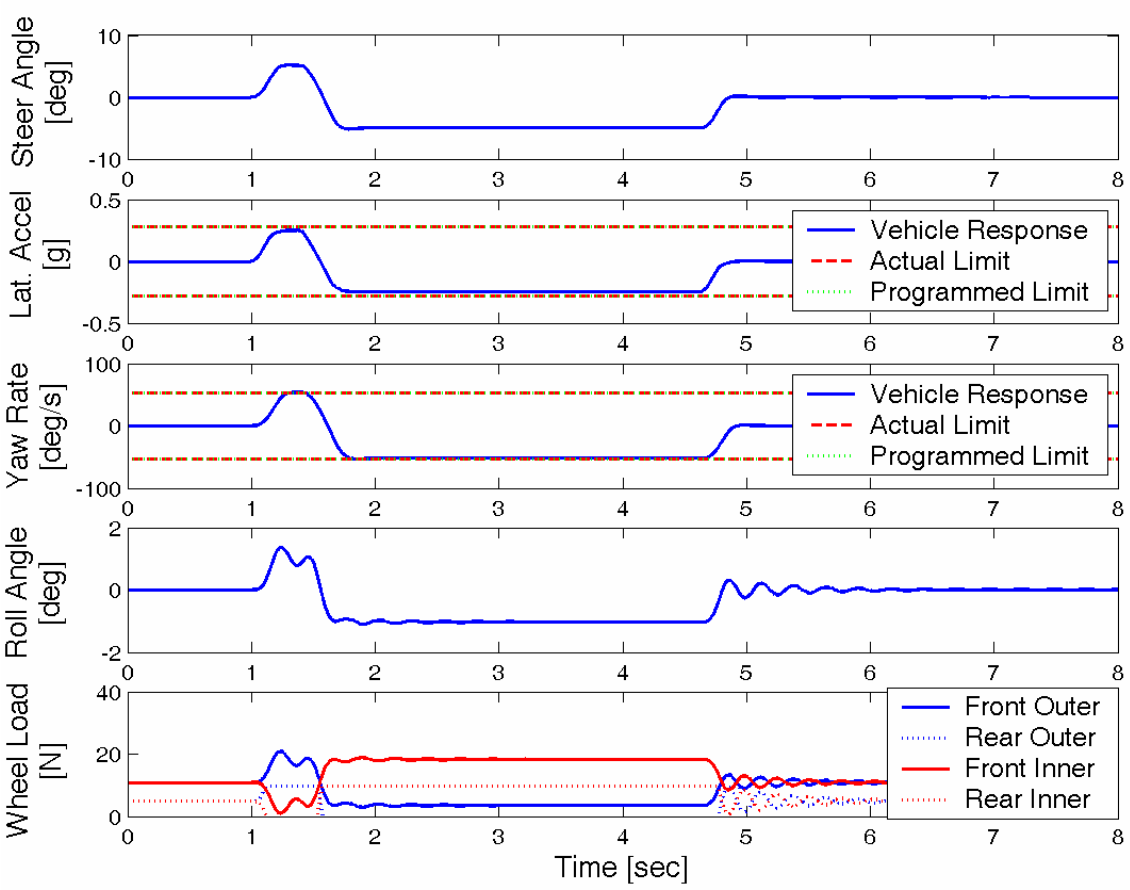

Figure 6.14. Results for the Fishhook 1a with 60:40 Weight Split

In the second configuration, the weight split is modified to 40:60. This new load condition results in a new stability limit of 0.183 g for lateral acceleration and 44.9 deg/s for yaw rate. The simulation was performed assuming the ESC is not equipped with the IVM. Therefore, the vehicle model still uses 0.270 g and 53.6 deg/s as the rollover stability limit. The same maneuver used for the 60:40 configuration causes this vehicle configuration to exceed the stability limit, causing rollover. Since the vehicle model is not updated, the ESC never intervenes and vehicle rollover occurs as shown in Figure 6.15.

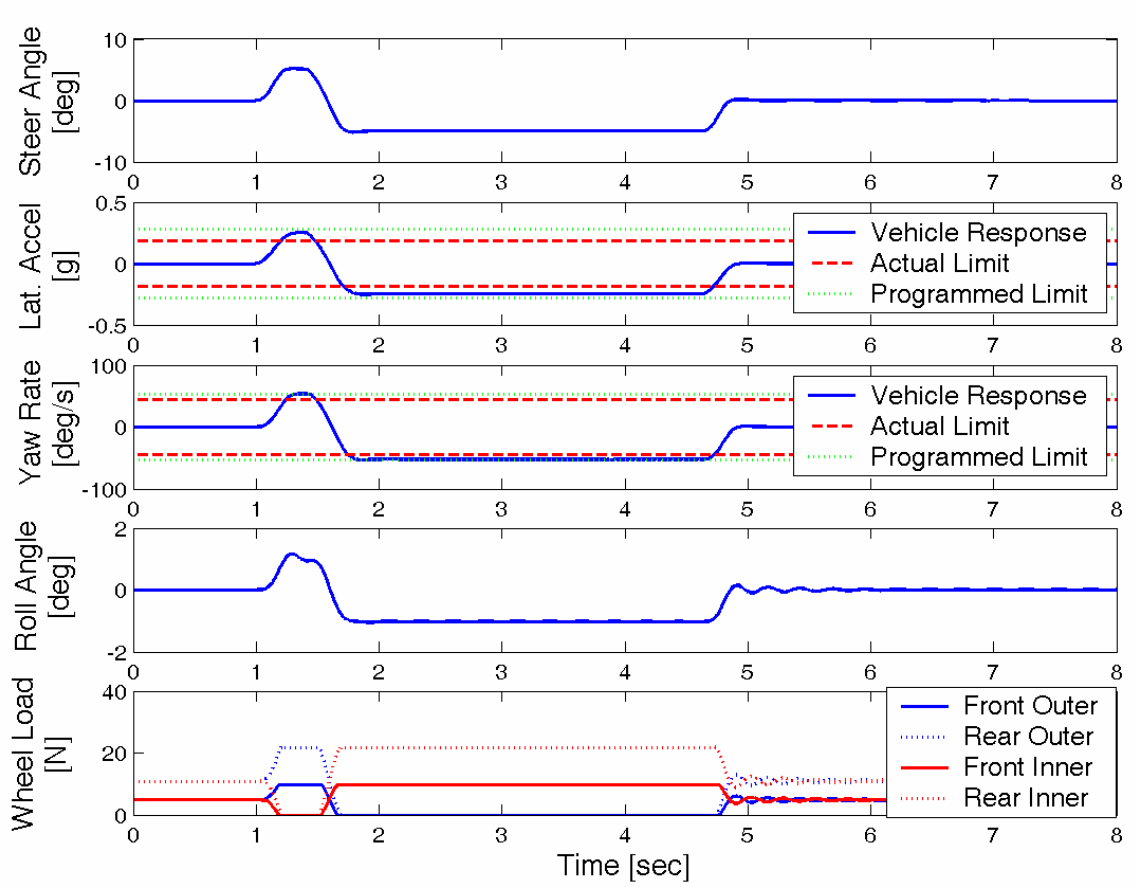

Figure 6.15. Results for the Fishhook 1a with 40:60 Weight Split

However, if the vehicle was equipped with the IVM along with the ESC, then the ESC would have known the correct stability limits. Therefore, the ESC could use the updated stability limit for the modified weight split. This would have enabled the ESC to correctly prevent the rollover as shown in Figure 6.13. A comparative analysis of these configurations is given in Table 6.2.

Table 6.2. ESC with and without IVM

	Weight Split Front:Rear		
	60:40	**40:60**	**40:60**
IVM	No	**No**	**Yes**
ESC	Engaged	**Disengaged**	**Engaged**
Rollover Incident	No	**Yes**	**No**
Maneuver Maximum Lateral Acceleration	0.25g	0.25g	0.18g
Maneuver Maximum Yaw Rate	53.6 deg/sec	53.6 deg/sec	44.0 deg/sec
Stability Threshold Lateral Acceleration	0.270g	0.183g	0.183g
Stability Threshold Yaw Rate	54.6 deg/sec	44.9 deg/sec	44.9 deg/sec

6.10 Summary and Conclusion

In this chapter, scaled vehicles have been shown to be valuable in evaluating vehicle loading conditions and their correlation with rollover. It has also been shown that scaled vehicles are valuable tools for studying ESC systems. Section 6.6 quantified a stability threshold in simulation for a scaled vehicle, and proposed the use of an IVM system. The IVM updates the stability threshold in the vehicle model for an ESC system

as the vehicle's payload changes. Section 6.7 verified the stability threshold with scaled vehicle experiments. Section 6.9 provided a scenario in which implementing an IVM would prevent rollover, while an ESC without IVM would not. Furthermore, this chapter has shown that scaled vehicles can be used to validate simulation results as well as provide valid information on the behavior of full scale passenger vehicles.

CHAPTER 7

CONCLUSION

7.1 Summary

An investigation of rollover propensity using simulation and experimental data has been presented. A vehicle model was developed and validated for studying rollover propensity. This vehicle model was then use to explore the changes that vehicle parameters have on rollover propensity. Stability thresholds for a range of vehicle load conditions were developed as well. An ESC was developed for mitigating rollover in simulation. Also, an IVM was developed and implemented with the ESC in order to improve ESC's effectiveness in preventing rollover. Finally, a scaled vehicle was used to validate the research. A summary of the research highlights in each chapter is provided below followed by a discussion of recommendations for future research.

In Chapter 2, a vehicle model was created to capture the major dynamics that govern vehicle rollover. Both non-linear yaw and roll dynamics were used to reproduce the transient dynamics in these axes. Newton's method, using FBDs, were used to develop the governing equations of motion. The non-linear, Pacejka, 'Magic Formula' tire model was used to model the tires. The diagrams and equations were detailed in the order in which they were used to develop the vehicle model.

Chapter 3 contains the evaluation and validation of the vehicle model developed in Chapter 2. In Section 2.2, the steady state results of the steady state roll equations were compared with those of the transient roll equations. The transient roll equations yielded the same steady state dynamic state values as the steady state roll equations. This validated the steady state dynamic states of the transient roll equations used in the vehicle model. Section 2.3 contained NHTSA Phase IV data which validated the transient dynamics of the yaw and roll equations in the vehicle model by matching with the simulation data. Experimental results using a transient maneuver with a Blazer at Auburn University provided further validation of the transient vehicle model. Finally, a discussion on the effect of roll centers below the un-sprung mass on weight transfer was given.

In Chapter 4, the correlation between vehicle load condition and rollover propensity was investigated. Analysis of the various load configurations of the NHTSA Blazer led to the development of a vehicle rollover stability threshold. The rollover stability threshold was derived as a function of various vehicle dynamic states such as lateral acceleration, yaw rate, and roll rate.

A simple ESC was developed in Chapter 5, and it is simulated on a Blazer. An IVM was developed to aid the ESC in preventing rollover. It utilized the stability threshold created in Chapter 4 with knowledge of vehicle properties changes to update the controller's vehicle model and state limits. It was shown that the IVM could improve ESC effectiveness during CG height changes. However, the IVM proved to be redundant as the vehicle's weight split was shifted to the rear axle.

In Chapter 6, the experimental test bed developed in this study allowed the robustness of ESC to be evaluated via changing vehicle properties such as weight split, center of gravity height, and suspension setup. These scenarios simulate changes in vehicle loading and suspension modifications, which are relevant in today's world of transporting children to soccer practice in SUVs, low rider hot rods, and modified four wheel drive vehicles. The scaled vehicle was used as a test bed to validate the stability limits created in simulation, explore vehicle properties that influence rollover, and investigate ESC algorithms. It is equipped with telemetry which consists of GPs and INS sensors. This chapter also quantified a rollover stability limit for the scaled vehicle and utilized the IVM, which updates the stability threshold in the vehicle model of an ESC. This chapter developed a scenario demonstrating that the IVM would aid in preventing rollover. The significance of the Intelligent Vehicle Model can be seen from the exercises in Section 6.9. IVM is a tool that ESC can use to improve its ability to prevent vehicle rollover.

7.2 Recommendations for Future Work

Results form this thesis should extended to derive the stability limit as a function of more vehicle properties. The vehicle properties that should be studied next include front and rear roll center heights as well as front and rear roll stiffness and damping. The

vehicle states that should be monitored in the stability threshold include yaw rate, lateral acceleration, roll angle, roll angle rate, side slip rate, and side slip angle.

The effect of tire properties should be further investigated for a wider range of paths and maneuvers, not just for steering profiles. This will provide a more accurate analysis of how a tire's cornering stiffness and peak lateral force effect vehicle rollover.

A higher DOF model, such as Adams or CARSIM, could also be used to derive the stability limits. The higher DOF models will include the suspension kinematics and dynamics of the un-sprung mass. These results should be compared with the results of the work presented in this thesis.

Since the ESC and IVM were only tested in simulation, further research could be conducted via experiments. Experimental data verifying the effectiveness that IVM has on preventing rollover is worth acquiring. Either a passenger vehicle or scaled vehicle could be used. Though the research presented in this thesis used the Fishhook maneuver, other maneuvers such as the ISO-3888 lane change maneuvers could be used. This maneuver requires a driver to follow a marked path instead of a steer profile. This would provide further validation of the ESC and IVM developed in this thesis.

Methods to inform the IVM of vehicle property changes should be explored. String potentiometers can be tuned to measure normal wheel loads. Accelerometers from an on-board IMU could be used with the wheel loads to determine the vehicle's weight split in a static case. Methods such as using a Kalman Filter to estimate the weight split should also be developed. A method to accurately estimate the CG height should also be derived and implemented. These methods to determine the vehicle load condition status could be implemented in simulation and experiments.

The scaled vehicle research in this thesis provided a relatively inexpensive means of acquiring real vehicle data. While this test bed provided experimental data, it could be improved. Because of the size of the 1:10th scale vehicle issues such as implementing sensors and finding a suitable test environment were never fully solved. For instance, a pebble to a full size vehicle is magnified 10 times for the 1:10th scale vehicle, and a seemingly smooth surface for a passenger vehicle is rough to a scaled vehicle. For future work, a larger scale vehicle (1:4th) should be used than the one used in this study. A larger vehicle, though more expensive, would be easier to instrument and might ultimately produce more accurate results.

REFERENCES

[1] Allen, R. W., Szostak,H.T, Rosenthal, T. J. and Klyde,D. H. 1990. "Field Testing and Computer Simulation Analysis of Ground Vehicle Dynamic Stability." SAE Paper No. 900127.

[2] Amberkar, S., et. al., "A Control System Methodology for Steer by Wire Systems." 2004. SAE Paper No. 2004-01-1106.

[3] Baumann, F.W., et. al., "Effects Causing Untripped Rollover of Light Passenger Vehicles in Evasive Maneuvers." 2004. SAE Paper No. 2004-01-1057.

[4] Bevly, D. M., Ryu, J., Sheridan, R., Gerdes, J. C, "Integrating INS Sensors with GPS Velocity Measurements for Continuous Estimation of Vehicle Side-Slip and Tire Cornering Stiffness," Proceedings of the 2001 American Control Conference, Vol.1, June 2001, pp.25-30.

[5] Brennan, S., et. al., "The Illinois Roadway Simulator – A Hardware-in-the-Loop Testbed Vehicle Dynamics and Control." Proceedings of the American Control Conference. June, 1998.

[6] Brennan, S. and Alleyne, A. "Using Scale Testbed: Controller Design and Evaluation." *IEEE Control Systems Magazine,* vol 21, 2001, pp. 15-26.

[7] Brennan, S. and Alleye, A. "Modeling and Control Issues Associated With Scaled Vehicles," 1999, University of Illinois at Urbana-Champaign.

[8] Brennan, S. and Alleyne, "The Illinois Roadway Simulator: A Mechatronic Testbed for Vehicle Dynamics and Control." *IEEE Transactions on Mechatronics.* Vol. 5, No. 4, pp. 349-359, December 2000.

[9] Brennan, S., "Similarity Conditions for Comparing Closed-Loop Vehicle Roll and Pitch Dynamics." Proceeding of the 2004 American Control Conference. Boston, MA. June 30 – July 2, 2004.

[10] Broulhiet, G., "The Suspension of the Automobile Steering Mechanism: Shimmy and Tramp", Bull Soc. Ing. Civ. Fr. 78, pp. 540-554, July 1925.

[11] Burns, Stephen R., O'Brien, Richard T., Piepmeier, Jenelle A., "Steering Controller Design Using Scale-Model Vehicles," 2002, IEEE Paper No. 0-7803-7339-1/02

[12] Carlson, C. R., and Gerdes, J. C., "Optimal Rollover Prevention with Steer by Wire and Differential." Proceedings of IMECE 2003.

[13] Christos, J. P. and Guenther, D. A. "The Measurement of Static Rollover Metrics," 1992, SAE Paper No. 920582

[14] Cooperrider, N. K., Hammound, S. A. and Thomas, T.M. "Testing and Analysis of Vehicle Rollover Behavior," 2000, SAE Paper No. 900366

[15] Day, T. D., and Garvey, J. T., "Applications and Limitations of 3-Dimensional Vehicle Rollover Simulation." 2000. SAE Paper No. 2000-01-0852.

[16] D'Entremont, K. L., Zhengyu, L. and Nalecz, A. G. "An Investigation into

Dynamic Measures of Vehicle Rollover Propensity," 1993, SAE Paper No. 930831

[17] Dixson, J. C., "Tires, Suspension and Handeling" Society of Automotive Engineers. Warrendale, PA. ISBN: 1-56091-831-4.

[18] Dugoff, H., Fancher, P.S., Segel, L., "Tire Performance Characteristics Affecting Vehicle Response to Steering and Braking Control Inputs." Report for Tire System Section, Office of Vehicle Systems Research. National Bureau of Standards, Washington, D.C. August, 1969

[19] Dugoff, H., Fancher, P.S., Segel, L., "An Analysis of Tire Traction Properties and their influence on Vehicle Dynamic Performance." SAE Paper 700377, 1970

[20] Eger, R., et. al., "Rollover Simulation Based on a Nonlinear Model." 1998. SAE Paper No. 980208.

[21] Ellis, J. R., "The Dynamics of Vehicles During Braking." Symposium on the Control of Vehicles, Institution of Mechanical Engineers, June 1963

[22] *Fatality Analysis Reporting System (FARS) Web-Based Encyclopedia*. National Center for Statistics and Analysis, National Highway Traffic Safety Administration, U.S. Department of Transportation. http://www-fars.nhtsa.dot.gov/.

[23] Forkenbrock, G.J., Garrott, W.R., Heitz, M. and O'Hara, B.C. NHTSA. 2002. "A Comprehensive Experimental Examination of Test Maneuvers that May Induce On-Road, Untripped, Light Vehicle Rollover – Phase IV of NHTSA's Light Vehicle Rollover Research Program" (October). Report No. DOT HS 809 513.

[24] Forkenbrock, G. J., Garrott, W.R., Heitz M. and O'Hara, B.C. 2003. "An Experimental Examination of J-Turn and Fishhook Maneuvers that May Induce On-Road, Untripped, Light Vehicle Rollover." SAE Paper No. 2003-01-1008.

[25] Fromm, H., "Brief Report on the History of the Theory of Shimmy", NACA TM 1395, pp. 181, 1954.

[26] Garrott, W. R., and Heydinger, G. J. 1992. An Investigation, Via Simulation, of Vehicle Characteristics that Contribute to Steering Maneuver Induced Rollover. SAE Paper No. 920585.

[27] Gillespie, T. D. 1992. "*Fundamentals of Vehicle Dynamics*." Society of Automotive Engineers. Warrendale, PA. ISBN: 1-56091-199-9.

[28] Ginsberg, J. H., "Advance Engineering Dynamics." 2nd ed. Cambridge University Press, 1998. ISBN: 0-521-47021-8.

[29] Hac, A. 2002. Rollover Stability Index Including Effects of Suspension Design. SAE Paper No. 2002-01-0965.

[30] Hac, A., et. al., "Detection of Vehicle Rollover." 2004. SAE Paper No. 2004-01-1757.

[31] Hallowell, Stephen J. and Ray, Laura R. "All Wheel Driving Using Independent Torque Control of Each Wheel, 2003," IEEE Paper No. 0-7803-7896-2/03

[32] Hilton, J., and Shankar, U., "Motor Vehicle Traffic Injury and Fatality Estimates – 2002 Early Assessment," Report No. DOT HS 809 586, May 2003, p. 15

[33] Huang, J., et. al., "Control Oriented Modeling for Enhanced Yaw Stability and

Vehicle Steerability." Proceeding of the 2004 American Control Conference. Boston, MA. June 30 – July 2, 2004.

[34] Johansson, B., and Gafvert, M., "Untripped SUV Rollover Detection and Prevention." 43rd IEEE Conference on Decision and Control. December 14 – 17, 2004.

[35] Klein, T. M., "A Statistical Analysis of Vehicle Rollover Propensity and Vehicle Stability." 1992. SAE Paper No. 920584.

[36] Milliken, D. L. and Milliken, W. F. 1995. *Race Car Vehicle Dynamics*. Society of Automotive Engineers. Warrendale, PA. ISBN: 1-56091-526-9.

[37] Morrison, W. R. B., "On the Lateral Dynamics of an Automobile in Accelerated Motions." Mechanical and Chemical Engineering Transactions, The Institution of Engineers, Australia, November 1967

[38] Newton, I., "Philosophiæ Naturalis Principia Mathematica." Londini : Jussu Societatis Regiae ac Typis Josephi Streater. Prostat apud plures bibliopolas, 1687.

[39] NHTSA. Phase IV Rollover Testing. 2002. George Washington Transportation Research Institute.

[40] NHTSA 2005: SafeCar.gov, Rollover. 18, Oct. 2005,

< http://www.nhtsa.dot.gov/cars/testing/ncap/Rollover/Index.htm>.

[41] Nishio, A., et. al., "Development of Vehicle Stability Control System Based on Vehicle Sideslip Angle Estimation." 2001. SAE Paper No. 2001-01-0137.

[42] Pacejka, H. B., Bakker, E., and Nyborg, L., "Tyre Modelling for Use in Vehicle Dynamics Studies." SAE Paper No. 870421, 1987

[43] Pacejka, H. B., Bakker, E., and Lidner L., "A New Tire Model with an Application in Vehicle Dynamics Studies." SAE Paper No. 890087, 1989.

[44] Plumlee, J. H., et. al. "Control of a Ground Vehicle Using Quadratic Programming Based Control Allocation Techniques." 2004.

[45] Ponticel, P. 2003. "Dynamic Testing Rollover on the Way," *Automotive Engineering International* (November 2003): 26-28.

[46] Radt, H. S., and Milliken, W. F., "Motions of Skidding Automobiles." Paper 205-A, Presented at SAE Summer Meeting, Chicago, June 1960

[47] Radt, H. S. and Pacejka, H. B., "Analysis of the Steady-State Turning of an Automobile." Symposium on the Control of Vehicles, Institution of Mechanical Engineers, June 1963

[48] Ryu, J., et. al., "Vehicle Sideslip and Roll Parameter Estimation using GPS." Design Division Stanford University.

[49] Schubert, P. J., et. al. "Electronic and Algorithms for Rollover Sensing." 2004. SAE Paper No. 2004-01-0343.

[50] Travis, W., Whitehead, R., Bevly, D. M., and Flowers G. T. "Using Scaled Vehicles to Investigate the Influence of Various Properties on Rollover Propensity." *Proceedings of the 2004 American Controls Conference, Boston, 30 June – 2 July, 2004*.

[51] Tseng, H. E., et.al., "Technical Challenges in the Development of Vehicle Stability Control System." Proceedings of the 1999 IEEE International Conference on Control Applications. August 22-27, 1999.

[52] U.S. Department of Transportation, National Highway Traffic Safety Administration, *The Economic Impact of Motor Vehicle Crashes 2000* (Washington, DC: 2002), also available at http://www.nhtsa.dot.gov/people/economic, as of December 2002.

[53] van Zanten, A.T., "Bosch ESP Systems: 5 Years of Experience." 2000. SAE Paper No. 2000-01-1633.

[54] Viano, D. C. and Chantal, P. "Case Study of Vehicle Maneuvers Leading To Rollovers: Need for a Vehicle Test Simulating Off-Road Excursions, Recovery and Handling," 2003 SAE Paper No. 2003-01-0169.

[55] Vilaplana, M.A., et. al., "Control of Sideslip and Yaw Rate in Cars Equipped with 4-Wheel Steer-by-Wire." 2004. SAE Paper No. 2004-01-2076.

[56] Voelcker, John. "Top Ten Tech Cars: A Year of Stability." *IEEE Spectrum*. March 2005: 22-30.

[57] Whitehead, R., Travis, W., Bevly, D. M., Flowers, G. T., "A Study of the Effect of Various Vehicle Properties on Rollover Propensity," 2004, SAE Paper No. 2004-01-2094.

[58] Wilde, J. R., et. al. "Experimental Evaluation of Fishhook Maneuver Performance of a Kinetic Suspension System." 2005. SAE Paper No. 2005-01-0392.

[59] Yih, Paul. "Radio Controlled Car Model as a Vehicle Dynamics Test Bed," Mechanical Engineering Department, Stanford University, Sept. 2000

APPENDICES

APPENDIX A

VEHICLE PROPERTIES

A.1 Introduction

Appendix A.2 contains a list and description of the vehicle properties used in the vehicle model developed in Chapter 2. Appendix A.3 contains the values of the vehicle properties for each of the Blazer configurations used in the NHTSA Phase IV experiments.

A.2 Garage Legend

Name	Description	Units
MT	Vehicle Total Mass	kg
M	Vehicle Sprung Mass	kg
m	Vehicle Un-Sprung Mass	kg
g	Gravitational Constant	m/s^2
W_t	Total Vehicle Weight	N
I_z	Vehicle Yaw Inertia	$N\text{-}m\text{-}s^2$
I_x	Vehicle Roll Inertia	$N\text{-}m\text{-}s^2$
WB	Vehicle Wheelbase	m
a	Distance from the CG to the front axle	m
b	Distance from the CG to the rear axle	m
h_{cgM}	CG height of Sprung Mass	m
h_{cgm}	CG height of Un-Sprung Mass	m
h_{rcf}	Front Roll Center height	m
h_{rcr}	Rear Roll Center height	m
trk_f	Front vehicle track	m
trk_r	Rear vehicle track	M
S_{kf}	Distance between front springs	M
S_{kr}	Distance between rear springs	M
S_{bf}	Distance between front dampers	M
S_{br}	Distance between rear dampers	M
K_{arbf}	Front Stabilizer, (anti-roll bar) Stiffness	N-m/rad
K_{arbr}	Rear Stabilizer, (anti-roll bar) Stiffness	N-m/rad
K_{sf}	Front Spring Stiffness	N/m
K_{sr}	Rear Spring Stiffness	N/m
B_f	Front Shock Damping Coefficient	N-s/m
B_r	Rear Shock Damping Coefficient	N-s/m

A.3 Garage Vehicles and Parameters

Parameter	Vehicle Description		
	Nominal Blazer	RRR Blazer	RMB Blazer
MT	1907 kg	1988.78 kg	2237.71 kg
M	1525 kg	1606.78 kg	1855.71 kg
m	382 kg	382 kg	382 kg
g	9.81 m/s^2	9.81 m/s^2	9.81 m/s^2
W_t	18707.67 N	19509.93 N	21951.94 N
I_z	3833.31 $N*m*s^2$	4094.98 $N*m*s^2$	$N*m*s^2$
I_x	734.04 $N*m*s^2$	813.49 $N*m*s^2$	$N*m*s^2$
WB	2.718 m	2.718 m	2.718 m
a	1.216 m	1.216 m	1.522 m
b	1.502 m	1.502 m	1.196 m
h_{cgM}	0.6629 m	0.6960 m	0.6614 m
h_{cgm}	0.35 m	0.35 m	0.35 m
h_{rcf}	-0.1 m	-0.1 m	-0.1 m
h_{rcr}	0.35 m	0.35 m	0.35 m
trk_f	1.445 m	1.445 m	1.445 m
trk_r	1.405 m	1.405 m	1.405 m
S_{kf}	0.7747 m	0.7747 m	0.7747 m
S_{kr}	0.9906 m	0.9906 m	0.9906 m
S_{bf}	0.7747 m	0.7747 m	0.7747 m
S_{br}	0.7620 m	0.7620 m	0.7620 m
K_{arbf}	700 N/deg	700 N/deg	700 N/deg
K_{arbr}	400 N/deg	400 N/deg	400 N/deg
K_{sf}	75000 N/m	75000 N/m	75000 N/m
K_{sr}	70000 N/m	70000 N/m	70000 N/m
B_f	5000 N*s/m	5000 N*s/m	5000 N*s/m
B_r	4000 N*s/m	4000 N*s/m	4000 N*s/m

APPENDIX B

SCALED VEHICLE PROPERTIES

B.1 Introduction

Appendix B contains the parameters of the scaled vehicle. These parameters are used in the vehicle simulation and come from the scaled vehicle that was used in the experiments.

B.2 Scaled Vehicle Parameters

Parameter	Description	Value	Units
MT	Vehicle Total Mass	3.20	kg
M	Vehicle Sprung Mass	2.	kg
m	Vehicle Un-Sprung Mass	0.276	kg
g	Gravitational Constant	9.81	m/s^2
W_t	Total Vehicle Weight	31.392	N
I_z	Vehicle Yaw Inertia	0.20	$N\text{-}m\text{-}s^2$
I_x	Vehicle Roll Inertia	0.10	$N\text{-}m\text{-}s^2$
WB	Vehicle Wheelbase	0.2556	m
a	Distance from the CG to the front axle	0.1374	m
b	Distance from the CG to the rear axle	0.1182	m
h_{cgM}	CG height of Sprung Mass	0.1565	m
h_{cgm}	CG height of Un-Sprung Mass	0.020	m
h_{rcf}	Front Roll Center height	0.010	m
h_{rcr}	Rear Roll Center height	0.0127	m
trk_f	Front vehicle track	0.1683	m
trk_r	Rear vehicle track	0.1746	M
S_{kf}	Distance between front springs	0.0492	M
S_{kr}	Distance between rear springs	0.0762	M
S_{bf}	Distance between front dampers	0.0492	M
S_{br}	Distance between rear dampers	0.0762	M
K_{sf}	Front Spring Stiffness	300	kN/m
K_{sr}	Rear Spring Stiffness	300	kN/m
B_f	Front Shock Damping Coefficient	100	N-s/m
B_r	Rear Shock Damping Coefficient	100	N-s/m

APPENDIX C

VEHICLE SIMULATION

C.1 Introduction

There are 15 MATLAB functions and scripts that make up the vehicle simulation. As stated in Chapter 2, the vehicle simulation is 3 DOF including the yaw and roll transient dynamics. The trapezoidal method is used to solve the integrals. The time step must be set at .001 seconds to achieve good results when using this method. The various pieces of MATLAB code are shown in the following sections of Appendix C.

C.2 Vehicle Simulation Layout

The simulation beings with the function 'main.m.' The vehicle, maneuver, and velocity profile are each chosen by the user in this function. The property variation can also be chosen from the 'main' function. The 'Garage.m' contains vehicle properties for various vehicles. The steering profile is produced in the 'steer_profile.m' function. 'Velocity.m' produces the longitudinal velocity profile for the maneuver. The 'property_changer.m' allows vehicle properties to be varied until two-wheel-lift is detected in the 'two_wheel_lift_detector' script. The simulation switch script contains

the numerical integration to solve the equations of motion and yield the vehicle's dynamic states. 'RubberandString.m' is called from the simulation switch when a value for tire lateral force is required. Various tire models are found in this function such as the non-linear, Pacejka 'Magic Formula,' and the linear tire model.

C.3 Main.m

```
% Vehicle Simulation
close all
clear all
clc

% Property you wish to vary
   % 0 - No Changes
   % 100 - Nominal Vehicle Condition looking for wheel lift
   % 1 - Weight Split
   % 2 - CG Height
   prop=1;

% Simulation type
   % '100' - Steady State Roll
   % '300' - Transient Roll
   sim=300;

% Vehicle Model
car='2001 Blazer Nom';

% Maneuver Profile
   % step -    Step Steer
   % 1a   -    Fishhook
   maneuver='1a';

% Max steer angle [deg]
   A=5;
   max_steer=A;

% Velocity Profile
       % step -    Step Profile
       % ramp a -  Contant ramp
```

```
    % ramp -    Ramp at a given acceleration
    % coast -   Coast Down
  vel_profile='step';
  if prop == 0 | 100
    ZZ=0;
    speed_i=15;     % [MPH] Velocity of No Change Option 0
  else
    ZZ=1;
   speed_i=15;      % [MPH] Initial Velocity of Property Changer Option 1:10
  end

% Wheel Lift Detector
  % 1   1-Wheel-Lift
  % 2   2-Wheel-Lift
  wheel_lift_detector=2;
  lift_time=1;     %ts*sec - value being the duratin of wheel lift  ie. value at 1000 = 1 sec
wheel lift

% Tire Model
  % Linear
  % Pacejka
  % Dugoff
  tire='Pacejka';

% Simulation Time
  endtime=8;         % 8 seconds is minimum time for steer profile 1a
  ts=0.001;          % Sample Time
  NN=endtime/ts;  % # of calculations

% Loading Vehicle Data
  [MT,M,m,g,Wt,Iz,Ix,zeta,a,b,h_cg_M,h_cg_m,h_rc_f,h_rc_r,trk_f,trk_r,...
    Sk_f,Sk_r,Sb_f,Sb_r,Sarb_f,Sarb_r,ks_f,ks_r,...
    karb_f,karb_r,Ca_f,Ca_r,SIS_const,steer_ratio,WB,b_f,...
    b_r] = garage(car);
  disp('Vehicle Parameters Loaded...')

% Loading Steering Profile
  del=steer_profile(maneuver,max_steer,SIS_const,endtime,ts,steer_ratio);
  disp('Steering Profile Loaded...')

% Roll Stiffness
  kphi_f = karb_f+0.5*ks_f*Sk_f^2;       % Front Roll Stiffness  [N*m*rad]
  kphi_r = karb_r+0.5*ks_r*Sk_r^2;       % Rear Roll Stiffness   [N*m*rad]
  kphi_t = kphi_f+kphi_r;                % Total Roll Stiffness

% Calculating the roll center at the CG
```

```
[h_rc_cg]=roll_center_height(WB,a,h_rc_f,h_rc_r);

% Property Changer
   Property_Changer
% Initial Conditions
   initial_variables

% Property Variation Loop
for qq = 1:QQ
   flag=0;
   two_wheel_lift_i(1:NN)=0;
   two_wheel_lift_o(1:NN)=0;
   t_w_l_i(1:NN)=0;
   t_w_l_o(1:NN)=0;
   w_l_fi(1:NN)=0;
   w_l_fo(1:NN)=0;
   w_l_ri(1:NN)=0;
   w_l_ro(1:NN)=0;
   zz=0;
   while zz <= ZZ
      while flag == 0
      % Velocity
      speed=speed_i+(zz/10);    %(zz increments 1 each step, adjust the denominator for
mesh density)
      % Ramp Acceleration    Note: Must be an even number
      accel=2;
      % Loading Velocity Profile
      vel=velocity(vel_profile,speed,accel,endtime,ts,MT);
      % Simulation Script
      Simulation_Switch
      % Roll Rate
      Roll_Rate(qq)=(((-M*g*d1(qq))/(-kphi_t+M*g*d1(qq))))*180/pi;     %deg roll/g
      % Index Counter
      zz=zz+1;
      if prop == 0
         flag = 1;
      end % (if statement)
      end % Flag while
   if flag == 1
      break
   end  % (Flag break)
   end % (Velocity while)
end % (Property while)
```

C.4 Garage.m

```
% Garage Function
% This function contains properties for the various cars in our "garage",
% which the main m-file calls for.  (Basically you get to pick which ride you want for each simulation)
% Input a Vehicle name:
%   RC
%   Neutral Blazer
%   2001 Blazer Nom
%   2001 Blazer RRR
%   2001 Blazer RMB

% Output:
%       MT     % kg      % mass of entire vehicle
%       M    % kg       % Sprung Mass
%       m     % kg       % Unsprung mass
%       g     % m/s^2    % Local Gravity
%       Iz    % N-m-sec^2  % Mass Moment of inertia about z-axis
%       Ix    % N-m-sec^2   % Mass Moment of inertia about x-axis
%       zeta            % Assumed damping coefficient
%       a    % m         % x-axis Distance from CG to front tire patch
%       b    % m         % x-axis Distance from CG to rear tire patch
%       h_cg_M   % m     % CG height in z-axis of Sprung Mass
%       h_cg_m   % m     % CG height of Un-Sprung mass
%       h_rc_f   % m     % Front Roll Center height in z-axis
%       h_rc_r   % m     % Rear Roll Center height in z-axis
%       trk_f    % m     % Front vehicle track
%       trk_r    % m     % Rear vehicle track
%       Sk_fM    % m     % Distance between front springs attachment points
                        % on Sprung Mass
%       Sk_fm    % m     % Distance between front springs attachment points
                        % on Un-Sprung Mass
%       Sk_rM    % m     % Distance between rear springs
                        % attachment points on Sprung Mass
%       Sk_rm    % m     % Distance between rear springs
                        % attachment points on Un-Sprung Mass
%       Sb_fM;   % m     % Distance between front dampers attachment
                        % points on Sprung Mass
%       Sb_fm;   % m     % Distance between front dampers attachment
                        % points on Un-Sprung Mass
%       Sb_rM;   % m     % Distance between rear dampers attachment
                        % points on Sprung Mass
%       Sb_rm;   % m     % Distance between rear dampers attachment
                        % points on Un-Sprung Mass
%       Sarb_f   % m     % Distance between front Anti-RBs
```

```
%       Sarb_r  % m     % Distance between rear Anti-RBs
%       k_f     % N/m   % Stiffness of front spring  (Individual Front Spring)
%       k_r     % N/m   % Stiffness of rear spring (Individual Rear Spring)
%       k_stabf  % N*m/rad     % Front Stabilizer Stiffness  Guess
%       k_stabr  % N*m/rad     % Rear Stabilizer Stiffness
%       Ca_f        % Front Axle Corning Stiffness
%       Ca_r        % Rear Axle Corning Stiffness
%       steer_ratio=18;     % handwheel/steer angle
%       SIS_const     % Steer angle (at the handwheel) at which .3g of lateral
                % acceleration is achieved on the SkidPad at 50 MPH

function [MT,M,m,g,Wt,Iz,Ix,zeta,a,b,h_cg_M,h_cg_m,h_rc_f,h_rc_r,trk_f,trk_r,...
      Sk_f,Sk_r,Sb_f,Sb_r,Sarb_f,Sarb_r,ks_f,ks_r,karb_f,karb_r,...
      Ca_f,Ca_r,SIS_const,steer_ratio,WB,b_f,b_r] = garage(car)

switch car;
      case 'Neutral Blazer'      % NHSTA Nominal Loading Configuration
      MT=1907.16;         % kg    % mass of entire vehicle
      M=MT*.8;            % kg    % Sprung Mass
      m=MT*.2;            % kg    % Unsprung mass
      g=9.81;             % m/s^2 % Local Gravity
      Wt=MT*g;            % Total weight of vehicle       (N)
      Iz=3833.31;         %N-m-sec^2  % Mass Moment of inertia about z-axis
      Ix=734.04;          %N-m-sec^2        % Mass Moment of inertia about x-axis
      WB=2.7180;
      a=WB*(.5);          % m     % x-axis Distance from CG to front tire patch
      b=WB-a;             % m     % x-axis Distance from CG to rear tire patch
      h_cg_M=.6629; %.6629  % m     % CG height in z-axis of Sprung Mass
      h_cg_m=.3;          %m      % CG height of Un-Sprung mass
      h_rc_f=.1;          % m     % Front Roll Center height in z-axis
      h_rc_r=.1;          % m     % Rear Roll Center height in z-axis
      trk_f=1.445;        % m     % Front vehicle track
      trk_r=trk_f;        % m     % Rear vehicle track
      Sk_f=0.7747;        % m     % Distance between front springs
      Sk_r=Sk_f;          % m     % Distance between rear springs
      Sb_f=Sk_f;          % m     % Distance between front dampers
      Sb_r=Sb_f;          % m  % Distance between rear dampers
      Sarb_f=1.0287;      % m   % Distance between front Anti-RBs
      Sarb_r=Sarb_f;      % m  % Distance between rear Anti-RBs
      karb_f=0;           % N*m/rad     % Front Stablizer Stiffness
      karb_r=0;           % N*m/rad     % Rear Stablizer Stiffness
      ks_f=60000;         % N/m   % Stiffness of front springs
      ks_r=40000;         % N/m   % Stiffness of rear springs
      b_f=5000;           % N/m/s  % Front dampers
      b_r=b_f;            % N/m/s  % Rear dampers
      Ca_f=1500;          % N/deg_slip     % Front tire Cornering Stiffness
```

```
Ca_r=Ca_f;          % N/deg_slip         % Rear tire Cornering Stiffness
steer_ratio=18;     % handwheel/steer angle
SIS_const=1.268*steer_ratio; %0.3282;   % Phase IV results = 0.3159  % degrees at handwheel
% Slowly Increasing Steer simulation where vehicle experiences 0.3g at this steer angle

case '2001 Blazer Nom'      % NHSTA Nominal Loading Configuration
MT=1907.16;         % kg    % mass of entire vehicle
M=MT*.8;            % kg    % Sprung Mass
m=MT*.2;            % kg    % Unsprung mass
g=9.81;             % m/s^2 % Local Gravity
Wt=MT*g;            % Total weight of vehicle       (N)
Iz=3833.31;         % N-m-sec^2  % Mass Moment of inertia about z-axis
Ix=734.04;          % N-m-sec^2         % Mass Moment of inertia about x-axis
a=1.216;            % m     % x-axis Distance from CG to front tire patch
b=1.502;            % m     % x-axis Distance from CG to rear tire patch
WB=a+b;             % m     % Wheelbase
h_cg_M=.6629;       % m     % CG height in z-axis of Sprung Mass
h_cg_m=.4;          % m     % CG height of Un-Sprung mass
h_rc_f=-0.1;        % m     % Front Roll Center height in z-axis
h_rc_r=0.35;        % m     % Rear Roll Center height in z-axis
trk_f=1.445;        % m     % Front vehicle track
trk_r=1.405;        % m     % Rear vehicle track
Sk_f=0.7747;        % m     % Distance between front springs
Sk_r=0.9906;        % m     % Distance between rear springs
Sb_f=Sk_f;          % m     % Distance between front dampers
Sb_r=.762;          % m     % Distance between rear dampers
Sarb_f=1.0287;      % m     % Distance between front Anti-RBs
Sarb_r=.6731;       % m     % Distance between frear Anti-RBs
karb_f=0;           % N*m/rad   % Front Stablizer Stiffness
karb_r=0;           % N*m/rad   % Rear Stablizer Stiffness
ks_f=75000;         % N/m   % Stiffness of front springs
ks_r=75000;         % N/m   % Stiffness of rear springs
b_f=1000;           % N/m/s % Front dampers
b_r=1000;           % N/m/s % Rear dampers
Ca_f=1500;          % N/deg_slip    % Front tire Cornering Stiffness
Ca_r=Ca_f;          % N/deg_slip    % Rear tire Cornering Stiffness
steer_ratio=18;     % handwheel/steer angle
SIS_const=1.268*steer_ratio; %0.3282;   % Phase IV results = 0.3159  % degrees  at handwheel ...
% Slowly Increasing Steer simulation where vehicle experiences 0.3g at this steer angle

case '2001 Blazer RRR'      % NHTSA Reduced Rollover Resistance Roof Ballast
MT=1988.78;         % kg    % mass of entire vehicle 4WD=(1963.95 kg)
```

```
M=MT*.8;          % kg    % Sprung Mass
m=MT*.2;          % kg    % Unsprung mass
g=9.81;           % m/s^2 % Local Gravity
Iz=4094.98*0.95;    % N-m-sec^2 % Mass Moment of inertia about z-axis
Ix=813.49*.75;      % N-m-sec^2 % Mass Moment of inertia about x-axis
zeta=.7;          % Assumed damping coefficient
a=1.216;          % m     % x-axis Distance from CG to front tire patch
b=1.502;          % m     % x-axis Distance from CG to rear tire patch
WB=a+b;           % m     % Wheelbase
h_cg_M=0.6960;       % m     % CG height in z-axis of Sprung Mass
h_cg_m=.4;        % m     % CG height of Un-Sprung mass
h_rc_f=-.1;       % m     % Front Roll Center height in z-axis
h_rc_r=0.35;      % m     % Rear Roll Center height in z-axis
trk_f=1.445;      % m   % Front vehicle track
trk_r=1.405;      % m     % Rear vehicle track
Sk_f=0.7747;      % m     % Distance between front springs
Sk_r=0.9906;      % m     % Distance between rear springs
Sb_f=Sk_f;        % m     % Distance between front dampers
Sb_r=.762;        % m  % Distance between rear dampers
Sarb_f=1.0287;     % m   % Distance between front Anti-RBs
Sarb_r=.6731;      % m  % Distance between frear Anti-RBs
Farb_f=700;         % N % Force/2 exerted by ARB per degree.  Creates a moment around roll center for Sprung and Un-Sprung mass
Farb_r=400;       % N % it is directly related to Roll stiffness created by the ARBs
k_stabf=0;        % N*m/rad     % Front Stablizer Stiffness  * Not used in Transient Simulation
k_stabr=0;        % N*m/rad     % Rear Stablizer Stiffness   * Not used in Transient Simulation
k_f=75000;              % N/m     % Stiffness of front springs      Estimate of hand calculation
k_r=70000;        % N/m   % Stiffness of rear springs
b_f=5000;         % N/m/s  % Front dampers
b_r=4000;         % N/m/s  % Rear dampers
Ca_f=2500;        % N/deg  % Front Axle Corning Stiffness
Ca_r=Ca_f;        % Rear Axle Corning Stiffness
steer_ratio=18;     % handwheel/steer angle
SIS_const=1.268*steer_ratio; %0.3282;   % Phase IV results = 0.3159  % degrees  at handwheel ...
% Slowly Increasing Steer simulation where vehicle experiences 0.3g at this steer angle

case '2001 Blazer RMB'      % NHTSA Rear-Mounted Basslast Configuration
MT=2237.71;       % kg    % mass of entire vehicle 4WD=(1963.95 kg)
M=MT*.9;          % kg    % Sprung Mass
m=MT*.1;          % kg    % Unsprung mass
g=9.81;           % m/s^2 % Local Gravity
```

```
Iz=4886.38*0.95;    % N-m-sec^2 % Mass Moment of inertia about z-axis
Ix=769.97*0.75;     % Mass Moment of inertia about x-axis
a=1.522;            % m     % x-axis Distance from CG to front tire patch
b=1.196;            % m     % x-axis Distance from CG to rear tire patch
h_cg_M=0.6614;      % m     % CG height in z-axis of Sprung Mass
h_cg_m=.4;          % m      % CG height of Un-Sprung mass
h_rc_f=-.15;        % m     % Front Roll Center height in z-axis
h_rc_r=0.3;         % m     % Rear Roll Center height in z-axis
trk_f=1.445;        % m     % Front vehicle track
trk_r=1.405;        % m     % Rear vehicle track
Sk_f=0.7747;        % m     % Distance between front springs
Sk_r=0.9906;        % m     % Distance between rear springs
Sb_f=Sk_f;          % m     % Distance between front dampers
Sb_r=.762;          % m  % Distance between rear dampers
Sarb_f=1.0287;      % m   % Distance between front Anti-RBs
Sarb_r=.6731;       % m  % Distance between frear Anti-RBs
Farb_f=700;         % N % Force/2 exerted by ARB per degree.  Creates a moment around roll center for Sprung and Un-Sprung mass
Farb_r=400;         % N % it is directly related to Roll stiffness created by the ARBs
k_stabf=0;          % N*m/rad     % Front Stablizer Stiffness  * Not used in Transient Simulation
k_stabr=0;          % N*m/rad     % Rear Stablizer Stiffness   * Not used in Transient Simulation
k_f=60000;              % N/m     % Stiffness of front springs      Estimate of hand calculation
k_r=60000;          % N/m   % Stiffness of rear springs
b_f=5000;           % N/m/s  % Front dampers
b_r=4000;           % N/m/s  % Rear dampers
Ca_f=2500;          % N/deg  % Front Axle Corning Stiffness
Ca_r=Ca_f;          % Rear Axle Corning Stiffness
steer_ratio=18;     % handwheel/steer angle
SIS_const=1.268*steer_ratio; %0.3282;   % Phase IV results = 0.3159  % degrees  at handwheel ...
% Slowly Increasing Steer simulation where vehicle experiences 0.3g at this steer angle

case 'RC'

%Weight Distribution
weight_front=0.809;         %kg  Mass on front of vehicle
weight_rear=0.941;          %kg   Mass on rear of vehicle
weight_left=0.899;          %kg   Mass on left of vehicle
weight_right=0.854;         %kg  Mass on right of vehicle
weight_split=[0.4623 0.5377];  %Front-Rear Weight Split
%Total Mass=1.65
wheelbase=0.2556;           %m  Wheelbase
```

```
%Unsprung Mass Components
wheel_mass=0.034;          %kg  Mass of wheel  x4 = .136
upper_arm_mass=0.001;      %kg  Mass of upper arm  x4=.004
lower_arm_mass=0.005;      %kg  Mass of lower A arm x4=.02
axle_mass=0.005;           %kg  Mass of Axle x4=.02
spindle_mass=0.024;        %kg  Mass of spindle x4=.096

MT=3.20;    % kg          % mass of entire vehicle
m=.276;             % kg              % Un-sprung mass
M=MT-m;          % kg       % Sprung Mass
g=9.81;             % m/s^2         % Local Gravity
Wt=MT*g;    % Total weight of vehicle       (N)
Iz=.20;        % N-m-sec^2         % Mass Moment of inertia about z-axis (yaw)
Ix=.10;     % N-m-sec^2           % Mass Moment of inertia about x-axis (roll)
Iy=.2;      % N-m-sec^2     % Inertia about y-axis (pitch)
a=0.1374;   % m               % x-axis Distance from CG to front tire patch
b=0.1182;   % m           % x-axis Distance from CG to rear tire patch
WB=a+b;
h_cg_M=.1565;   % m             % CG height (in z-axis) of Sprung Mass
h_cg_m=.02;     % m      % CG height of Un-Sprung mass
h_rc_f=0.010;     % m    % Front Roll Center height in z-axis
h_rc_r=0.0127;  % m      % Rear Roll Center height in z-axis
trk_f=0.1683;   % m       % Front vehicle track
trk_r=0.1746;   % m       % Rear vehicle track
Sk_fM=0.0492;   % m   % Distance between front spring attachment points on sprung mass
Sk_fm=0.1016;   % m    % Distance between front spring attachment points on un-sprung mass
Sk_f=(Sk_fM+Sk_fm)/2;
Sk_rM=0.0762;  % m       % Distance between rear springs attachment points on Sprung Mass
Sk_rm=0.1206;   % m    % Distance between rear springs attachment points on Un-Sprung Mass
Sk_r=(Sk_rM+Sk_rm)/2;
Sb_fM=0.0492;  % m    % Distance between front dampers attachment points on Sprung Mass
Sb_fm=0.1016;   % m    % Distance between front dampers attachment points on Un-Sprung Mass
Sb_f=(Sb_fM+Sb_fm)/2;
Sb_rM=0.0762;   % m   % Distance between rear dampers attachment points on Sprung Mass
Sb_rm=0.1206;  % m       % Distance between rear dampers attachment points on Un-Sprung Mass
Sb_r=(Sb_rM+Sb_rm)/2;
karb_f=0;
```

```
    karb_r=0;
    Sarb_f=0;          % m     % Distance between front Anti-Roll Bars
    Sarb_r=0;          % m     % Distance between rear Anti-RBs
    ks_f=150*100;    % N/m   % Stiffness of front spring (Individual Front Spring)
    ks_r=150*100;    % N/m           % Stiffness of rear spring (Individual Rear Spring)
    b_f=100;
    b_r=100;
    k_stabf=0;         % N*m/rad     % Front Stabilizer Stiffness
    k_stabr=0;         % N*m/rad     % Rear Stabilizer Stiffness
    Ca_f=100;       % N/rad  % Front Axle Corning Stiffness
    Ca_r=100;       % N/rad  % Rear Axle Corning Stiffness
    steer_ratio=1;
    SIS_const=2.787*steer_ratio;

  otherwise
    disp('We do not have the car you request in the garage. See "help garage" and pick a
car in the garage, or start walking.')
end
```

C.5 Initial Conditions

```
% Initializing Variables
% Initial Conditions
a_f(1:NN)=0;
a_r(1:NN)=0;
r(1:NN)=0;
r_dt(1:NN)=0;
Vy(1:NN)=0;
Vy_dt(1:NN)=0;
B(1:NN)=0;
B_dt(1:NN)=0;
t(1:NN)=0;
ay(1:NN)=0;
phiM(1:NN)=0;
phiM_ddt(1:NN)=0;
phiM_dt(1:NN)=0;
Fy_fl(1:NN)=0;
Fy_fr(1:NN)=0;
Fy_rl(1:NN)=0;
Fy_rr(1:NN)=0;
Fy_total(1:NN)=0;
ay(1:NN)=0;
```

```
Fz_fi(1:NN)=0;
Fz_fo(1:NN)=0;
Fz_ri(1:NN)=0;
Fz_ro(1:NN)=0;
d1(1:NN)=0;
d1_dt(1:NN)=0;
d1_ddt(1:NN)=0;
y(1:NN)=0;
y_dt(1:NN)=0;
y_ddt(1:NN)=0;
z_b_r(1:NN)=0;
z_b_r_dt(1:NN)=0;
z_b_r_ddt(1:NN)=0;
z_b_f(1:NN)=0;
z_b_f_dt(1:NN)=0;
z_b_f_ddt(1:NN)=0;
z_k_r(1:NN)=0;
z_k_r_dt(1:NN)=0;
z_k_r_ddt(1:NN)=0;
z_k_f(1:NN)=0;
z_k_f_dt(1:NN)=0;
z_k_f_ddt(1:NN)=0;
dFz_f(1:NN)=0;
dFz_r(1:NN)=0;
Fy_f(1:NN)=0;
Fy_fi(1:NN)=0;
Fy_fo(1:NN)=0;
Fy_r(1:NN)=0;
Fy_ri(1:NN)=0;
Fy_ro(1:NN)=0;
Fy_t(1:NN)=0;
Vx(1:NN)=0;
a_cen(1:NN)=0;
two_wheel_lift_o(1:NN)=0.125;
two_wheel_lift_i(1:NN)=0.150;
Marb_f(1:NN)=0;
Marb_r(1:NN)=0;
Fb_f(1:NN)=0;
Fb_r(1:NN)=0;
Fk_f(1:NN)=0;
Fk_r(1:NN)=0;
Ry(1:NN)=0;
Ry_f(1:NN)=0;
Ry_r(1:NN)=0;
Rz(1:NN)=0;
RS(1:NN)=0;
```

```
RD(1:NN)=0;
fo_lift(1:NN)=0;
fi_lift(1:NN)=0;
ro_lift(1:NN)=0;
ri_lift(1:NN)=0;
two_wheel_lift_i(1:NN)=0;
two_wheel_lift_o(1:NN)=0;
t_w_l_i(1:NN)=0;
t_w_l_o(1:NN)=0;
w_l_fi(1:NN)=0;
w_l_fo(1:NN)=0;
w_l_ri(1:NN)=0;
w_l_ro(1:NN)=0;
roll_ay(QQ)=0;
roll_r(QQ)=0;
roll_V(QQ)=0;
roll_B_dt(QQ)=0;
roll_B(QQ)=0;
roll_phiM(QQ)=0;
roll_phiM_dt(QQ)=0;
roll_a_f(QQ)=0;
roll_a_r(QQ)=0;
roll_Fy_f(QQ)=0;
roll_Fy_r(QQ)=0;
roll_Fy_t(QQ)=0;
roll_dFz_f(QQ)=0;
roll_dFz_r(QQ)=0;
roll_del(QQ)=0;
roll_t(QQ)=0;
Fz_fo_lift = 0;
Fz_ro_lift = 0;
Fz_fi_lift = 0;
Fz_ri_lift = 0;
counter=0;
```

C.6 roll_center_height.m

```
function[h_rc_cg]=roll_center_height(WB,a,h_rc_f,h_rc_r)
if h_rc_f < h_rc_r;
   theta=atan((h_rc_r-h_rc_f)/WB);
   x=a*tan(theta);
   h_rc_cg=x+h_rc_f;
else
if h_rc_f > h_rc_r;
```

```
   theta=atan((h_rc_f-h_rc_r)/WB);
   x=a*tan(theta);
   h_rc_cg=x+h_rc_r;
else
if h_rc_f == h_rc_r;
   h_rc_cg=h_rc_f;
end
end
end
```

C.7 Velocity.m

```
function [vel]=velocity(profile,speed,accel,endtime,ts,MT);
NN = endtime/ts;
milephour2meterpsec = 1606.344/3600;    % Conversion from mph to meter/s
vel(1:NN) = 0*milephour2meterpsec;       % initializing the velocity vector
switch profile
   case 'step'
      vel(1:NN)=speed*milephour2meterpsec;

   case 'ramp a'   % constantly increasing ramp
      for k=1:NN-1
         vel(k+1)=(speed/NN)+vel(k);
      end
      vel(1:NN)=vel(1:NN)*milephour2meterpsec;
   case 'ramp'     % starting the vehicle from standstill to designated velocity
                   % Both Maximum speed and acceleration are user defined
      period_1 = 5;    % [sec]
      index_1  = period_1/ts;
      period_2 = (1/accel)*speed+period_1;
      index_2 = period_2/ts;
      for k=index_1:index_2
         vel(k) = vel(k-1)+ts*accel;
      end
      vel(index_2+1:NN)=vel(index_2);
      vel(1:NN)=vel(1:NN)*milephour2meterpsec;
   case 'coast'  % Coast Down
      drag=0.85;
      F_fric=600;
      t_coast(NN)=0;
      vel_dt(NN)=0;
      start_time=2/ts;
      vel(1:start_time)=speed;
      for cc=start_time:NN
```

```
        vel_dt(cc+1)= -drag/MT*vel(cc)^2-F_fric/MT;
        vel(cc+1)=vel(cc)+ts*0.5*(vel_dt(cc+1)+vel_dt(cc));
        t_coast(cc+1)=t_coast(cc)+ts;
    end
    vel=Velocity_Smoothing(vel);
    vel=vel*milephour2meterpsec;
end
```

C.8 Velocity_Smoothing.m

```
function[vel_out]=Velocity_Smoothing(vel_in)
% Velocity Profile Smoothing
% This file takes out the sharp changes in velocity
wn=100;
[B,A]=butter(2,wn/1000*2*pi);
vel_out=filter(B,A,vel_in);
```

C.9 Steer_Profile.m

```
function [del_out]=steer_profile(maneuver,max_steer,SIS_const,endtime,ts,steer_ratio);
NN=endtime/ts;
del(1:NN)=0;    % initializing del
switch maneuver
% Slowly Increasing Steer (SIS) Maneuver
        case 'SIS'
                ramptime=30; % sec
                for n=1:NN
                        del(n+1)=(max_steer*pi/180)/(ramptime/ts)+del(n);
                end
% Step Maneuvers
   case 'step'
      del(1:NN)=max_steer*pi/180;    % Radians
 % Ramp Maneuvers
   case 'ramp'
      ramptime=5;     % the time it takes to ramp linearly from zero to the set steer angle
      del(1)=0;
      t(1)=0;
      for n=1:NN;
         if n <= ramptime/ts
            del(n+1)=(max_steer*pi/180)/(ramptime/ts)+del(n);
```

```
        end
        if n > 5/ts
           del(n+1)=del(n);
        end
      end
% Sinusoidal Maneuvers
  case 'sine'
      del(1)=0;
      t(1)=0;
      for n=1:NN
         wn=n*180/pi/20000;
         del(n+1)=(max_steer*pi/180)*sin(wn);
      end
% Fishhook 1a
  case '1a'
      period_1=2;
      index_1=period_1/ts;
      A=chop(max_steer*pi/180,4);
      steer_rate=chop(40*pi/180,2);
      period_2=chop(A/steer_rate+period_1,4);
      index_2=period_2/ts;
      for k = index_1:index_2
         del(k+1)=steer_rate*ts+del(k);
      end
      period_3=.25+period_2;
      index_3=period_3/ts;
      for kk=index_2:index_3
         del(kk+1)=del(kk);
      end
      period_4=chop(2*A/steer_rate+period_3,4);
      index_4=period_4/ts;
      for k=index_3:index_4
         del(k+1)=del(k)-steer_rate*ts;
      end
      period_5=3+period_4;
      index_5=period_5/ts;
      for k=index_4:index_5
         del(k+1)=del(k);
      end
      period_6=chop(A/steer_rate+period_5,4);
      index_6=period_6/ts;
      for k=index_5:index_6
         del(k+1)=steer_rate*ts+del(k);
      end
      del(index_6+1:NN)=0;
end
```

```
[del_out] = Steering_Smoothing(del);
```

C.10 Steering_Smoothing.m

```
function[del_out]=Steer_Smoothing(del_in)
% Steering Profile Smoothing
% This file takes out the sharp changes in steering angle
wn=.5;
[B,A]=butter(2,wn/1000*2*pi);
del_out=filter(B,A,del_in);
```

C.11 RubberandString.m

```
function [Fy]=rubberandstring(Ca,tire,alpha,Fz)
alpha=-alpha*180/pi;    % There is a sign change here do to my sign convention on my FBD
Fz=Fz/1000;           % Conversion from N to kN
switch tire
   case 'Pacejka'
      % The stadard Pacejka "Magic Tire Model" found is SAE 870421
      % Pacejka Parameters
      a0=0;             % 0
      a1=-10.1;          % -22.1
      a2=1011;           % 1011
      a3=1578;           % 1078
      a4=1.82;           % 1.82
      a5=0.208;          % 0.208
      a6=0;             % 0
      a7=-0.352;         % -0.354
      a8=.707;           % 0.707
      % Pacejka Equations
      if Fz <= 0;
         Fy = 0;
      else
         C = 1.30;                        % Shape Factor  % 1.30
         D = a1*Fz^2+a2*Fz;                % Peak Factor
         E = a6*Fz^2+a7*Fz+a8;  % -1.5  % Curvature Factor
         BCD= a3*sin(a4*atan(a5*Fz));  % Ca  % Cornering Stiffness Parameter (Calpha)
```

```
      B=BCD/(C*D);                    % Stiffness Factor
      phi = (1-E)*alpha+(E/B)*atan(B*alpha);
      Fy = D*sin(C*atan(B*phi));
      mu=Fy/Fz/1000;
   end
case 'Linear'
   % This is a simple linear tire model.  Not realistic, but it is
   % used to debug code, and to see what is happening in the simulation

   Ca=2500.0;   % N/deg_slip    Cornering Stiffness per tire
   Fy=Ca*alpha;

case 'Dugoff No Fz'
   % This is a Dugoff type model, however Fz is set at 5 kN
   Ca=1002.5;      % N/deg_slip    Cornering Stiffness per tire
   Fy_Max=5000;    % Newtons
   saturation_alpha=Fy_Max/Ca;     % degress   Saturation tire slip angle
   if alpha <= saturation_alpha
      Fy=Ca*alpha;
   end
   if alpha >= -saturation_alpha
      Fy=Ca*alpha;
   end
   if alpha > saturation_alpha
      Fy=Fy_Max;
   end
   if alpha < -saturation_alpha
      Fy=-Fy_Max;
   end

case 'Dugoff'
   % This is a variation of Dugoff's tire model.  Fy_Max is a funtion
   % of Fz and the coefficent of friction.
   % SAE 700377
   mu=1.02;
   Fy_Max=Fz*mu*1000;
   Ca=1002.5;
   saturation_alpha=Fy_Max/Ca;
   if alpha <= saturation_alpha
      Fy=Ca*alpha;
   end
   if alpha >= -saturation_alpha
      Fy=Ca*alpha;
   end
   if alpha > saturation_alpha
      Fy=Fy_Max;
```

```
    end
    if alpha < -saturation_alpha
       Fy=-Fy_Max;
    end
end
```

C.12 Property Changer

```
% Property Changer Switch
switch prop
 case 0
 % No Changes
[a,b,Wf,Wr,M_f,M_r,m_f,m_r,h_cg_M,Iz,Ix,d1,h1,Ca_f,Ca_r]
=No_Change(a,b,g,m,WB,MT,Wt,h_cg_M,Iz,Ix,M,h_rc_cg,Ca_f,Ca_r);
QQ=length(a);
case 100
 % No Changes but looking for wheel lift
[a,b,Wf,Wr,M_f,M_r,m_f,m_r,h_cg_M,Iz,Ix,d1,h1,Ca_f,Ca_r]
=No_Change(a,b,g,m,WB,MT,Wt,h_cg_M,Iz,Ix,M,h_rc_cg,Ca_f,Ca_r);
QQ=length(a);
case 1
 % Weight Split Change
  [a,b,Wf,Wr,M_f,M_r,m_f,m_r,h_cg_M,Iz,Ix,d1,h1,Ca_f,Ca_r]
=Weight_Split_Changer(a,b,g,m,WB,MT,Wt,h_cg_M,Iz,Ix,M,h_rc_cg,Ca_f,Ca_r);
 QQ=length(a);
case 2
 % CG Height Change
[h_cg_M,a,b,Wf,Wr,M_f,M_r,m_f,m_r,Ix,Iz,h_cg_Percent,d1,h1,Ca_f,Ca_r]
=CG_Height_Changer(h_cg_M,a,b,g,m,WB,MT,Wt,M,Ix,Iz,h_rc_cg,Ca_f,Ca_r);
QQ=length(h_cg_M);
end
```

C.13 No Change

```
function[a,b,Wf,Wr,M_f,M_r,m_f,m_r,h_cg_M,Iz,Ix,d1,h1,Ca_f,Ca_r]=No_Change(a_ol
d,b_old,g,m,WB,MT,Wt,h_cg,Iz_old,Ix_old,M,h_rc_cg,Ca_f_old,Ca_r_old);
% This function causes no change to the initial vehicle properties
qq=1;
h_cg_M(qq)=h_cg;
a(qq)=a_old;
b(qq)=b_old;
```

```
 h1(qq)=h_cg_M(qq)-h_rc_cg;      % Negative number means that the CG is below the
roll center
d1(qq)=h1(qq);
Ix(qq)=Ix_old;
Iz(qq)=Iz_old;
d1(qq)=h1(qq);
Ca_f(qq)=Ca_f_old;
Ca_r(qq)=Ca_r_old;
% Weight ratio
 Wr(qq)=a(qq)*MT*g/(a(qq)+b(qq));    % Total weight on rear tires    (N)
 Wf(qq)=MT*g-Wr(qq);         % Total weight on front tires   (N)
 M_f(qq)=Wf(qq)/g;           % Sprung Mass on front axle     (kg)
 M_r(qq)=Wr(qq)/g;           % Sprung Mass on rear axle      (kg)
% I assume that the un-sprung mass has same weight split as the sprung mass
 m_f(qq)=m*Wf(qq)/Wt;        % Un-Sprung Mass on front axle  (kg)
 m_r(qq)=m*Wr(qq)/Wt;        % Un-Sprung Mass on rear axle   (kg)
```

C.14 Weight_Split_Changer.m

```
function
[a,b,Wf,Wr,M_f,M_r,m_f,m_r,h_cg_M,Iz,Ix,d1,h1,Ca_f,Ca_r]=Weight_Split_Changer(a
_old,b,g,m,WB,MT,Wt,h_cg,Iz_old,Ix_old,M,h_rc_cg,Ca_f_old,Ca_r_old);
% This function changes vehicle weight split
% It makes vectors of the variable it is outputting

% Weight Split Changer
      QQ=80;
      qq=1;
      for qq = 1:QQ
         a(qq)=.28*WB+WB*(qq/160);
         b(qq)=WB-a(qq);
         h_cg_M(qq)=h_cg;
         Iz(qq)=Iz_old;
         Ix(qq)=Ix_old;
         h1(qq)=h_cg_M(qq)-h_rc_cg;
         d1(qq)=h1(qq);
         Ca_f(qq)=Ca_f_old;
         Ca_r(qq)=Ca_r_old;
      % Weight ratio
         Wr(qq)=a(qq)*MT*g/(a(qq)+b(qq));    % Total weight on rear tires    (N)
         Wf(qq)=MT*g-Wr(qq);         % Total weight on front tires   (N)
         M_f(qq)=Wf(qq)/g;           % Sprung Mass on front axle     (kg)
         M_r(qq)=Wr(qq)/g;           % Sprung Mass on rear axle      (kg)
      % I assume that the un-sprung mass has same weight split as the sprung mass
```

```
        m_f(qq)=m*Wf(qq)/Wt;        % Un-Sprung Mass on front axle  (kg)
        m_r(qq)=m*Wr(qq)/Wt;        % Un-Sprung Mass on rear axle   (kg)
    end
```

C.15 CG_Height_Changer.m

```
function
[h_cg_M,a,b,Wf,Wr,M_f,M_r,m_f,m_r,Ix,Iz,h_cg_Percent,d1,h1,Ca_f,Ca_r]=CG_Heigh
t_Changer(h_cg_M_old,a_old,b_old,g,m,WB,MT,Wt,M,Ix_old,Iz_old,h_rc_cg,Ca_f_old,
Ca_r_old)
% This function changes the CG height
QQ=40;
for qq=1:QQ
   h_cg_M(qq)=((.60)+(qq/2)/(QQ/2))*h_cg_M_old;
   h_cg_Percent(qq)=h_cg_M(qq)/h_cg_M_old*100;
   a(qq)=a_old;
   b(qq)=b_old;
   h1(qq)=h_cg_M(qq)-h_rc_cg;
   d1(qq)=h1(qq);
   Ix(qq)=Ix_old;
   Iz(qq)=Iz_old;
   Ca_f(qq)=Ca_f_old;
   Ca_r(qq)=Ca_r_old;
   % Weight ratio
    Wr(qq)=a(qq)*MT*g/(a(qq)+b(qq));    % Total weight on rear tires    (N)
    Wf(qq)=MT*g-Wr(qq);         % Total weight on front tires   (N)
    M_f(qq)=Wf(qq)/g;           % Sprung Mass on front axle     (kg)
    M_r(qq)=Wr(qq)/g;           % Sprung Mass on rear axle      (kg)
   % I assume that the un-sprung mass has same weight split as the sprung mass
    m_f(qq)=m*Wf(qq)/Wt;        % Un-Sprung Mass on front axle  (kg)
    m_r(qq)=m*Wr(qq)/Wt;        % Un-Sprung Mass on rear axle   (kg)
end
```

C.16 Simulation Switch

```
% Simulation Switch
switch sim
   case 100
      n=1;
      while n <= NN
         d1=h1;
```

```
% Velocity in x-axis
   Vx(n)=vel(n)*cos(B(n));   % m/s
% Tire Slip Angles
   a_f(n)=atan((Vy(n)+a(qq)*r(n))/Vx(n))-del(n);   % tire slip angle front  (rad)
   a_r(n)=atan((Vy(n)-b(qq)*r(n))/Vx(n));          % tire slip angle rear   (rad)
% Spring and Damper Displacement and Velocity
   z_k_f(n) = (Sk_f/2)*sin(phiM(n));      % Front Spring Displacement [m]
   z_k_r(n) = (Sk_r/2)*sin(phiM(n));      % Rear Spring Displacement [m]
   z_b_f_dt(n) = phiM_dt(n)*(Sb_f/2)*cos(phiM(n)); % Front Damper
Displacement [m/s]
   z_b_r_dt(n) = phiM_dt(n)*(Sb_r/2)*cos(phiM(n)); % Rear Damper Displacement
[m/s]
% Spring Forces (Individual springs)
   Fk_f(n) = ks_f*z_k_f(n);      % Front Individual Spring Force [N]
   Fk_r(n) = ks_r*z_k_r(n);      % Rear Individual Spring Force [N]
% Damper Forces (Individual dampers)
   Fb_f(n) = 0;    % Front Indiviual Damper Force [N]  Zero for SS
   Fb_r(n) = 0;    % Rear Individual Damper Force [N]  Zero for SS
% Anti-Roll Bar Moment
   Marb_f(n) = phiM(n)*karb_f;   % [N*m]
   Marb_r(n) = phiM(n)*karb_r;   % [N*m]
% Reaction Forces
   Ry(n) = ay(n)*M;                  %(ay(n)+y_ddt(n))*M;     % [N]
   Ry_f(n) = Ry(n)*M_f(qq)/M;         % Ry allocated to the Front [N]
   Ry_r(n) = Ry(n)*M_r(qq)/M;         % Ry allocated to the Rear [N]
   Rz(n) = M*g;                      % [N]
% Weight Transfer
   % Fzo-Fzi
   dFz_f(n)=(2/trk_f)*(Marb_f(n)+Sk_f*Fk_f(n)+Sb_f*Fb_f(n)+...
      Ry_f(n)*(h_rc_f-h_cg_m)+Fy_f(n)*h_cg_m);    % Front Lateral Weight
Transfer
   dFz_r(n)=(2/trk_r)*(Marb_r(n)+Sk_r*Fk_r(n)+Sb_r*Fb_r(n)+...
      Ry_r(n)*(h_rc_r-h_cg_m)+Fy_r(n)*h_cg_m);    % Rear Lateral Weight
Transfer
% This is a cap for the dFz so you don't have more mass transfer than is physically
possible
if abs(dFz_f(n)) >= Wf(qq)/2
   dFz_f(n)=sign(dFz_f(n))*Wf(qq)/2;
end
if abs(dFz_r(n)) >= Wr(qq)/2
   dFz_r(n)=sign(dFz_r(n))*Wr(qq)/2;
end
% Calculating the new Fz value at each wheel
   Fz_ri(n)=Wr(qq)/2-dFz_r(n);     % Force in the z-axis on rear inner tire  [N]
   Fz_ro(n)=Wr(qq)/2+dFz_r(n);     % Force in the z-axis on rear outer tire  [N]
   Fz_fi(n)=Wf(qq)/2-dFz_f(n);     % Force in the z-axis on front inner tire [N]
```

```
    Fz_fo(n)=Wf(qq)/2+dFz_f(n);     % Force in the z-axis on front outer tire [N]
  switch wheel_lift_detector
    case 1
      % Individual Wheel-Lift detector
      One_Wheel_Lift_Detector
    case 2
      % Two Wheel Lift Detector
      Two_Wheel_Lift_Detector
  end
  % Lateral Forces from Non-Linear Pacejka Tire Model
  % Send rubberandstring.m slip angles in radians and Fz in N
    Fy_fo(n+1)=rubberandstring(Ca_f(qq),tire,a_f(n),Fz_fo(n));   % Lateral Force
    Front inner   (N)
    Fy_fi(n+1)=rubberandstring(Ca_f(qq),tire,a_f(n),Fz_fi(n));   % Lateral Force
    Front outer    [N]
    Fy_ro(n+1)=rubberandstring(Ca_r(qq),tire,a_r(n),Fz_ro(n));   % Lateral Force
    Rear inner  (N)
    Fy_ri(n+1)=rubberandstring(Ca_r(qq),tire,a_r(n),Fz_ri(n));   % Lateral Force Rear
    outer  (N)
    Fy_f(n)=Fy_fo(n)+Fy_fi(n);
    Fy_r(n)=Fy_ro(n)+Fy_ri(n);
    Fy_t(n)=Fy_f(n)+Fy_r(n);
  % Yaw Dynamics
    r_dt(n+1) = (-b(qq)*Fy_r(n)+a(qq)*Fy_f(n)*cos(del(n)))/Iz(qq);      % Yaw
    Accel. [rad/sec^2]
    r(n+1)=r(n)+0.5*ts*(r_dt(n+1)+r_dt(n));               % Yaw Rate [rad/sec]
    Vy_dt(n+1)= (Fy_r(n)+Fy_f(n)*cos(del(n)))/MT-vel(n)*r(n)*cos(B(n));
    Vy(n+1)=Vy(n)+ts*0.5*(Vy_dt(n+1)+Vy_dt(n));
    B_dt(n)=asin((Vy_dt(n)/vel(n)));
    if Vx(n) == 0
      B(n+1)=0;
    else
      B(n+1)=atan((Vy(n+1)/Vx(n)));          % Vehicle Sideslip [rad/sec]
    end
    a_cen(n)=r(n)*vel(n);                    % Centripital Acceleration [m/sec^2]
    ay(n+1)=Vy_dt(n+1)+a_cen(n)*cos(B(n+1));    % Lateral Acceleration [m/sec^2]
  % Steady State Roll
    phiM(n+1)=((M*g*d1(qq))/(kphi_t-M*g*d1(qq)))*(ay(n+1)/g); % Roll Angle
    [rad]
  % Time Counter
    t(n+1)=t(n)+ts;                          % Time [sec]
  % Index Counter
    n=n+1;
  end

case 300
```

```
n=1;
d1=h1;
% Velocity in x-axis
   Vx(n)=vel(n)*cos(B(n));   % m/s
% Tire Slip Angles
   a_f(n)=atan((Vy(n)+a(qq)*r(n))/Vx(n))-del(n);   % tire slip angle front  (rad)
   a_r(n)=atan((Vy(n)-b(qq)*r(n))/Vx(n));          % tire slip angle rear   (rad)
% Spring and Damper Displacement and Velocity
   z_k_f(n) = (Sk_f/2)*sin(phiM(n));      % Front Spring Displacement [m]
   z_k_r(n) = (Sk_r/2)*sin(phiM(n));      % Rear Spring Displacement [m]
   z_b_f_dt(n) = phiM_dt(n)*(Sb_f/2)*cos(phiM(n)); % Front Damper
Displacement [m/s]
   z_b_r_dt(n) = phiM_dt(n)*(Sb_r/2)*cos(phiM(n)); % Rear Damper Displacement
   [m/s]
% Spring Forces (Individual springs)
   Fk_f(n) = ks_f*z_k_f(n);      % Front Individual Spring Force [N]
   Fk_r(n) = ks_r*z_k_r(n);      % Rear Individual Spring Force [N]
% Damper Forces (Individual dampers)
   Fb_f(n) = b_f*z_b_f_dt(n);    % Front Indiviual Damper Force [N]
   Fb_r(n) = b_r*z_b_r_dt(n);    % Rear Individual Damper Force [N]
% Anti-Roll Bar Moment
   Marb_f(n) = phiM(n)*karb_f;   % [N*m]
   Marb_r(n) = phiM(n)*karb_r;   % [N*m]
% Reaction Forces
   Ry(n) = ay(n)*M;                  %(ay(n)+y_ddt(n))*M;     % [N]
   Ry_f(n) = Ry(n)*M_f(qq)/M;        % Ry allocated to the Front [N]
   Ry_r(n) = Ry(n)*M_r(qq)/M;        % Ry allocated to the Rear [N]
   Rz(n) = M*g;                      % [N]
% Weight Transfer
   % Fzo-Fzi
   dFz_f(n)=(2/trk_f)*(Marb_f(n)+Sk_f*Fk_f(n)+Sb_f*Fb_f(n)+...
      Ry_f(n)*(h_rc_f-h_cg_m)+Fy_f(n)*h_cg_m);    % Front Lateral Weight
   Transfer
   dFz_r(n)=(2/trk_r)*(Marb_r(n)+Sk_r*Fk_r(n)+Sb_r*Fb_r(n)+...
      Ry_r(n)*(h_rc_r-h_cg_m)+Fy_r(n)*h_cg_m);    % Rear Lateral Weight
   Transfer

% This is a cap for the dFz so you don't have more mass transfer than is physically
   possible
if abs(dFz_f(n)) >= Wf(qq)/2
   dFz_f(n)=sign(dFz_f(n))*Wf(qq)/2;
end
if abs(dFz_r(n)) >= Wr(qq)/2
   dFz_r(n)=sign(dFz_r(n))*Wr(qq)/2;
end
% Calculating the new Fz value at each wheel
```

```
        Fz_ri(n)=Wr(qq)/2-dFz_r(n);     % Force in the z-axis on rear inner tire  [N]
        Fz_ro(n)=Wr(qq)/2+dFz_r(n);     % Force in the z-axis on rear outer tire  [N]
        Fz_fi(n)=Wf(qq)/2-dFz_f(n);     % Force in the z-axis on front inner tire [N]
        Fz_fo(n)=Wf(qq)/2+dFz_f(n);     % Force in the z-axis on front outer tire [N]
      switch wheel_lift_detector
        case 1
          % Individual Wheel-Lift detector
          One_Wheel_Lift_Detector
        case 2
          % Two Wheel Lift Detector
          Two_Wheel_Lift_Detector
      end
      % Lateral Forces from Non-Linear Pacejka Tire Model
      % Send rubberandstring.m slip angles in radians and Fz in N
        Fy_fo(n+1)=rubberandstring(Ca_f(qq),tire,a_f(n),Fz_fo(n));   % Lateral Force
Front inner   (N)
        Fy_fi(n+1)=rubberandstring(Ca_f(qq),tire,a_f(n),Fz_fi(n));   % Lateral Force
Front outer    [N]
        Fy_ro(n+1)=rubberandstring(Ca_r(qq),tire,a_r(n),Fz_ro(n));   % Lateral Force
Rear inner  (N)
        Fy_ri(n+1)=rubberandstring(Ca_r(qq),tire,a_r(n),Fz_ri(n));   % Lateral Force Rear
outer  (N)
        Fy_f(n)=Fy_fo(n)+Fy_fi(n);
        Fy_r(n)=Fy_ro(n)+Fy_ri(n);
        Fy_t(n)=Fy_f(n)+Fy_r(n);
      % Yaw Dynamics
        r_dt(n+1) = (-b(qq)*Fy_r(n)+a(qq)*Fy_f(n)*cos(del(n)))/Iz(qq);      % Yaw
Accel. [rad/sec^2]
        r(n+1)=r(n)+0.5*ts*(r_dt(n+1)+r_dt(n));              % Yaw Rate [rad/sec]
        Vy_dt(n+1)= (Fy_r(n)+Fy_f(n)*cos(del(n)))/MT-vel(n)*r(n)*cos(B(n));
        Vy(n+1)=Vy(n)+ts*0.5*(Vy_dt(n+1)+Vy_dt(n));
      % Side Slip Angle (Beta)
        B(n+1)=asin((Vy(n)/vel(n)));              % Vehicle Sideslip [rad]
        B_dt(n+1)=(B(n+1)-B(n))/ts;       % Vehicle Sideslip rate [rad/sec]
      % Lateral Acceleration
        a_cen(n)=r(n)*vel(n);                  % Centripital Acceleration [m/sec^2]
        ay(n+1)=Vy_dt(n+1)+a_cen(n)*cos(B(n+1));    % Lateral Acceleration [m/sec^2]
        ay_test(n)=vel(n)^2/R;
      % Roll Stiffness
        RS=kphi_t;
        RSM(n)=RS*phiM(n);
      % Roll Damping
        RD(n)=(0.5*b_f*Sb_f^2*cos(phiM(n))+0.5*b_r*Sb_r^2*cos(phiM(n)));
        RDM(n)=RD(n)*phiM_dt(n);
      % Roll Dynamics
```

```
        phiM_ddt(n+1)=(1/Ix(qq))*(-RSM(n)-
        RDM(n)+Rz(n)*d1(qq)*sin(phiM(n))+Ry(n)*d1(qq)*cos(phiM(n)));
        phiM_dt(n+1)=phiM_dt(n)+ts*0.5*(phiM_ddt(n+1)+phiM_ddt(n));    % Roll
Velocity [rad/s]
        phiM(n+1)=phiM(n)+ts*0.5*(phiM_dt(n+1)+phiM_dt(n));      % Roll Angle [rad]
      % Time Counter
        t(n+1)=t(n)+ts;                    % Time [sec]
      % Index Counter
        n=n+1;
      end
end
```

C.17 Two-Wheel-Lift Detector

```
% Script of Two-Wheel-Lift Detector
% Detects wheel lift of both 'inside' or 'outside' tires
% Depending on the maneuver the 'outside' tires may have wheel lift.  This
% does not actually mean that the outside tires lift.  The terms outside
% and inside were used instead of left and right for ease in debugging step
% inputs.

   % Two wheel-lift detector of outside tires
      if Fz_fo(n) <= 0 & Fz_ro(n) <= 0
         counter=1+counter;
         fo_lift(n) = 1;
         ro_lift(n) = 1;
         roll_fo_lift(qq) = 1;
         roll_ro_lift(qq) = 1;
         two_wheel_lift_o(n)=1;
         roll_ay(qq)=max(ay(1:n));
         roll_r(qq)=(r(n));
         roll_V(qq)=(vel(n));
         roll_B_dt(qq)=(B_dt(n));
         roll_B(qq)=(B(n));
         roll_phiM(qq)=(phiM(n));
         roll_phiM_dt(qq)=(phiM_dt(n));
         roll_a_f(qq)=(a_f(n));
         roll_a_r(qq)=(a_r(n));
         roll_Fy_f(qq)=(Fy_f(n));
         roll_Fy_r(qq)=(Fy_r(n));
         roll_Fy_t(qq)=(Fy_t(n));
         roll_dFz_f(qq)=(dFz_f(n));
         roll_dFz_r(qq)=(dFz_r(n));
         roll_del(qq)=del(n);
```

```
        roll_t(qq)=t(n);
    end
   t_w_l_o(n+1)=two_wheel_lift_o(n)+t_w_l_o(n);

% Two wheel lift detector of inside tires
    if Fz_fi(n) <= 0 & Fz_ri(n) <= 0
        counter=1+counter;
        fi_lift(n) = 1;
        ri_lift(n) = 1;
        roll_fi_lift(qq) = 1;
        roll_ri_lift(qq) = 1;
        two_wheel_lift_i(n)=1;
        roll_ay(qq)=max(ay(1:n));
        roll_r(qq)=(r(n));
        roll_V(qq)=(vel(n));
        roll_B_dt(qq)=(B_dt(n));
        roll_B(qq)=(B(n));
        roll_phiM(qq)=(phiM(n));
        roll_phiM_dt(qq)=(phiM_dt(n));
        roll_a_f(qq)=(a_f(n));
        roll_a_r(qq)=(a_r(n));
        roll_Fy_f(qq)=(Fy_f(n));
        roll_Fy_r(qq)=(Fy_r(n));
        roll_Fy_t(qq)=(Fy_t(n));
        roll_dFz_f(qq)=(dFz_f(n));
        roll_dFz_r(qq)=(dFz_r(n));
        roll_del(qq)=del(n);
        roll_t(qq)=t(n);
    end
    t_w_l_i(n+1)=two_wheel_lift_i(n)+t_w_l_i(n);


     if prop == 0
         % Do Nothing
     else if prop == 100 | 1 | 2 | 3 | 4 | 5 | 6 | 7 | 8 | 9 | 10
       if t_w_l_i(n+1) > lift_time
          flag=1;
          break
       end
       if t_w_l_o(n+1) > lift_time
          flag=1;
          break
       end
     end,end
```